A unified fracture mechanics approach to fretting fatigue crack growth

by

Laurent Chambon

Submitted to the Department of Aeronautics and Astronautics
in partial fulfillment of the requirements for the degree of

Master of Science

at the

MASSACHUSETTS INSTITUTE OF TECHNOLOGY

February 2001

Author ....
Department of Aeronautics and Astronautics
January 18, 2001

Certified by..... .....
Subra Suresh
R. P. Simmons Professor of Materials Science and Engineering,
Head of the Department of Materials Science and Engineering
Thesis Supervisor

Certified by..... .....
Mark Spearing
Esther and Harold E. Edgerton Associate Professor of Aeronautics
and Astronautics
Thesis Supervisor

Accepted by .....
Wallace E. Vander Velde
Professor Emeritus,
Chairman, Department Graduate Office

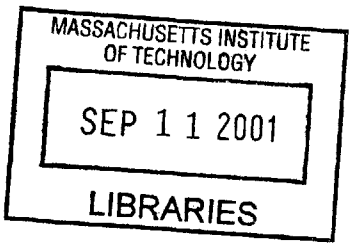

A unified fracture mechanics approach to fretting fatigue crack growth

by

Laurent Chambon

Submitted to the Department of Aeronautics and Astronautics
on January 18, 2001, in partial fulfillment of the
requirements for the degree of
Master of Science

Abstract

The purpose of this work is to demonstrate the adequacy of a modeling approach of fretting fatigue for a sphere-on-flat geometry entirely based on fracture mechanics. All stages of damage evolution, from initiation to failure, are encompassed within the framework of fracture mechanics, in contrast with the general use of stress based criteria to predict crack initiation. A comparison with the classical approaches show how this methodology allows to circumvent the problem of the length scale for initiation by using the crack analogue methodology of contact of Giannakopoulos, Venkatesh, Lindley and Suresh. On the other hand, another length scale, identified as the region of dominance of the singular adhesive stresses, is introduced by the model, and experimental methods to validate it are suggested.

The comparison of simulations with three sets of experiments performed on a titanium alloy, with a good control of the normal, tangential and axial loads, shows that the qualitative trends are captured. Good quantitative agreement is also obtained for some of them, depending on the details of the crack growth law.

Experimentally, results on the same material after shot peening are reported and used to evaluate the ability of the approach to cope with residual stresses. A good qualitative explanation of the fretting fatigue resistance of the shot peened material is demonstrated. These experiments also serve to illustrate possible testing methods and observations which could yield more useful information than the "classical" fretting fatigue test to failure, and to emphasize the need for a careful stress analysis to avoid plastification under certain material and experimental conditions.

Thesis Supervisor: Subra Suresh
Title: R. P. Simmons Professor of Materials Science and Engineering,
Head of the Department of Materials Science and Engineering

Thesis Supervisor: Mark Spearing
Title: Esther and Harold E. Edgerton Associate Professor of Aeronautics and Astronautics

Acknowledgments

Many different people contributed to making my MIT experience the incredible time it was, but I'll try to keep it brief.

On the academic side, it won't be a surprise that working for Professor Subra Suresh was an incredible intellectual and personal experience. As once said about Gen. Doolittle, he's a man with more gifts than any one man has a right to be blessed with, from whom it is a chance and a pleasure to learn. I am equally thankful, and greatly indebted to Professor Mark Spearing, to have been accepted as a part-time member of his lab, for being exposed to the wealth of composite knowledge of the TELAC members was a delight, and also because I now have another puzzle to solve: how can one combine intellectual excellence, good character and outstanding teaching abilities altogether to the level Professor Mark Spearing does?

I also need to thank Dr. Antonios Giannakopoulos and Professor Trevor Lindley for sharing some of their immense knowledge of contact problems through helpful comments and discussions. They helped me understand what the famous quotes about seeing far by standing on the shoulders of giants meant; too bad I have been short-sighted since I was 19, but thanks for the lift anyway. I am also grateful to Dr. T. A. Venkatesh, for his constructive criticism, and his effort to put some academic perspective in my admittedly very engineering approach to research.

I will remember all LEXCOM members as talented, fun individuals, to whom I am grateful for the good time I had in the lab. George LaBonte, Andrew Gouldstone, Brett Conner, Anders Salomonsson, Krystyn Van Vliet, Raj Vaidyanathan, Kob Chollacoop, Yoonjoon Choi, Tae-Soon Park, Tim Hanlon, Dr. Chong Soo Lee: these are names that will always mean something to me. A special thanks to then Second Lieutenant Conner, for getting me up to speed on fretting so effectively, and to Dr. Lee for invaluable insights on the material side of things and for the help in performing some of the experiments.

On the industry side, I am more than deeply grateful to M. Didier Guedra-Degeorges, M. Jocelyn Gaudin, and M. Bertrand Journet for their trust, support

and advice. The continuous financial support of Aerospatiale, Aerospatiale-Matra, and EADS is gratefully acknowledged.

On the personal side, well, there would be many contributors. To Ben, Fred, Gwen, Arrow 813ND, Derek Ruetsch and David Schoneman, for being there in the best and worst moments. My family was also a great support, especially considering how little they know about what I am doing.

And first should have come the one to whom I owe most. To make a long and complex story short, had she not entered my life, I would not be writing this today. Thank you Aude.

Contents

List of Figures

List of Tables

Chapter 1

Introduction

Fretting fatigue is a surface damage process which arises when small oscillatory relative displacements exists between two components in contact (see Section 2.1 for more details on a definition of fretting fatigue). It is of particular importance for fitted, bolted or riveted components, and for jet engine compressor blade roots (see Hattori [13] for a review of fretting problems in structural applications). The knowledge of fretting failure requires an understanding of the interaction among fatigue, contact mechanics, materials science and fracture mechanics, which has made it a challenging topic for research community for many decades. No one can yet claim to have given a completely consistent picture of the phenomenon, and the design of the much needed palliatives has primarily drawn on experience and "trial and error". In addition, part of the uncertainty has come from the difficulty in controlling and/or measuring of the large number of intricate parameters.

It is nevertheless well known that the crack propagation taking place during the failure process can be relatively well described by fracture mechanics, although the complexity of loading encountered in contact problems are not well captured by current methodologies [14][15][16][17]. The practical problem of predicting the number of cycles to failure of a component subjected to fretting fatigue can be (and has been) thus approached to a first order in a way that resembles well-known damage tolerance methodologies. However fretting fatigue does not easily lend itself to be characterized on the basis of an assumed or measured initial defect size[18] on which the calculation

could be based, since the location of damage is determined by the contact problem, not materials characteristics: failure is not brought about by some weakness in the material, but rather by the mechanics of the problem. But, in its traditional form, the contact problem doesn't provide the necessary length scale (see Fouvry et al. [19] on the need for a length scale). Consequently, life calculations traditionally rely on an educated guess of what a reasonable initial crack size after a certain likely number of cycles may be, often presented in the form of a stress criterion. Although good guesses may allow to correlate predictions with specific experimental data, the method is satisfactory neither from a scientific nor from an engineering point of view. Proposed methodologies, their advantages and shortcomings are discussed in the first part of this thesis.

An alternative has been offered by the "crack analogue methodology" developed by Giannakopoulos et al. [2][20]. With this approach, some contact problems can be recast into a fracture mechanics problem. One option, outlined by the authors, could then be to treat the entire problem purely in term of crack propagation. The details of the methodology are also presented in part I, with an emphasis on the sphere-on-flat geometry dealt with experimentally later in this report. The first and major objective of this work is to assess the validity and possible benefits of such an approach, and indicate possible areas of improvement. To this end, the comparison of a model, using the adhesive version of the crack analogue methodology [20] and fracture mechanics only, with a set of experiments with carefully controlled loads performed on Ti-6Al-4V is presented.

In order to better evaluate the relevance to practical applications, the ability to account for the effect of palliative surface treatments was considered crucial. Therefore, a second objective was to generate carefully documented data on material treated against fretting. Fretting tests were performed on shot-peened Ti specimens, in addition to the extensive database available on untreated Ti alloys [21]. Other palliatives were also evaluated, and the results discussed in the appendices as they are less directly related to the modeling effort. The principles of shot peening are explained in the third part of this work, after the introduction to modeling, as an introduction to

the experimental observations.

Chapter 4 is devoted to a thorough discussion of the stress state for the geometry of interest, with particular emphasis on the conditions for plastification, the predictions of the model, and the comparisons with the unique set of experiments recently produced by Conner [3]. Overall, it is shown that the model qualitatively captures all the reported trends due to variations in the load parameters, even with residual stresses. Quantitatively, a systematic study of the effect of the crack growth law parameters is carried out, which indicates that physically meaningful parameters yield good agreement with experiments. The benefits of differentiating between different regimes of crack growth rate, depending on the length of the crack, are analyzed. Limitations, mainly due to closure effects, to the uncertainty in the strength of adhesion, the quantitative values of the crack growth threshold, and the size of the dominance region of the adhesive stresses, are finally pointed out, and possible developments are outlined.

Chapter 2

Overview of current modeling approaches to fretting fatigue

2.1 Motivation for the study

Fretting is well known to reduce the fatigue life of a variety of materials (for instance [22][23]). The reduction of the endurance limit observed in laboratory tests for engineering alloys vary widely, but a reduction to only 30% of the plain fatigue endurance limit is not uncommon. This degradation of mechanical properties is of major practical importance. In the mid 1980's, fretting and stress corrosion were reported to account for about 30% of the crack induced failures in aircraft in service in the United States, with the former generating an increasing number of failures, commonly occurring before 50% of the expected life was expended [24]. Therefore, much effort has been devoted to try and explain this phenomenon, but the task is far from complete.

Various definitions of the condition of fretting have been given. The definition as "an interfacial damage process that arises from a tripartite interaction among wear, corrosion and fatigue phenomena", found in [25], seems sometimes to be considered acceptable, although it is less appropriate than "a surface damage phenomenon occurring on two contacting surfaces having oscillatory relative displacements" (National Materials Advisory Board definition cited in [26]). The former indeed, together with

the common use of the term fretting *fatigue* to designate fretting, seems to imply that bulk loading is required to grow fretting damage, as in the case of plain fatigue, which is contrary to experience [1]. In spite of the large number of contact conditions that can be studied, much work has been devoted to the case of a sphere or flat punch "sliding" on a plane, under a constant normal force and varying tangential force, a sometime relevant laboratory picture of the practical situation. Usually a bulk uniaxial stress is imposed on one of the components, with the purpose of accounting for service loads. This leads to the phenomenon of fretting-initiated fatigue, or fretting fatigue, investigated in this report, "a condition where the material fatigue strength is degraded by the presence of surface stress concentrations resulting at site of fretting pits, and surface and subsurface stresses resulting from rubbing friction contact combined with the stresses resulting from the overall fluctuating stress field" (in [26]). As noted before, this practice may have contributed to the overemphasis placed on bulk stress in fretting damage evolution.

Of course, once the potential danger of fretting has been identified, the next question is how to understand, model, predict and prevent it. Although a "unified" theory of fretting palliatives took some time to emerge [27] and is still not complete, it has been recognized that nucleation occurred quite early, and that the phenomenon was therefore propagation-driven [23][28][29]. Among all the palliatives strategies cited by Foulquier and Petiot [29], only the modification of surface properties and/or contact stresses and the prevention of crack propagation are used in practice. Therefore, the beneficial effect of imparting residual stresses in the fretted components was soon tested and recognized [22]. In some cases, an almost complete recovery of plain fatigue strength can be obtained [23] [22]. More recently, the achievement of a greater peening depth using the high pressure produced by an expanding plasma generated by laser illumination of a painted surface (see, for instance, [30]) has demonstrated substantial improvement over shot peening in plain fatigue. In many applications, the protection provided in the bulk of the material by residual stresses may be preferred to surface coatings, for simplicity, as the resistance of the coating may be harder to evaluate and predict. Treatments affectng the material itself, such as shot-peening,

ion implantation or heat treatments, have been the focus of the experimental part of this work.

In spite of the progress made to alleviate fretting fatigue, modeling-based palliative design is still in its early stage, due to lack of modeling for the phenomenon itself. The question of the principal relevant parameters in fretting fatigue, crucial to any modeling attempt, is not yet fully settled: surface condition, temperature, coefficient of friction, mechanical and hardening characteristics of the materials, contact geometry and loading and/or displacement parameters can usually be considered the most relevant. On the other hand, the phenomenology of the damage process is now well established, and illustrated on Figure 2-1. The propagation of fretting cracks in metallic materials may be divided in (at least) four stages:

1. stage I is the initiation stage, corresponding to the propagation of microstructurally short cracks over a length comparable to relevant microstructural features

2. stage II corresponds to the stable propagation of a physically short crack at some angle to the surface, under the influence of the contact (and the bulk) load, over a distance of a few grains. Closure effects need to be taken into account at this stage

3. stage III encompasses the stable propagation in mode I, driven by the bulk stress, of a physically long crack

4. stage IV is related to the catastrophic failure

In addition to the choice of relevant variables, a central problem for any modeling attempt is its capability to account for the main features of the phenomenon. Modeling should take into account the fact that (see [31] for a review):

1. fretting cracks develop in two stages, with an inward crack angle in stage I (see later for a definition of the stages of fretting crack propagation) that becomes steeper with increasing normal pressure

2. nucleation occurs earlier at higher normal pressure

3. fretting is not solely a crack nucleation controlled process

4. the effect of the stress created by normal pressure is mainly felt during crack initiation and early propagation in stage I

The main aim of any modeling attempt is of course to account for the main features mentioned above, as well as some other well established observations. For instance, early stages of crack growth are strongly influenced by the contact loads, as evidenced by the effect of the normal pressure on crack geometry for the case of a flat pad [31], by the effect of the contact loads on the number of cycles in stage I and II [21], or the absence of further propagation of crakcs initiated under fretting conditions when the pad is removed.

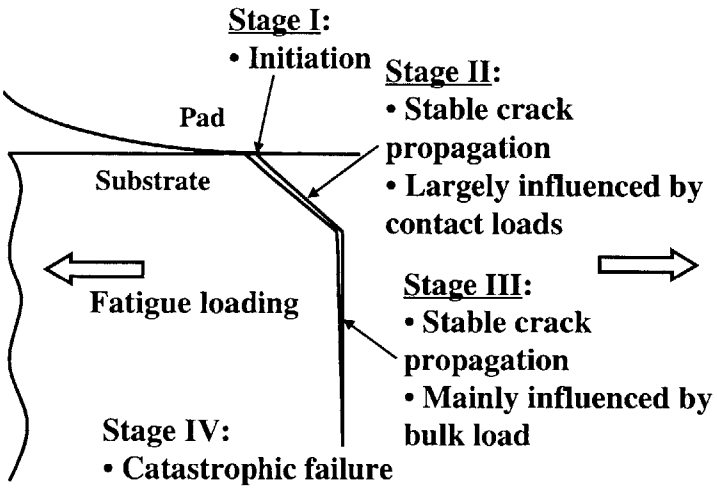

Figure 2-1: Schematic of the various stages of fretting fatigue crack growth

Consequently different modeling approaches might be used, one for the early stage, that should include the effect of normal pressure, geometry and short crack closure, and another for a later propagation stage, that should account for the effect of the fatigue stress, frequency and environment. Other experimental evidence may be used

in the evaluation of a model, notably the occurrence of fretting in the absence of bulk stress ([1] for static bulk stress, and [26] for pads' observations), and for non-metallic materials.

Another critical aspect of modeling, presented in the introduction, is the ability to estimate the number of cycles at which reliable fracture mechanics calculations can be started. Stress-based criteria are often awkwardly invoked for that purpose. A discussion of their limitations will be included in the subsequent review on modeling, which form the first part of this chapter.

2.2 Fretting modeling

The distinction between the various modeling approaches is essentially in stage I and II, as linear elastic fracture mechanics is usually used to calculate the portion of the life in stage III, and stage IV is neglected. The various attempts to model fretting (or rather fretting-induced fatigue in a stricter sense) can be roughly divided into three categories: the stress-based models, the fracture mechanics-based models, and the crack-analogue models. Most stress-based models are in essence limited to the prediction of the endurance limit, although attempts have been made to predict the number of cycles to a given length on the basis of stresses and strains only, to provide a starting length for fracture mechanics calculations. The fracture mechanics-based models try to apply fracture mechanics to short cracks of somewhat arbitrary length to model the whole life as a crack-propagation problems. An interesting modeling approach, at the crossroad of the two previous ones, relies on dislocation theory to predict such features as the initial crack angle and the number of cycles to failure in a somewhat unified way. A large section is devoted to the details of the novel approach developed by Giannakopoulos et al. [2][20], as it is at the root of the life prediction methodology developed in this investigation. The fundamentals of each approach will be presented, together with a few examples, and their performance with respect to the criteria mentioned above will be discussed.

2.2.1 Stress-based models

The models in this class rely on stress criteria to predict the location, and the initial orientation of cracks. A variety of stress-based criteria may be used in principle, provided they perform well for multi-axial, non-proportional loadings (a requirement that makes the pool of candidates not so large actually). These criteria usually have some physical basis: a combination of stress invariants or shear and normal stresses is used to account for the effect of shear and normal stress on the dislocation motion. Some combination of maximum shear stress or maximum shear stress amplitude and maximum normal stress is usually invoked in critical plane theories (for example in maximum shear or McDiarmid criteria). Of the various combinations offered by stress-invariant criteria, the Crossland and Dang Van criteria seem to be the most widely used to date in engineering against fatigue[1]. Alternatively, an energy-type of threshold may be postulated (as in the case of the Smith-Watson-Topper criterion). Various studies in plain fatigue ([32][33]) suggest that modified version of the Dang Van and Crossland criteria may best suited for fretting fatigue loading, although they were not developed for out-of-phase loading[2].

A comparative study by Wittkowsky et al. [34] shows that most of these criteria predict crack initiation in the slip zone (with a slight preference for the edge of contact) with the notable exception of the modified Smith-Watson-Topper criterion that clearly designate the edge of contact as the site of initiation. It is also important to note that two orthogonal directions of damage are predicted by the critical-plane criteria, while the modified SWT criterion considers cracking normal to the surface by definition. Therefore, the stress-based criteria fail to account for experimental observations on three points. The first one, relatively minor for engineering purposes, is that cracks may appear anywhere in the annular slip zone, and not necessarily at the edge of contact. As just noted, this deficiency is relatively minor, since the numerical variation of these criteria over the slip zone may be limited. Considering the

[1]The Dang Van criterion is strictly speaking of the critical plane type but has also been formulated in terms of stress invariants

[2]Papadopoulos et al. [32] have shown that phase does not affect the fatigue strength of hard materials, which may partly justify the use of such criteria

pointwise nature of theses criteria and their inability to deal with stress gradients, it is indeed unrealistic to strictly assign an initiation site only by numbers. A more global interpretation of the numerical prediction as an overall margin to crack initiation threshold seems more relevant, and suitable for engineering purposes. The second point of disagreement between criteria and observations is that only inward cracks (that is cracks propagating towards the center of the contact zone) have ever been observed. Although it is natural to simply eliminate the wrong direction, there is clearly a deficiency in the approach. A third weakness of the formulation is that it encompasses both the contact and bulk stress in the computation, whereas we have seen that initiation and initial propagation are expected to be primarily driven by the contact stress field.

Some other limitations appear when these criteria are used to actually predict fretting life, as can be seen in the work of Szolwinski and Farris [35][25]. In this case, the criteria are modified so that the equivalent stress is taken to indicate failure at a given number of cycles, instead of the endurance limit. Problems arise because of the pointwise nature of these criteria, when dealing with inhomogeneous stress fields. Practically, gradients induce pronounced variations of the numerical value of the criteria under the contact, so the natural tendency would be to take an average over a certain volume. Physically, such a procedure is meaningful too, because although the strain energy density that drives dislocation motion during initiation is a point quantity, it is truly the limit of a volumic quantity, and some volume of material is physically needed to define it[3]. But the volume of averaging can only be arbitrary, and, as noted by Couratin et al. [36] when comparing the fatigue strength for various loadings with criteria predictions, this may actually increase the scatter of the predictions. This averaging procedure amounts to arbitrarily specifying the length of the crack at the end of the initiation/nucleation stage, when used as a starter to a fracture mechanics calculation. Whether the stresses are averaged or not, obtaining relevant parameters for the criteria appears extremely difficult. When used to predict a num-

[3]The same is true for the stress, although it may be less intuitive due to its great familiarity as a point quantity

ber of cycles to initiation, the required parameters are usually derived from plain fatigue data. The procedure is meaningful only if the critical crack length used to fit the criterion parameters in the plain fatigue tests is similar to the length arbitrarily chosen as the length to initiation (which is not always the case when picking data from the literature). When the stress field is not uniform, another serious difficulty appear: part of the growth to the specified length will occur under the influence of a varying stress field. In order for the calibration test to capture the influence of the stress gradient, similarity should be insured between the calibration test and the intended application. If the stress gradient is due to geometric effects, similarity can be ensured by using the same geometry for the calibration test, which is not practical. For a contact problem, where the stress gradient is notoriously sharp and problem-dependent, the only way to capture the gradient effect is actually to perform a calibration test on the intended application. Of course, if the stress gradient is not sharp or the length to initiation small enough so that the effect of a gradient is minimal, this concern is alleviated and a classical calibration test under uniaxial uniform loading may yield useful information. Unfortunately, in the absence of a rigourous specification for the severity of the gradient and its influence on crack growth, it must be realized that one has actually not control on the accuracy of a stress criterion when used in a complex stress field. Attempts to include gradient effects in fatigue criteria, such as the work of Papadopoulos and Panoskaltsis [37], are limited to a constant gradient, so their ability to deal with fretting situations remains to be demonstrated. As emphasized by Bleuzen et al. in a comparative study of endurance limit prediction in multiaxial loadings [38], a good correlation in the absence of gradient consideration is a matter of luck, and they suggest that fracture mechanics be used as much as possible in this situation.

Another objection to the use of fatigue criteria is that they fail to predict the observed behavior in the case of normal fatigue. In the absence of tangential force, shear indeed is maximum on the axis of symmetry, at a depth of about half the contact radius. Therefore, initiation should take place at this location according to most shear-based criteria, whereas surface cracks are observed in practice. In the

case of fretting fatigue, this potential deficiency is commonly overcome by using the criteria at the surface only, which is a convenient but not a rigorous methodology.

Despite their limitations, stress-based endurance criteria are well-established in the engineering community, and relatively straightforward to use. For reference, four criteria used in fretting fatigue are briefly presented:

1. a modified version of the Crossland criterion, that coincide with the mesoscopic criterion of Papadopoulos [32]

2. a simple maximum shear amplitude criterion, that can be linked to the dislocation approach of Yamashita and Mura [1]

3. the Ruiz-Chen model, actually based on the density of frictional energy dissipated, as explained in [39]

4. another energy-based model, developed by Farris and coworkers [25] on the basis of a modified Smith-Watson-Topper criterion

The first one is truly an endurance criterion, the other two are rather indicators of severity that have been used to predict the location of damage, and the last one is a true finite life criterion. Another stress-based approach, using dislocation theory, will be discussed further in the following section devoted to fracture mechanics approaches, as it is included in a coherent fretting fatigue model that uses dislocations to explain both the initiation behavior in terms of stress and the propagation behavior in the framework of fracture mechanics.

2.2.2 Modified Crossland criterion

The well-known Crossland criterion, which postulates a dependence of the failure envelope on the J_2 amplitude and maximum hydrostatic pressure, can be modified to better account for the case of non-proportional biaxial loadings, by maximizing the stress amplitude with respect to the phase. The modification amounts to neglecting phase effect in the calculation of the stress invariant. The criterion then almost coincides with the mesoscopic criterion of Papadopoulos, and reads:

$$\frac{Max_{\Phi}\sqrt{J_{2,a}} + \alpha\sigma_{H,max}}{\beta} = 1 \tag{2.1}$$

where Φ is the phase.

The parameters α and β are defined from uniaxial tests as:

$$\alpha = \frac{3t_{-1}}{f_o} - \sqrt{3} = \frac{\sqrt{3}f_{-1}}{\sigma_f} \text{ and } \beta = t_{-1} \tag{2.2}$$

where:

- t_{-1} is the endurance limit in torsion
- f_o is the endurance limit in repeated bending
- f_{-1} is the endurance limit in fully reversed bending
- σ_f is the ultimate tensile strength of the material

For self-consistency, the model requires that $\frac{t_{-1}}{f_{-1}} = \frac{1}{\sqrt{3}}$. For the titanium alloy used by Conner [3] (Ti-6Al-4V STOA), some of the above values can be obtained from the literature ([12]):

- f_{-1}=779 MPa at 10^7 cycles
- f_o=488 MPa at 10^7 cycles

Note these are values for the exact same material and heat treatment used in the HCF program (but of course not necessarily from the same batch). Conner [3] showed that the criterion is fairly conservative for the sphere-on-flat configuration.

2.2.3 Maximum shear amplitude criterion

The criterion predicts the initiation of a crack on the planes where the shear amplitude is maximal during a cycle. It has been physically related to the motion of dislocations along such planes by Tanaka and Mura. Their model is closely linked to the concept of shear banding. A simple Mohr's circle diagram indicates that such

a criterion will predict two possible orthogonal planes. Various attempts have been made to try and justify why cracks develop only on one of these planes. The value of the traction normal to the plane is usually invoked. Although the arguments often make sense physically, they are absolutely never quantitative[4], and will not be discussed here (see Lamacq [1] for an extensive discussion of these approaches). Similarly, it must be emphasized that this approach is strictly limited to the prediction of the initiation angle, and cannot quantitatively predict a threshold condition: no validated model allows to link a critical shear amplitude for the occurrence of damage.

In principle, the non-proportionality of the contact loading requires a complete description of the loading path to determine the plane of maximum shear. The problem is further complicated by the asymmetry in the contact condition introduced in most fretting fatigue experiments by the use of the axial load to produce the relative displacement. However, in the case of the sphere-on-flat geometry, since the component of stress normal to the surface vanishes at the contact edge, there is a biaxial state of stress at this particular location. Consequently the maximum shear amplitude planes are necessarily oriented at 45° from the surface.

2.2.4 Ruiz-Chen criterion

This criterion relates the initiation of a crack to the frictional energy dissipated, in the simple form of the product of the surface shear traction τ and the relative tangential displacement δ. In order to account for the effect of in-plane stresses on the opening of cracks normal to the surface, the authors added the component of stress parallel to the free surface σ_t in the product. This version of the criterion reads:

$$\kappa_1 = (\sigma_t)_{max}(\tau\delta)_{max} \tag{2.3}$$

They also derived a different form using the maximum value of the product of the three parameters, for the case when the maximum tangential stress and frictional

[4]With the exception of the McDiarmid criterion

work don't occur at the same location, which as the form:

$$\kappa_2 = (\sigma_t \tau \delta)_{max} \tag{2.4}$$

In the non-dimensional form $\frac{\sigma\tau\delta E}{p_o^3(1-\nu^2)a}$ (a being classically the contact radius and p_o the mean normal pressure), it may be used only as an index of the severity of the contact, and hence an indicator of crack location. It suffers from the same limitation as the preceding criterion: in the absence of a theoretical threshold value associated with the index, it cannot be used to predict whether failure will actually occur. Lykins et al. [40] unsuccessfully looked for an empirical correlation between this parameter and the number of cycles to a given length.

2.2.5 Modified Smith-Watson-Topper criterion

This criterion, proposed by Farris and coworkers [25], is in essence a Smith-Watson-Topper criterion of the form:

$$\sigma_{max}\frac{\Delta\epsilon}{2} = \frac{{\sigma_{f'}}^2}{E}(2N_f)^{2b} + \sigma_{f'}\epsilon_{f'}(2N_f)^{b+c} \tag{2.5}$$

where σ_{max} is the maximum stress normal to the crack plane during a loading cycle, $\Delta\epsilon$ is the equivalent strain amplitude, and the coefficients and exponents on the right hand side are to be derived from low and high cycle fatigue tests.

The authors simplified the analysis by assuming a crack direction normal to the surface, neglecting the variation in the stress introduced by the asymmetric distribution of slip (after numerical estimation of its magnitude), and limiting the calculation to the edge of contact. In that case, the maximum traction simply becomes:

$$\sigma_{max} = 2p_o\sqrt{\frac{\mu Q}{P}} + \sigma_o \tag{2.6}$$

where p_o is the mean normal pressure due to the normal load P (equal to $(\frac{3P(1-\nu^2)^2}{2\pi^3E^2R^2})^{\frac{1}{3}}$ for a sphere of radius R on a flat surface), Q is the tangential load and σ_o is the

maximum applied bulk load.

The general applicability of neglecting the traction due to the slip distribution is not guaranteed. However, the normal load reported by the authors is very high compared to the tangential load ($\frac{Q}{P} \simeq 0.1\%$), so the approximation may well fit their particular experimental conditions. Another possible limitation is that the coefficients need to be generated by recording the number of cycles to the arbitrarily defined crack length in plain fatigue for the same geometry to obtain a good agreement. As in the case of Lykins et al. discussed in the next paragraph, if the contact conditions are not too severe, the agreement only means that a bulk-dominated crack propagation can be described using fatigue tests.

The remark certainly applies to the recent review by Lykins et al. [40] of some of these criteria, namely the SWT and Ruiz criteria, plus the Fatemie-Socie criterion and the maximum strain and maximum principal strain criteria. All criteria, but the κ_1 parameter predicted more or less the same location for crack initiation, which agreed with experimental observations. The maximum strain, maximum principal strain (both corrected for strain ratio effects) and SWT criteria also provided a good estimate of the number of cycles for initiation of a 380 μm crack for various loads and stress ratii. The number of cycles was not directly obtained experimentally, but calculated by subtracting from the total life an estimated propagation life, based on striation measurements. The conclusion of the authors was that fretting fatigue can be assessed exactly like fatigue, which is somewhat surprising, considering the amount of work devoted to understanding the peculiarities of fretting fatigue in the past three decades. Some points of their analysis worthy of further discussion are their definition of initiation, the accuracy of the procedure to estimate the number of cycles it takes, the size of the crack at initiation with respect to the size of the zone affected by the contact, and the relative magnitude of the contact stresses and the axial stress. It is not obvious from their published data whether their experimental data represent severe contact conditions, or if the failure is essentially dictated by the axial stress. Based on their published data, it appears for instance that the contribution of the contact to the axial stress at the trailing edge is at most one third, in contrast with

Conner's experiments [3] where this contribution is at least two third. This relates to the point made earlier that stress criteria work well if the stress distribution is similar in the problem of interest and the experiments from which the parameters where derived. It is interesting to note that the authors did fit the stress criteria for a length-to-initiation with specimens on the same geometry in plain fatigue. As pointed out earlier, it is the most accurate way to do it, but it also implies that in order to estimate the life of a component under fretting fatigue, a similar one has to be broken in plain fatigue.

In view of the above discussion, it appears that stress-based approaches require in principle and in effect the collecting of "ad-hoc" data (for a specific length and possibly geometry), which was not attempted in the course of this work.

2.2.6 Fracture mechanics-based models

Several researchers have indeed tried to assess the "initiation" stage using fracture mechanics only, meaning that they use only fracture-mechanics to predict the fretting-fatigue life. Usually, some specific crack geometry ([14],[41]) is assumed [5], and an initial crack size is postulated, although it is rarely clearly stated ([14],[15],[13],[41]). The mode II solicitation is neglected as discussed by Araújo and Nowell in [41], probably as much because it is not significant as because the constant variation of mode mixity throughout a cycle is very hard to deal with. When this methodology is applied to calculate an endurance limit, the assumption of an arbitrary initial crack length is unsatisfactory in principle, but not very harmful in practice. This crack-arrest methodology did not give very good results in the preliminary investigation by Araújo and Nowell, who used dislocations distributions to compute the stress intensity factor of cracks normal to the surface, and Kitagawa-Takahashi diagrams to predict crack arrest. Two different arrest criteria may in fact be written, due to the non-uniform stress field, one describing the short crack regime with a critical

[5] This simplification is not a prerequisite of the method, and, since the computational effort is usually significant, one might in fact as well look at realistic slant cracks instead of cracks normal to the surface

stess intensity factor amplitude and crack length, and the other with a critical stress intensity factor amplitude and stress amplitude. While the former is rather more legitimate from a mechanics point of view, the prediction of the latter seemed to match the experimental data better. As pointed out by the authors, improvement in short crack analysis may be needed to overcome this anomaly. The general trend of an increase in life with increasing pad size is nevertheless correctly captured. On the other hand, the work of Hattori and Nakamura [14] seems to compare rather well with experimental data. The analysis also involves pure mode I only, and invoke only a stress intensity factor amplitude threshold in the short crack regime of the form:

$$\Delta K_{th}(a) = \Delta K_{th}(a = \infty)\sqrt{\frac{a}{a + a_o}} \tag{2.7}$$

where a_o is a critical crack length derived from the long crack threshold with a simple $\Delta K = \Delta\sigma\sqrt{\pi a}$ relation. Their analysis predicts a strong influence of a superimposed mean stress on the fretting fatigue endurance.

These authors also tried to extent their methodology to fatigue life prediction, taking advantage of the singularity at the edge of contact in a flat-on-flat configuration to apply fracture mechanics concepts. For the case of a wedge in contact with an infinite half-plane, they compare the stress intensity factors at the edge of contact, obtained numerically, with a stress-based initiation criterion of their own in order to predict initiation, and proceed to analyze the propagation of very short cracks (typically 20 μm) in the singular stress field. For the geometry examined, for which the stress state at the edge of contact is singular, the predictions of the fretting fatigue strength agree well with experiments.

Dislocation-based models

These models are in essence based on the representation of crack displacement discontinuity by dislocations. The initiation of a crack is modeled by the motion of edge dislocations of opposite sign on two planes parallel and close to each other, as can be seen on Figure 2-2. The assumption is that a crack develops on the slip plane

on which the shear (Tanaka and Mura model) or shear amplitude (Yamashita and Mura model) is maximal, if the stress normal to the plane (taking into account the dislocation interaction) is large enough. A number of cycles to initiation is computed by comparing the stored strain energy to the energy needed to create new surfaces.

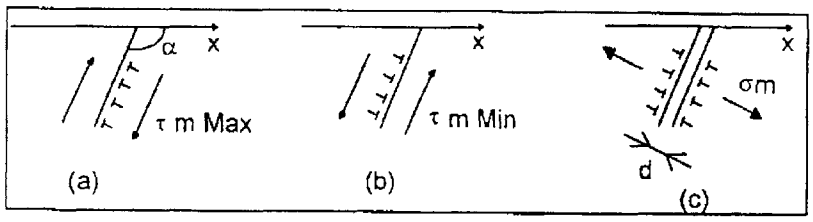

Figure 2-2: Representation of initial crack by two planes of dislocations, from Lamacq [1]

As explained by Lamacq [1], the formulation suffers from nearly the same inadequacies as the shear-based criteria, since they use essentially the same driving parameters: the representative volume for the computation of the strain energy has to be set arbitrarily, and two planes of initial propagation are predicted. Lamacq modified the Yamashita and Mura model to obtain two conditions for initial propagation, one governed by maximum shear amplitude (type I crack), and the other by maximum normal stress (type II crack). In the former case, the condition imposed to discard one of the two planes is the continuity of mechanism between initiation and early propagation: the mean normal stress is higher on the outward plane, which is supposed to favor a branching in mode I, whereas the initiation is driven by shear. The advantage of this modification is that it correlates well with the observations of two planes of initial cracking, at a shallow and steep angle, made by the author on aluminum alloys. But the prediction of the site of initiation is not very satisfactory, so the initiation criteria are finally interpreted in a loose sense: a "high" value of either criterion indicates a "high" probability of initiation. For lack of quantification, this assertion actually amounts to not considering too strictly the prediction of criteria that have not been designed to account for gradient effects, as discussed about the work of Wittkowsky et al. A large outer region of the slip plane is then predicted

to be a zone of initiation, but, on the other hand, type I cracks become very likely to appear outside the contact zone (which is not contradictory to observations: only the probability of occurrence is an issue here). Although some fundamental questions, such as the crack location and number of cycles to initiation lack satisfactory answers, this approach showed a rather correct agreement with the data presented in [1].Especially, the loose interpretation of the criteria (which might nonetheless gain to be formally stated in a probabilistic manner) allows to model the phenomenon of multiple cracking.

Following the idea of Keer and Bryant, Lamacq et al. [16][42] model the displacement field at the lips of a crack by a continuous distribution of dislocations to treat the propagation problem. The propagation of several cracks, inclined or normal to the surface, can be modeled, including their interaction, using an influence function approach. The superposition of the interaction stress field and the contact stress field for the uncracked body (obtained analytically or numerically, depending on the contact geometry), with appropriate boundary conditions at crack interfaces, allows the calculation of the displacement and stress fields along the crack faces. Stress intensity factors can then be obtained, reflecting the influence of both the loading and the interactions between cracks. The stress intensity factors can be significantly altered by the latter, depending on the distance between cracks, the relative position with respect to the loading zone, the interfacial friction coefficient and the loading mode. With a suitable Paris-type of propagation law, the propagation of each crack can be assessed for a given loading history.

This model for the first time accounts for the multiple cracking reported in fretting [1], and the effect of crack interaction on the propagation of the critical crack(s) that will lead to failure, and the conclusions are on the whole quite satisfactory. But, as the implementation by Dubourg and Lamacq [16] shows, there are a number of limitations: it is not clear whether the contact and interaction fields alone would be able to account for the propagation in the absence of bulk stress, and although the mathematical description of crack face displacements in term of dislocation distribution can be applied to any material, it is physically meaningful only in the case of

metallic materials.

2.2.7 Crack-analogue models

The approach proposed by Giannakopoulos, Lindley and Suresh [2] is based on the asymptotic identity between the contact stress field and the stress field at the tip on an appropriate cracked geometry, under certain conditions that will be developed below. Once the identity is established, considering the relatively large size of the K-dominance zone (about 20% of the contact radius on each edge) and the probable limited distorsion of the contact stress field due to the propagating crack (see Figure 2-4), the problem of the propagation of the fretting crack becomes the problem of propagation of preexisting crack under mixed-mode loading, which can be more conveniently treated using known results of linear elastic fracture mechanics. The analogy is illustrated by Figure 2-3, where the corresponding parameters are given.

The geometries investigated so far are the case of a flat punch with generatrices normal to an infinite half-plane (not necessarily cylindrical) [2], and of a rounded punch on an infinite half-plane [20]. In the former case, the square root singularity at the edge of contact is inherent to the contact solutions of Sadowski and Nadai. In the latter case, adhesion has to be invoked to recover the singular stress field. Briefly speaking, adhesion is due to the decrease of energy consecutive to the increase of the contact area between two bodies. Physically, the origin of adhesion is to be sought in the unbalance of bonding energy of the atoms at the surface of a solid body compared to the ones in the interior. The situation where the surface is increased to bond with atoms on the surface on the contacting surface is energetically more favorable than keeping the unbalanced bonding to the atoms beneath the surface. In other words, the surface energy of the separated surfaces is greater than the interface energy of the contacting surfaces. An illustration of the phenomenon is the case of a droplet on a solid surface: it will neither remain spherical, nor usually expand into a thin layer, but rather assume an hemispherical-cap shape to maximize the work of adhesion. In the case of a rounded contact, the effect of adhesion is to both to increase the area of contact compared to the geometrical solution given by Hertz, and to create a

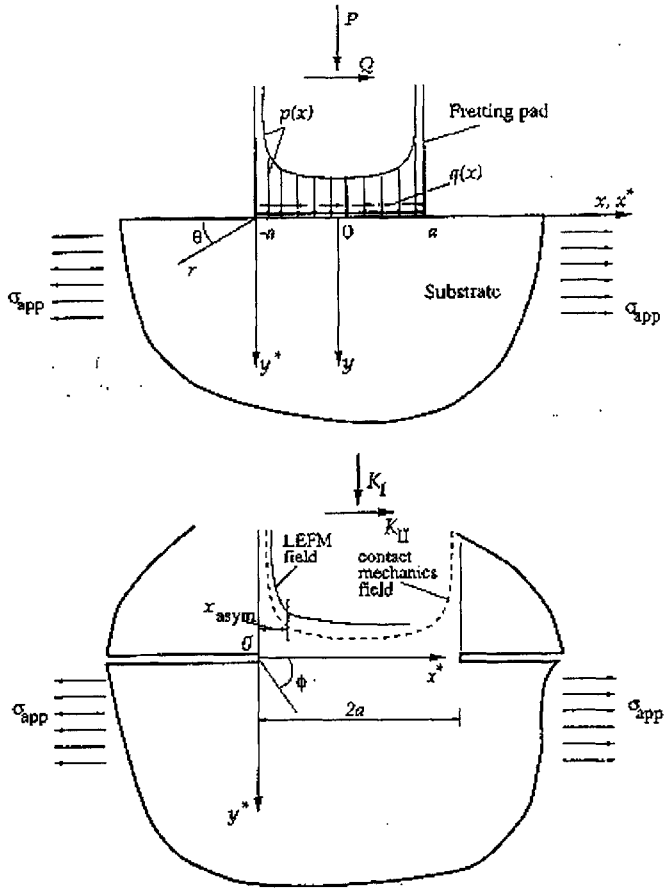

Figure 2-3: Flat punch on an infinite half-plane and the crack analogue, from Giannakopoulos et al. [2]

square-root singular stress field at the edge of contact.

The remarkable result is that in both cases, the stress field at the edge of contact is asymptotically identical to the stress field at the tip of the crack in a circularly cracked in a rod of inner diameter equal to the diameter of the contact zone. As a result, a natural length is introduced in the problem for the computation of the stress intensity factors, which contrasts with the arbitrary length scale invoked in the other models. Another unique feature is the prediction of a single, definite, inward initial propagation angle, that correlates fairly well with observations in the case of the flat punch [2]. Also, contrary to other models, a definite location is assigned to the initial crack, that may be either at the edge of contact or at the stick-slip zone

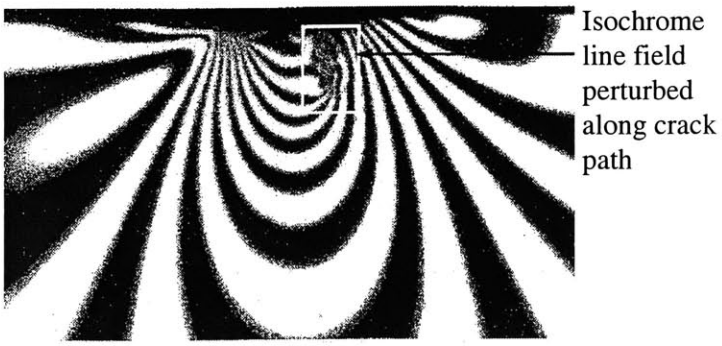

Figure 2-4: Photoelasticimetry visualization of the distorsion of the contact field by a crack in PSM 5 polymer, for a normal load of 200 N and a tangential load of 90 N, from Lamacq [1]

boundary depending on the adhesion conditions. This clearcut answer to a problem loosely treated elsewhere may be a limitation of the model, since it excludes multiple cracking, or cracking outside the contact zone. Yet if the behavior of the critical crack (the one leading to failure) is to be captured, this would not be a problem. Finally, it is worth noting that this analysis rationalizes the different crack angles observed for different static and cyclic loadings, as demonstrated in [2]. For instance, in the case of normal fatigue, the maximum shear stress amplitude occurs in depth, so subsurface initiation would be expected from a stress analysis, whereas surface cracks are observed in practice. This shortcoming is easily overlooked because most fretting investigations involve cyclic tangential loading, and this illustrates the benefit of trying to apply models in various contexts to get some sense of their fundamental capabilities.

A thorough overview of the methodology is now given, although the interested reader is referred to [2][20]. The origin of the model can be traced back to both the elastic contact solution of a flat punch on a flat substrate by Sadowski in the 1930's,

and the Johnson-Kendall-Roberts theory of adhesive hertzian contact [43]. The latter incorporates the effect of surface energy in the formulation of the Hertz problem. The influence of a tangential traction was introduced by Savkoor and Briggs [44], and, although the analogy between the adhesive theory of contact and fracture mechanics had been more or less pointed out earlier, it was formally established by Barquins and Maugis [45]. Surprisingly the strength of the approach and its application to contact problems was not realized until the work of Giannakopoulos, Lindley and Suresh [2] for the case of a flat punch, and the comprehensive theory of contact fatigue by Giannakopoulos et al. [20].

In both cases, the authors have taken advantage of the asymptotic identity between the stress distribution at the edge of contact and the stress field at the tip of a circumferentially cracked specimen. In the case of a round pad on a flat surface that is of particular interest to us[6], they use the contact radius corrected for the effect of adhesion:

$$a_{max} = \left[\frac{3D(1-\nu^2)}{4E}\left(P_{max} + \frac{3\pi D}{2} + \sqrt{3\pi D w P_{max}} + \left(\frac{3\pi D w}{2}\right)^2\right)\right]^{\frac{1}{3}} \tag{2.8}$$

where D is the pad radius, and w the work of adhesion between the contacting solids (usually approximated to 1 $\frac{\mathrm{N}}{\mathrm{m}}$ for all metals), and $\mathrm{P_{max}}$ is the maximum normal load.

An equivalent load $\mathrm{P_{max}}^*$ is defined as the one that gives the same contact radius in Hertz theory:

$$P^*_{max} = \frac{4Ea^3_{max}}{3(1-\nu^2)D} \tag{2.9}$$

The stress field developed at the edge of contact under the influence of a normal load $\mathrm{P_{max}}$ and a tangential load $\mathrm{Q_{max}}$ is asymptotically in the form of a crack tip stress field:

$$\sigma_{rr} = \frac{K_I}{\sqrt{2\pi\rho}}\cos\frac{\theta}{2}(1-\sin\frac{\theta}{2}\sin\frac{3\theta}{2}) + \frac{K_{II}}{\sqrt{2\pi\rho}}(-\sin\frac{\theta}{2})(2+\cos\frac{\theta}{2}\cos\frac{3\theta}{2}) \tag{2.10}$$

[6]Note that the stress field for a flat punch and a rounded punch are actually the same; only the derivation of the stress field and the discussion of strong vs. weak adhesion is particularized

$$\sigma_{zz} = \frac{K_I}{\sqrt{2\pi\rho}} \cos\frac{\theta}{2}(1 + \sin\frac{\theta}{2}\sin\frac{3\theta}{2}) + \frac{K_{II}}{\sqrt{2\pi\rho}} \sin\frac{\theta}{2}\cos\frac{\theta}{2}\sin\frac{3\theta}{2} \quad (2.11)$$

$$\sigma_{rz} = \frac{K_I}{\sqrt{2\pi\rho}} \cos\frac{\theta}{2}(sin\frac{\theta}{2}\cos\frac{3\theta}{2}) + \frac{K_{II}}{\sqrt{2\pi\rho}} \cos\frac{\theta}{2}(1 - \sin\frac{\theta}{2}\sin\frac{3\theta}{2}) \quad (2.12)$$

where ρ and θ are local polar coordinates at the contact edge.

The stress intensity factors for mode I and mode II are respectively:

$$K_I = \frac{P^* - P_{max}}{2a_{max}\sqrt{\pi a_{max}}} \quad (2.13)$$

$$K_{II} = \frac{Q_{max}}{2a_{max}\sqrt{\pi a_{max}}} \quad (2.14)$$

Under cyclic tangential loading, the stress intensity factor amplitude depends on whether the tangential force exceeds the force that can be sustained by adhesion, which is:

$$\bar{Q}_{max} = 2\sqrt{\frac{2-2\nu}{2-\nu}\pi a_{max}^3 \left[G_d^{II}\frac{E}{1-\nu^2} - \left(\frac{3G_d^I\pi D}{4a_{max}^{\frac{3}{2}}}\right)^2\right]} \quad (2.15)$$

where G_d^I and G_d^{II} are the critical debonding energies under a normal and tangential load respectively. As for the work of adhesion, which represents the same quantity for advancing rather than receding contact, these values lack precise measurement. A correlation with friction was derived by McFarlane and Tabor:

$$G_d = 14.3651\sqrt{0.3 + \mu^2} \text{ (units of } \frac{N}{m}) \quad (2.16)$$

where μ is the coefficient of friction.

If the tangential load Q_{max} is less than or equal to $\bar{Q}_{max}$, adhesion over the maximum contact radius a_{max} can overcome it. In this case named strong adhesion by the authors, a crack is predicted to appear at the edge of contact, whose stress intensity factor amplitude is:

$$\Delta K_{II} = \frac{Q_{max}}{a_{max}\sqrt{\pi a_{max}}} \quad (2.17)$$

On the other hand, if Q_{max} is larger than $\bar{Q}_{max}$, the material debonds at the edge of contact, and the tangential force sustained in the stick zone is the driving force for

propagation of a crack at the edge of stick-slip. The tangential force balanced in the stick zone is:

$$Q_{max}^{stick} = Q_{max} - \mu \frac{P_{max}}{a_{max}^3} \left(a_{max}^2 - c^2\right)^{\frac{3}{2}} \tag{2.18}$$

where c is the size of the stick zone, determined by Mindlin [46] to be:

$$c = a_{max} \left(1 - \frac{Q_{max}}{\mu P_{max}}\right)^{\frac{1}{3}} \tag{2.19}$$

The stress intensity factor amplitude in this so-called weak adhesion case is:

$$\Delta K_{II} = 2 \times \left(\frac{Q_{max}^{stick}}{2c\sqrt{\pi c}}, \sqrt{\frac{G_d^{II} E}{1-\nu^2}}\right) \tag{2.20}$$

It should be noted that in this case, the load ratio becomes R=-1, whatever the actual tangential loading cycle. Compared to the models presented before, this so-called crack-analogue methodology presents the advantage of clearly defining the crack angle and the crack location, and to allow the use of fracture mechanics concepts at a very early stage in the crack life. In principle, fracture mechanics may be used to describe the entire life of the crack. However, some simplifying assumptions may have a bearing on the accuracy of the methodology suggested in [2], particularly:

- the use of a criterion for the initial kinking that does not take into account the non-proportionality of K_I and K_{II} (see Section 2.2.8)
- the use of a single stress intensity factor to describe the stress field in stage I-II
- the use of a single stress intensity factor throughout stage I-II
- the use of a single crack propagation law for all stages

These assumptions will be discussed further in the following section. The model presented in Section 4.2.1 is essentially a somewhat more rigorous implementation of the representation of fretting fatigue as a pure propagation problem.

2.2.8 Deflection criteria

Whether derived in a "classical" or analogue context, one of the first use of stress intensity factors is to try and predict the crack path [42][2]. A variety of criteria have been proposed, mostly in the context of uniaxial or proportional loading. The review by Khan and Khraisheh [47] of the predictions for various loading configurations of the maximum tensile stress (MTS) criterion, the maximum stress triaxiality criterion, the minimum strain energy density (S) criterion, and variants of the MTS and S criteria show that none is able to fit all experimental data, which incidentally are scarce. Moreover, the limited set of data available appears not to be very discriminatory. For the particular case of combined tension and shear of interest in fretting, which happens to be discriminatory, no experimental observations are reported in this review. When applied to fretting fatigue, the use of deflection criteria is made even more hazardous by the non proportional stress state for two reasons, as explained in [42]. One is that, from limited experimental data, there may be a dependence of the direction of propagation on the phase, or alternatively on a combination of stress intensity factors amplitude and maximum value, which are not included in the criteria cited above. Another difficulty comes from the fact that, under such conditions, the direction predicted by the classical criteria is varying during a loading cycle. A direction can be singled out either by maximizing one of the above criteria over a load cycle (since they are in the form of an optimization problem), or using another criterion to determine the point of the cycle when the crack advances. Alternatively, Hourlier and Pineau have proposed to select the step of the load cycle and direction that maximize the crack growth rate. In any case, there aren't enough experimental and theoretical study to favor any approach.

The life prediction methodology outlined by Giannakopoulos et al. [2] uses the MTS criterion to predict the initial angle of propagation under a static mode I-alternating mode II condition. For the sphere on flat geometry, the problem of non-proportionality is circumvented by neglecting the effect of the static mode I, which

yields a theoretical angle close to 70.5° for any loading condition[7]. This assumption is specific to this geometry and was not made by the authors for the flat punch [2]. In that case, the contribution of the mode I is significant, as suggested by the observation of Hoeppner et al. [31] of steeper initial crack angle with increasing normal pressure. Note, however, that the simplification is compatible with observations by Kitagawa et al. [48] on slant cracks under biaxial stress in cross-shape specimens, who advocate an entirely different use of the criterion by using stress intensity factor amplitudes instead of magnitude. As will be seen in Section 4.2.1, the distinction is secondary for the sphere-on-flat geometry. The local stress intensity factors at the tip of an infinitesimally kinked crack are given by:

$$k_1 = a_{11}(\Phi)K_I + a_{12}(\Phi)K_{II} \tag{2.21}$$

$$k_2 = a_{21}(\Phi)K_I + a_{22}(\Phi)K_{II} \tag{2.22}$$

where Φ is the angular coordinate in polar coordinates at the tip of the unkinked crack and:

$$a_{11}(\Phi) = \frac{1}{4}\left(3\cos\frac{\Phi}{2} + \cos\frac{3\Phi}{2}\right) \tag{2.23}$$

$$a_{12}(\Phi) = -\frac{3}{4}\left(\sin\frac{\Phi}{2} + \sin\frac{3\Phi}{2}\right) \tag{2.24}$$

$$a_{21}(\Phi) = \frac{1}{4}\left(\sin\frac{\Phi}{2} + \sin\frac{3\Phi}{2}\right) \tag{2.25}$$

$$a_{22}(\Phi) = \frac{1}{4}\left(\cos\frac{\Phi}{2} + 3\cos\frac{3\Phi}{2}\right) \tag{2.26}$$

A contribution of the normal load via K_I is thus expected using any of the methods described previously to predict deflection.

On the other hand, under a fixed normal load and cyclic tangential load, the local mode I stress intensity factor fluctuates due to mode II variations only, and provides

[7]Note that for the case of weak adhesion, the mode I contribution truly vanishes

the driving force for crack advance. If Φ_{in} represents the initial crack angle:

$$\Delta k_1 = \pm\frac{3}{4}K_{II|max}\left(\sin\frac{\Phi_{in}}{2} + \sin\frac{3\Phi_{in}}{2}\right) \tag{2.27}$$

Whatever the deflection criterion, an important feature of the initial angle computed in the analogue framework is that it depends exclusively on the adhesion-induced singularity, and not at all by any bulk or residual stresses. This is strongly supported by the observations by Lamacq et al. [42] of crack propagating at the same angle in a specimen subjected to a constant axial load and in the pads, submitted to the contact load only.

In the model described in [2], the crack is predicted to propagate at a constant angle Φ_{in} and then turn in a direction normal to the remote loading when the stress intensity factor for a doubly kinked crack exceeds the local Δk_1 stress intensity factor. The two-angle path is in good agreement with experimental observations[8]. The propagation before the turning point is the so-called stage I-II, whereas the propagation in mode I after the turning point is denominated stage III by the authors. The methodology assumes that the local mode I stress intensity factor Δk_1 in stage I-II is constant, so the number of cycles in stage I-II is easily calculated using some Paris-law to describe the crack advance per cycle. After the crack bifurcates, standard stress intensity factor solutions may be used to compute the life in stage III. The final failure, corresponding to the so-called stage IV, is considered to occur very suddenly, and does not enter the life calculation.

[8]In reality, it seems that the crack angle gradually changes from the initial angle to the final 90^o angle, but the idealization introduced by the model seems quite legitimate to start with

Chapter 3

Experimental work

This section contains information relative to the experimental testing performed during the study, starting with the characteristics of the base material and the test apparatus. Three different kinds of potential fretting palliatives were investigated: ion-glazing, heat treatment and shot-peening. Characteristics of the untreated material and the experimental set-up are given here before a review on shot peening, which introduces the work on shot peened specimens. The results for the ion glazing and heat treatments, which relate less directly to the modeling discussed in Section 4, are given in Appendix A and B.

3.1 Experimental set-up and material description

3.1.1 Experimental apparatus

A complete description of the fretting set-up is given in [49]. The schematic of the authors is reproduced on Figure 3-1. The apparatus is composed of an Instron fatigue machine, on which specially designed pad supports have been added. The strength of the apparatus lies in the adjustable points of support on the side, which, combined with load trains of different compliance, allow to change the value of the tangential load for a given bulk load, and in the monitoring of the normal load and the tangential load (and possibly the relative displacement between the specimen and

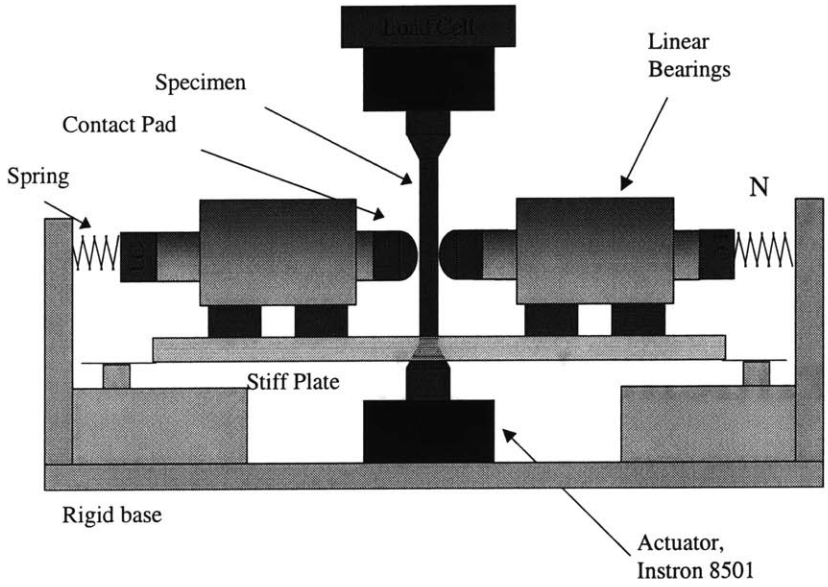

Figure 3-1: Schematic of the fretting set-up, showing the various adjustment and measurement capabilities, from Conner [3]

the pads). A variety of loading conditions may be investigated with optimal control of the loading parameters.

3.1.2 Material description

The material used for this investigation is titanium alloy Ti-6Al-4V in the solution-treated and 5 (STOA) condition. After forging, the material was solution-treated at 925°C for 1 hour, and vacuum annealed at 700°C for 2 hours for stabilization. The treatment results in a bimodal microstructure (approximately 60 vol% of primary α and 40 vol% of lamellar colonies of $\alpha + \beta$).The details on composition, treatments and material characteristics, taken from [50] and material data sheets, are reported in Table 3.1 and Table 3.2.

The specimen and pad geometries are identical to those reported by Conner [3]. The size of the square section of the specimen is about 4.76 mm, with a useful gauge length of 50.8 mm (see Figure 3-2). Only 12.7 mm radius pads were used in this

Al	V	Fe	O	N
6.3	4.17	0.19	0.19	0.13

Table 3.1: Percentage weight of alloying elements in the Ti-6Al-4V alloy used in the study

Tensile strength (MPa)	Yield strength (MPa)	Young's Modulus (GPa)	$\Delta K_{threshold}$ estimate (MPa$\sqrt{m}$)
1025	960	116	2

Table 3.2: Mechanical properties of the Ti-6Al-4V alloy used in the study

study.

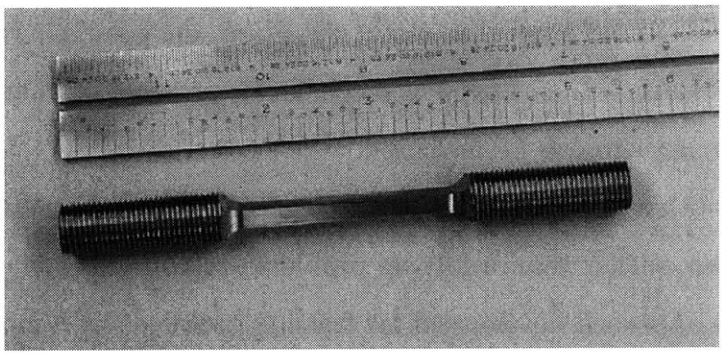

Figure 3-2: Specimen used for fretting fatigue experiments, from Conner [3]

3.2 Influence of shot peening on fretting fatigue resistance

This section provides a brief overview of the shot peening process, and its effect on fretting fatigue resistance. The rationale for and physical effects of the process are discussed to help understand its benefits and limitations, and familiarize the reader with the technique before presenting experimental results on shot peened Ti-6Al-4V in the next chapter.

3.2.1 Principles of surface design

The idea behind most surface treatments suggested for fretted components draws on the extensive experience in design against pure fatigue: in this case, fatigue damage is created by slip at the surface. Any surface modification that tends to prevent slip by pinning dislocations may enhance fatigue strength. If fretting fatigue is thought of as a fatigue process under a peculiar stress condition, the principle remains valid. As summarized in Figure 3-3, a variety of mechanical, physical or chemical tretaments that aim at reducing slip can be proposed.

Obvioulsy, another way to tackle the problem of fretting fatigue is to think of it as a contact problem, rather than a fatigue problem. In this case, as demonstrated by the fretting map approach developped for fretting problems by Vincent and coworkers [51], or the stress-based approach of Chivers and Gordelier [27], friction becomes a key parameter, and partial slip condition must be avoided to increase the resistance against fretting. Coatings or change in the surface composition are typically recommended by this approach.

A third way to design against fretting fatigue is to consider it as a crack-propagation process. The crack-analog model and experimental evidence of early crack nucleation in fretting fatigue support this approach. The good results obtained by shot peening also give a large credit to this stategy, since the improvement is attributed mainly to the closure effect of the residual stresses. Interestingly, although most of the treat-

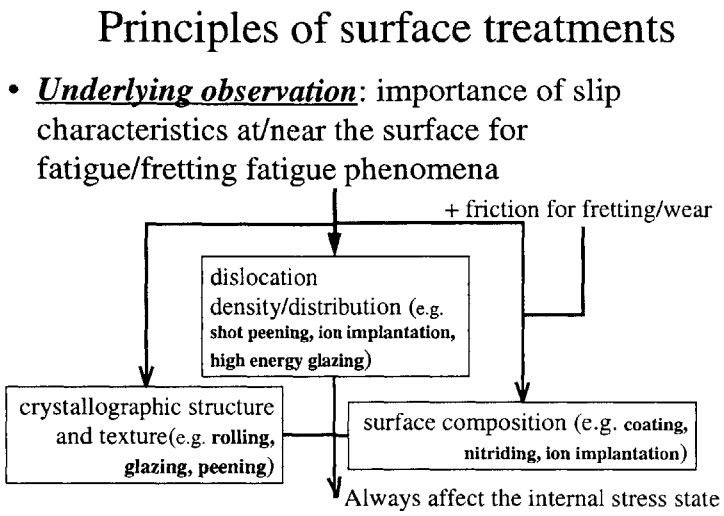

Figure 3-3: A summary chart of the design approach against shot peening and their justification

ments devised by following the first two design methodologies also generate residual stresses which are often invoked to explain the results (see [52] for a discussion of ion implantation, or [53] for a discussion on coatings), the idea of designing against propagation (by modifying the toughness or the microstructural characteristics close to the surface for instance) is seldom emphasized or aggressively pursued.

3.2.2 Shot peening: influence on material's properties in relation to fretting fatigue

Influence of materials characteristics on fatigue and fretting fatigue properties

For alloys of medium hardness ($300 \leq HV \leq 600$), fatigue and fretting fatigue resistance depend primarily on five parameters: microstructure, surface roughness, hardening, residual stresses and loading characteristics. The influence of microstructure will not be discussed here (few studies have been devoted to the subject, see [54] for

a discussion of the influence of microstructural features on crack path in aluminum, or [55] for consideration of possible microstructural changes in titanium alloys). The effect of most other parameters can be analyzed from Figure 3-4. A brief description of the parameters will be presented before a more detailed discussion of two particular processes used to enhance fatigue properties, namely shot peening and laser shock peening. The later was not directly investigated for this report but is given for completeness. As often as possible, results will be particularized for titanium alloys.

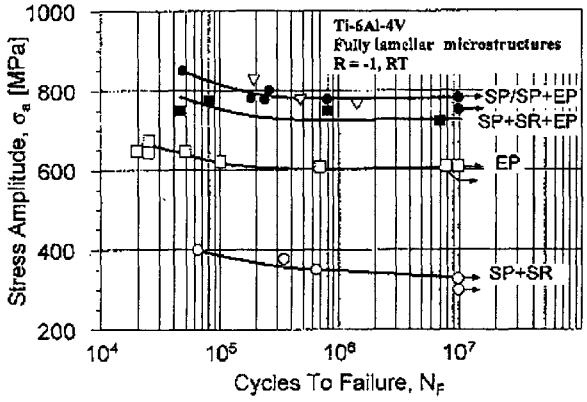

Figure 3-4: Effects on various surface conditions on fatigue strength: SP refers to shot-peening, MP to mechanical polishing, EP to electropolishing and SR to thermal stress relieving treatment, from Wagner [4]

Surface roughness has a negative effect on plain fatigue resistance [56][4], because surface microcracks nucleate more easily on a rough surface. Contradictory evaluations of the same parameter can be found in the case of fretting fatigue: it is can be found that cracks initiate more easily on rough surfaces([23] on steel, or [57] on titanium), but it is more often reported that a rough surface increases the life of fretted components (see the extensive work of Waterhouse [22],[5],[58],[59]). Typical results are shown in Figure 3-5. This is attributed either to the smaller area affected by contact, and hence the scarcer number of initiation site [22], or to the shielding effect of the resilience of the "peaks" on a rough surface [60][61].

Work hardening has no clear cut effect on plain fatigue life. A high number of dislocations makes crack nucleation more difficult, and is usually highly beneficial if

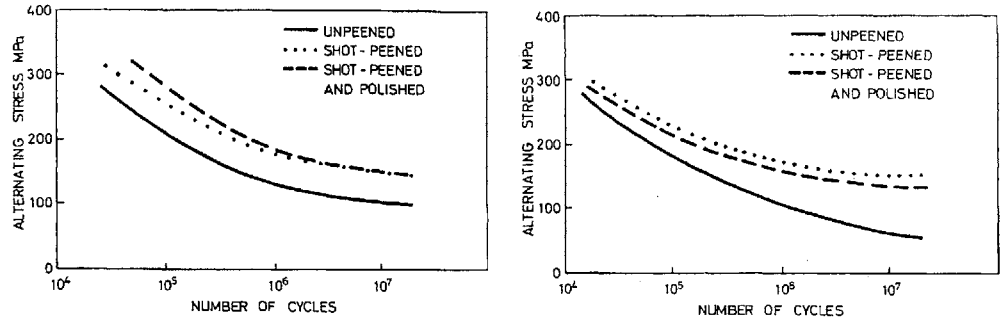

Figure 3-5: Effect of surface roughness on the fretting fatigue resistance of 2014A aluminum, naturally aged (top) and artificially aged (bottom) from Waterhouse [5]

the time to failure is crack-nucleation dependent, as can be from Figure 3-4. Yet cracks tend to propagate more easily in dense dislocation fields, and a hardened material may be very susceptible to fatigue if a crack is present before the load is applied [56], that is if the evolution is crack-propagation controlled.

Compressive residual stresses usually prove beneficial for test pieces or parts in plain fatigue [4][62][28][63]. The decrease of crack growth rate induced by the shielding effect of compressive stresses results in an increased life, provided the time to failure is crack propagation-controlled [56]. However, adverse effects after introduction of residual stresses have also been reported [64][65], and this can be rationalized by observing that crack nucleation may occur beneath the surface in plain fatigue, particularly for positive R ratio in tension tests [66][67]. Since compressive residual stresses in some parts of a sample must be counterbalanced by tensile ones in others to ensure global equilibrium, it may happen that the crack nucleate in a region of tensile stresses, which can both accelerate nucleation and increase the crack growth rate. Shot peening may even increase the depth of crack nucleation, which annihilate the beneficial effects of compressive residual stresses. In other words, the expected influence of compressive residual stresses can only be assessed together with the depth of initiation: the greater the time spent by the crack in the compressive stress field, the greater the enhancement of fatigue strength. In this regard, notched specimens, on which cracks initiate at the surface, may benefit from peening more than smooth

ones with subsurface crack nucleation [65].

The S-N curve is finally influenced by the type of loading. Some titanium alloys, such as TIMETAL 1100 for instance, are very sensitive to stress gradient. This is also the case for Ti-6Al-4V [65], which is 100% fatigue notch sensitive. In any case, the effect of stress gradient is largely related to nucleation site: if cracks initiate at subsurface locations, the lower due to stress gradient for a given maximum amplitude will result in a significantly improved strength. An important feature of Ti-6Al-4V is the dependence of the fatigue behavior on the R-ratio in two separate ways: a shifting of crack nucleation to subsurface for $R \geq 0$ in axial loading, and an anomalous dependence of fatigue resistance on mean stress for material forged in the $(\alpha+\beta)$ phase [56][66][67].

Enough has been said to suggest that a process that would induce compressive stresses and a high dislocation density at some depth below the surface of a cyclically loaded component could significantly enhance its fatigue and fretting fatigue capabilities. The most common of these processes are mechanical treatments such as cold-rolling or shot peening. These methods also affect surface roughness, which may partially or totally overcome the expected benefit in fatigue, but is helpful in fretting. On the other hand, the use of laser shock peening allows residual stresses to be introduced without much affecting the surface condition or the microstructure, which can both be an asset in fatigue (although the greater depth of treatment (see below) may easily counterbalance the issue of surface roughness in fretting), and a convenient mean to decouple the effects of the various parameters in the lab.

3.2.3 Shot peening

Mechanisms of residual stress creation

As described by Wohlfhart [6], two mechanisms related to local plastification are responsible for the occurrence of residual stresses. The first one is due to the compression of the surface layer under local pressure. This tends to stretch the surface layer, and therefore expand it radially, but it is confined by the surrounding elastic

material: the mismatch results in compressive tangential and radial residual stresses being developed. The magnitude of the residual stress field decreases from the (most stretched) surface to the (less stretched) core. The second mechanism is due to the Hertzian stress field that develops when a shot piece impacts the material. Similarly, local plastification occurs when the flow stress is exceeded, but the maximum equivalent stress now occurs below the surface (at a depth which is function of the contact pressure, see [68]). Consequently, the maximum amplitude of the residual stress field is located below the surface. These mechanisms are illustrated on Figure 3-6.

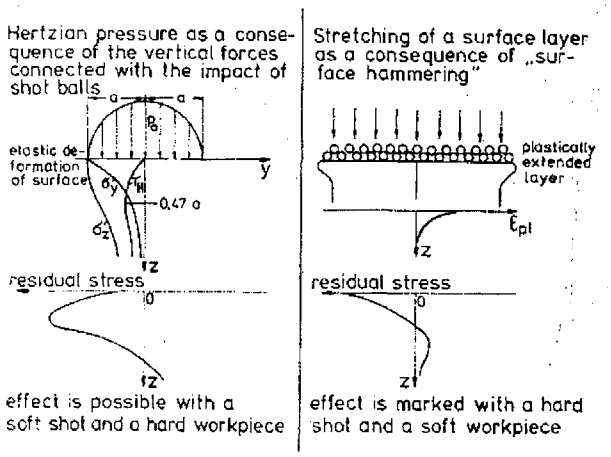

Figure 3-6: Illustration of the two competing mechanisms responsible for shot peening residual stresses, as given by Wohlfhart [6]

The relative importance of both mechanism depends mainly on the ratio of the shot hardness to the material hardness, the shot size and energy [6][28]. For usual steel shot (45 to 55 HR_c), this generally means that "soft" materials (HV$\leq$300) will have a decreasing stress profile, whereas "hard" materials (HV$\geq$600) will develop large maximum residual stresses below the surface.

Our material, with its medium hardness (365-370 HV reported by Broichhausen and Calles [64] and extrapolated from [69]), falls in the category of materials that can exhibit both types of residual stress profiles [70][29][64][71] [1]. In general, it seems that usual parameters lead to in-depth maximum stress. It is worth mentioning that

[1] It is, however, not clear whether some decreasing profiles are not due to lack of resolution

an untreated component should not be regarded as residual stress free, as opposed to a "stress full" peened component. Any mechanical process may induce residual stress in a component. Surface compressive stresses of 450 MPa can be induced by a rough mechanical polishing [56]. Some implications on crack observation will be mentioned in Section 4.2.5.

Material and process parameters affecting residual stress profiles

The parameters influencing the residual stress profile obtained by shot peening (and laser shock peening to a great extent) in a particular component can be grouped in three categories [72]:

1. component parameters, which include both material parameters and the geometry. The extensive work on the process modeling by Castex and coworkers tends to indicate that parameters describing both the monotonic and cyclic elastoplastic behavior are needed to understand the process

2. shot parameters: this covers both materials parameters such as the shape, size, and hardness hardness of the shot, and variables describing the energy of the shot flow, such as the velocity of the shot, the angle of impingement, or the duration of treatment

3. contact parameters, namely the coefficient of friction and the ratio of the hardnesses of the materials

The maximum stress achievable with shot peening is primarily a function of the hardening characteristics of the material. As a rule of thumb, the maximum stress is approximately two third of the yield strength of the hardened material, and the surface stress one half the yield strength of the hardened material [73]. The coverage, which is the percentage of the surface that has actually been shot, as a similar effect on maximum stress, since hardening increases with coverage. Increasing the Almen intensity, defined as the stabilized curvature of standard SAE 1070 spring steel specimens, slightly increases maximum stress, except for ceramic shot, that exhibit an

adverse effect [62]. A maximum stress in the range of 800-900 MPa seems to be a good practical limit for titanium alloys.

On the other hand, the maximum depth, i.e. the depth at which residual stresses turn from compressive to tensile, is a function of the shot size, shot hardness and velocity, and of the material's hardness, strength and hardening characteristics. The maximum depth is approximately the order of the shot size, and, in any practical case, under 0.25 mm[2]. It can be varied for given parameters by multiple peening, without much affecting the maximum values. Typical stress profiles, obtained with glass beads and steel shots, are shown on Figure 3-7.

The depth at which the magnitude of the residual stress field is maximum depends both on material and process parameters. It can be brought closer to the surface by using hard shot (glass or ceramic). The use of glass beads also achieves higher surface stress and similar maximum stress at lower intensity, which has a good influence on surface smoothness of glass peened specimens. For steel and ceramic, the depth of maximum stress is a linear function of intensity, with a coefficient that depends on the shot size for a given shot medium, whereas it is not intensity-related with glass beads [62]. Depth of 25 μm and below are commonly obtained.

3.2.4 Influence of shot peening on fretting fatigue resistance

Several studies report a large increase of fretting fatigue resistance after shot peening ([53],[57] on Ti-6Al-4V, or [58],[59] for aluminum alloys), and this beneficial aspect is well known. More detrimental effects have yet been observed and are worth keeping in mind when using shot peening in a design. As usual, the most efficient use of the technique may often be a matter of compromise.

[2]Twice higher values may be achieved by increasing coverage, at the expense of surface smoothness

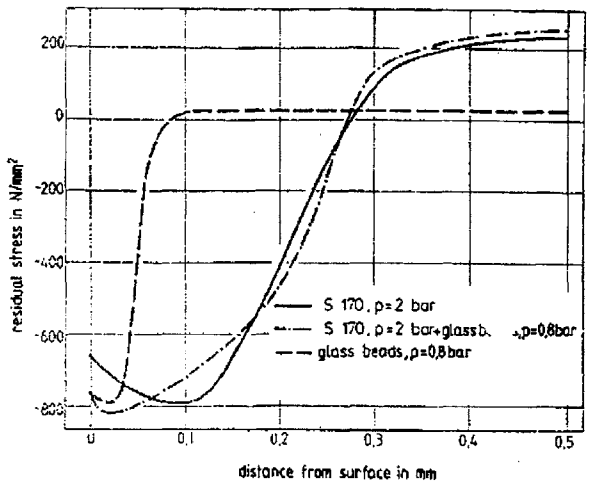

Figure 3-7: Residual stress profiles on Ti6Al-4V for various treatments, from Hirsch et al. [7]

Surface damage due to shot peening: influence on failure mechanism and modeling

Although it can be said, as a general design rule, that shot peening improves fretting fatigue resistance, it is nevertheless a relatively "harsh" process, whose beneficial effect results from a compromise. It is particularly important to be aware of the possibly drastic modification of surface characteristics due to shot peening, since it may significantly affect the mechanisms of fretting fatigue failure, and invalidate some of the most common modeling approaches. Surface damage is obviously the main drawback of shot peening. It may create stress concentrations, which may combine with the localized residual stress distribution to promote fracture. As observed by Waterhouse and coworkers [5] on aluminum alloys, damage may also take the form of "folding", a process in which slabs of material are detached under the shock of a shot and folded back onto the surface. As suggested by Figure 3-8, such a defect can be viewed as a subsurface damage (subsurface cavities were actually observed), which will provide easy propagation path to the surface.

A major change in the crack propagation behavior correlated with the damage: steep slant crack at 50-60° on the unpeened specimens were replaced by cracks at

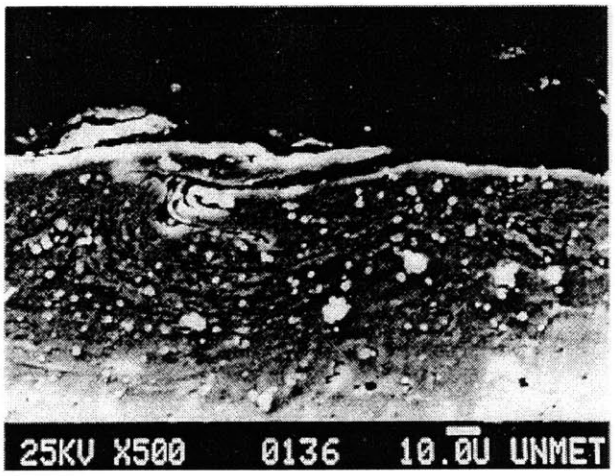

Figure 3-8: Folding surface defect observed by Waterhouse et al. on aluminum

much more shallower angles, sometime running parallel to the surface, and leading to delamination. The authors argued that the change was facilitated by the rotation of the principal stresses directions due to the biaxial compressive residual stress. Similar changes in crack pattern after shot peening can be found in a review on surface treatments by Lindley and Waterhouse [8], but in conjunction with heavily deformed surface. On Figure 3-9, the shift from a crystallographic failure to a much more tortuous crack pattern is striking. It implies that the behavior of unpeened 8090 alloy specimens is amenable to relatively simple mechanical modeling, whereas the modeling of peened specimens becomes very complicated.

Waterhouse et al. also reported a change in the aspect of the fretted zone: whereas the scar consisted of smeared and broken metal and oxide in the case of unpeened aluminum specimens, the fretted zone of peened specimens was covered with round debris, and subsurface cavities filled with the same debris were observed. This change was attributed to the break-up of heavily work hardened, and was invoked to explain the measured difference in the coefficient of friction and opposite trends of variation between unpeened and peened aluminum alloys.

All these observations clearly indicate that the surface state after peening may significantly alter the cracking behavior. In the latter case, it also affect a major mechanical parameter, the coefficient of friction. Consequently, the actual type of

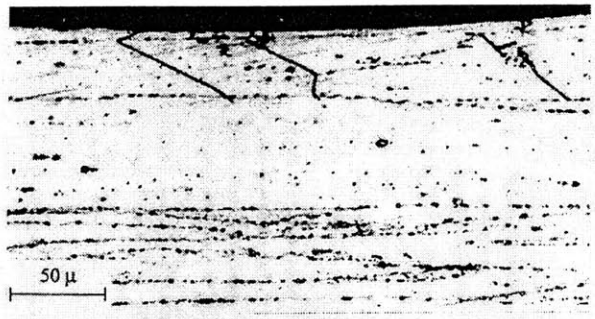

Figure 5. Cracks initiated in unpeened surface of aluminium alloy 8090.

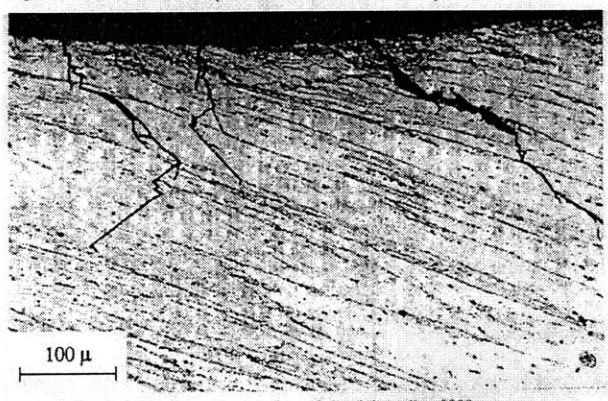

Figure 6. Cracks initiated in peened surface of aluminium alloy 8090.

Figure 3-9: Influence of shot peening on cracking pattern in aluminum 8090, from Lindley and Waterhouse [8]

damage occurring during the tests should be carefully assessed, as this may impact the fretting resistance, and significantly impact the relevant modeling of the phenomenon.

Optimization of shot peening treatment for fatigue applications and stress profile prediction

Optimizing fatigue properties through shot peening obviously implies a trade-off between the parameters. The magnitude and depth of compressive residual stresses usually play a key role, because fatigue resistance is very often propagation-controlled (specially in the case of fretting [23]). However, detrimental effects of high intensities are often reported [10] in plain fatigue: the Almen intensity limit of 5C has been proposed by Gillespie. High coverage has a similar adverse effect, and the optimum coverage seems to be in the range 100-200%. Furthermore, the optimal treatment may be microstructurally dependent (see [28] for steel, or possibly in relation to initiation

site on titanium). In addition, the optimum intensity for maximum fatigue strength or time strength differs for conventional shot media [62]. Finally, the solicitation has to be taken into account, mainly to ensure that compressive stresses are not rapidly relaxed upon loading (see below).

A variation of the process, called dual peening, is proven to be very effective and consists in peening the specimen twice, first with a large, hard steel shot that induces deep compressive stresses, then with glass beads in order to improve the surface smoothness.

Predictive models of the residual stress field may be helpful in selecting optimal parameters. The more advanced program, called Peenstress^{TM}, is based on the work of Castex [74], that models the evolution of a material with kinematic and isotropic hardening over cyclic application of a Hertzian stress field. Another earlier model by Al-Hassani [75] follows the same approach. It seems that the Peenstress^{TM} program has been improved over the years to capture the stress field near the surface with increased accuracy [76][77].

3.2.5 Laser shock peening

Principles of the technique

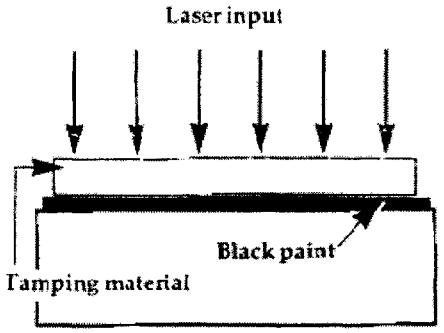

Figure 3-10: Schematic illustration of laser shock process, from Dane et al. [9]

The laser shock technique makes use of the very high pressure developed by a plasma confined by water to induce shock waves into the material. The plasma is produced by the vaporization of a paint layer on the surface of the specimen by a short laser pulse. The process is schematically depicted on Figure 3-10. The pressure can exceed twice the dynamic yield strength of the material for a very short time, and may be limited to 5-6 GPa at high power density by the formation of a parasitic plasma at the water/air interface (due to hot spots or surface impurities [78]). Compressive residual stresses are induced by a mechanism identical to the first one described for shot peening, the only difference being a shift in the value of the yield strength from the static value (in the range of 1000 MPa) to the dynamic value (about 2.8 GPa for Ti6Al-4V). The latter is only an extrapolation, based on its reported log-linear dependence for strain rates up to $10^4 s^{-1}$ [79]. It usually brings significant improvement over shot peening characteristics, notably as regard damage tolerance: damaged laser shocked blades can sustain loads exceeding the maximum design load for undamaged blades by 20%, which cannot be achieved by shot peening, as shown on Figure 3-11. Combined with the absence of surface roughness deterioration (which means no adverse effect and the possibility to comply with tight design specification), it explains why this technique, in spite on its cost[3], has received much attention from the jet engine industry [10].

Stress profiles characteristics

The maximum compressive stress, at most comparable to the one achieved by shot peening, is found at the surface, and decreases over a length of a least 1 mm for single shock [79][30][9]. There is no doubt that multiple peening can largely increase this value, but relaxation has also been reported on 316L at high power density (in the order of 10 GW/cm^2 [78]). The maximum stress increases with either intensity or multiple peening up to a saturation point where only the in-depth magnitude and

[3]Initially the frequency of one shot every 20 minutes limited the interest for large components, but later developments allowed to reach one shot every 2 minutes, and probably much more recently [78]

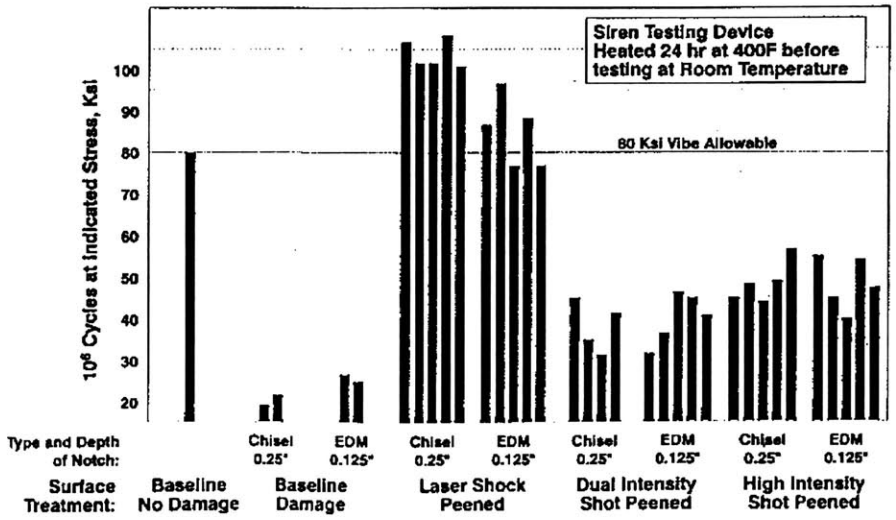

Figure 3-11: Comparison of the improvement of fatigue allowable on damaged blades: note how the specification for the undamaged component is matched by the laser shocked specimen, and that specimens have been damaged prior to peening, and subjected to thermal relaxation (400°F for 24 hours) before testing, from Thompson et al. [10]

affected depth are increased [30]. For thin sections however, such as 1.5 mm steel plates, only the in-depth magnitude and of course the tensile core are affected by multiple peening [30]. This may be related to interaction between shock waves (due to simultaneous shocking of opposite faces). This type of treatment is advised to avoid curvature on specimens less than 12 mm thick, but seems to produce high tensile stresses in the middle of the specimen. In addition to the axial stress profile, that is the stress profile in the direction normal to the surface, the radial profile at the surface must also be considered. The focusing of waves at the center of the spot eliminate the compressive stress at the center of the spot [79][30]. Rectangular spots alleviate the problem somewhat. At the edge of the spot, a tensile stress may appear on the radial component of the residual stress field [30], which is no longer axially symmetric. This effect is more than compounded by the fact that laser spots are usually small (2.5 to 25 mm in diameter), so that a computer-controlled scanning process with overlap is used to treat a large surface.

Influence on surface condition

The surface is essentially unaffected by this process. The energy of the shot (usually about 50 to 100 joules) is applied over a very short period of time (about 50 ns at most), so that there is theoretically no heat effect, and no microstructural changes. However, for cost efficiency reason, a small heat effect may be tolerated [30]. Another possible effect on soft materials, such as aluminum alloys, is a depression of the surface (in the order of up to 6 μm)[30].

Prediction of stress profiles

Analytical modeling of laser shock peening seems to have been seriously undertaken only recently in France and in the United States [79]. The first step consisted in fundamental work on the modeling of shock waves [78]. In principle, modeling relies on the idea that plastification occurs when the Hugoniot elastic limit is exceeded, using a yield criterion of the form:

$$\text{HEL} = (1 + \frac{\lambda}{2\mu})\sigma_{\text{dynamic}} \tag{3.1}$$

where HEL is the Hugoniot elastic limit, λ and μ are Lame coefficients, and σ_{dynamic} the stress due to the propagation of the elastic shock wave. Braisted and Williams [79] have shown that a finite element approach based on this principle could capture all trends of the stress profiles, but with mediocre accuracy.

3.2.6 Relaxation of residual stress fields

Relaxation of the residual stress field occurs when the equivalent stress due to the superposition of the load and the residual stress field exceeds the yield of the material, either in tension or in compression [28][26][11][4]. Under cyclic sollicitation it is not clear whether the stress field is relaxed immediately (mentioned in [28] for steel) or progressively. In the latter case, a log-linear decrease has been reported

[4]Not to mention of course the thermally activated relaxation that can occur at high temperatures

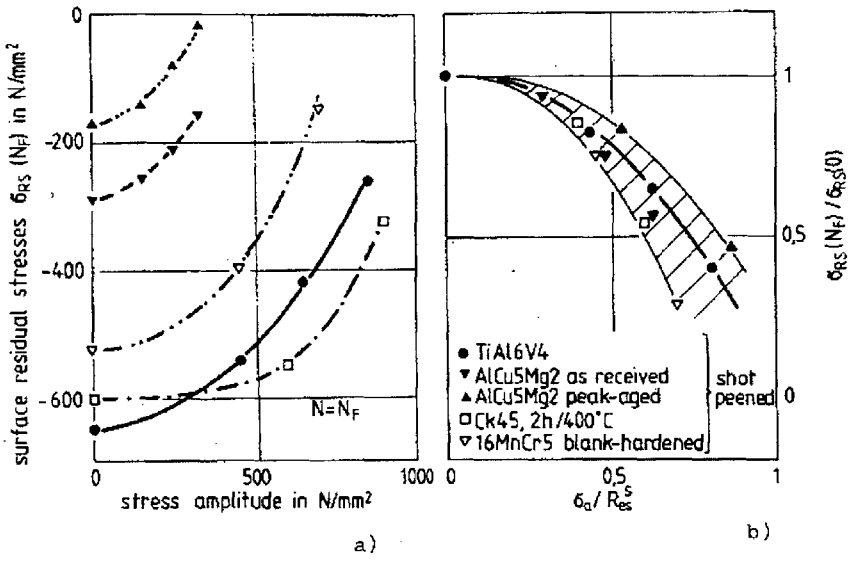

Fig. 9: Surface residual stresses after fatigue fracture as a function of stress amplitude of different shot peened materials (4, 8, 10).
a) σ_{RS}, σ_a-diagram, b) σ_{RS}/R_e^s, $\sigma_{RS}(N_F)/\sigma_{RS}^{(0)}$-diagram

Figure 3-12: Relaxation of residual stresses in various materials as a function of the loading conditions, from Vöringer et al. [11]

[80][81] for high number of cycles, but detailed observations by Vöhringer et al. [11] and Bignonnet et al. [82] tend to prove that relaxation occurs upon first compressive and second tensile half-cycle, then stabilizes for severals thousands of cycles, actually until cracks (from 0.3 to 0.7 mm length as observed by the authors) appear. Then relaxation occurs again. These authors have also established correlations between the initial and final surface residual stress and the loading amplitude (see Figure 3-12), that may be used as a first indicator of the expected magnitude of relaxation. In our case, a surface residual stress of 800 MPa at most is expected, and the maximum stress amplitude is likely to be under 400 MPa. Using the authors'diagrams, we may expect a surface residual stress at failure in the range of 550 to 600 MPa *in plain fatigue.* The actual stress level would be lower for our fretting experiments, as Waterhouse's work indicates that relaxation is more pronounced in fretting. Experimentally, it is also observed that the phenomenon is faster if the load is applied parallel to the residual

stress field [28][81].

As explained by Vöhringer et al. , relaxation is controlled by the surface and core yield strength and residual stress. It can be rationalized with simple models [11][26], by superposition of the applied stress field, of the contact stress field (using, for instance, the analytical solution of Hamilton [83]), and of a given residual stress field. The work of Kirkpatrick [26] describes a procedure to check the depth to which yielding can occur for the case of a sphere sliding over a semi-infinite substrate. As it is based on elastic calculations, it is strictly speaking a procedure to account for the occurence of stress redistribution, not for its amount. The computational tool developed in this work allows to check for the occurence of yielding in the case of a fretting sphere.

If plasticity appears, it may shakedown to an elastic state. The problem of calculating the variation of the residual is more complex. As a full elastic-plastic calculation seems impractical [5], the derivation of bounds for elastic and plastic shakedown may be a convenient way to partially answer the question of the stress state evolution. Using the static and kinematical shakedown theorem, Johnson and coworkers [68][85] derived an exact value for a line contact under repeated sliding. The same geometry was studied numerically by Dang Van and Maitournam [86] in the case of fretting, for which the elastic shakedown limit was found to be lower. In principle, the same kind of study can be carried out for a point contact. However, the analytical derivation relies on simplification of the admissible residual stress field (for the static shakedown theorem), and of the yield mechanism (for the kinematical shakedown theorem), which are no longer valid for a point contact even in the case of repeated sliding. Therefore, for our fretting problem, a numerical optimization scheme based on our stress computation program could be a basis, although the expected computational cost is high.

[5] See, for instance, the computational effort associated with running the model of Giannakopoulos and Suresh [84] several times

3.3 Peened material characterization

Specimens similar to those used in [3] were subjected to two different shot peening treatments: a simple peening denoted T1 (whose normalized characteristics are GP50 F15F20N 100%),and a duplex peening denoted T2+T1, consisting of a treatment MI230R F22F28A 100% followed by T1. The idea behind these specifications is to obtain both a shallow depth of peening (below 100 μm)with substantial residual stresses at the surface (which is achieved by the glass-bead T1 treatment), and a deeper depth of peening (around 200 μm) with a similar profile near the surface (which is achieved by T2+T1, as the lighter final peening affects mainly the near-surface profile). These two characteristic lengths are believed to bracket the typical depths of transition to mode I on the untreated specimens.

Hardness was measured by Vickers indentation (50 g load), and came out to 372 +10%/-7% for the T1 treatment and 448 +11%/-15% for the duplex peening T2+T1. The hardness for the untreated STOA material under the same conditions is 379 $\pm$5%. Only the duplex peening seems to significantly affect the surface hardness. Yet both peening treatments introduce significant scatter in the measurements, consistent with the observations reported in x-ref.

Friction was characterized using the same procedure as Conner [3]. The first break-away was observed for a $\frac{Q}{N}$ ratio of 0.75 and 0.95 for the simple and duplex treatment after polishing respectively, whereas the gross slip coefficient of friction was close to 0.65. These values are close to that obtained by Conner on the untreated material, with also break-aways at ratios beyond 1.

For consistency with the experimental procedure of [3], most specimens were mechanically and manually polished, finishing with 0.05 μm alumina paste. The process removes less than 10 μm of material, which does not significantly affect the expected residual stress distribution. The stress profiles for the polished and unpolished material are given in Table 3.3, which also contains the profilometry data.

The surface residual stresses were obtained by X-ray diffraction for the T1 polished, T1 as peened and T2+T1 polished specimens. The magnitudes of the residual

	Near center			Near center		
	R_a	R_t	R_z	R_a	R_t	R_z
T1 as peened	1.16 μm	8.43 μm	6.25 μm	1.16 μm	10.14 μm	8.18 mum
T1 polished	0.08 μm	0.80 μm	0.55 μm	0.10 μm	1.77 μm	1.25 μm
T2+T1 polished	0.07 μm	0.90 μm	0.50 μm	0.09 μm	1.40 μm	0.97 μm

Table 3.3: Profilometry data for the two shot-peened treatments and different finish conditions

stresses are -545 MPa, -516 MPa (with very little shear), and -541 MPa, $\pm$ 30%. The duplex peening is seen to be effective in harmonizing the surface stresses, while polishing induces only a slight redistribution of the surface stresses.

3.4 Experimental results

3.4.1 Tests to failure

Due to considerations of the magnitude of the equivalent stress developed in Section 4.1, a load ratio of 0.1 was chosen for the experiments on the shot-peened specimens. The pads were pressed on the specimen after pre-loading to the required mean stress, in order to keep a symmetric surface traction history. Although the effective loads were close to the chosen values, the effective load ratio turned out to be close to 0.085, due to the controls capability of the set-up. Figure 3-13 summarizes the results.

The number of valid experiments was low, with numerous non-fretting fatigue failure in the fillet or thread of the specimens. An attempt to decrease the axial stress below a critical load for these locations resulted in no failure nor visible cracking after more than five millions of cycles. Moreover, the observation of the scars revealed poor quality in general: the wear marks were often exceedingly large, with no definite stick-slip zone, and elongated (see Figure 3-14). Three phenomena could account for this deterioration of the scar quality:

1. an excessive eccentricity: based on the simplified analysis of Wittkowsky et al. [34], for a given axial load, a minimum tangential force is required to prevent

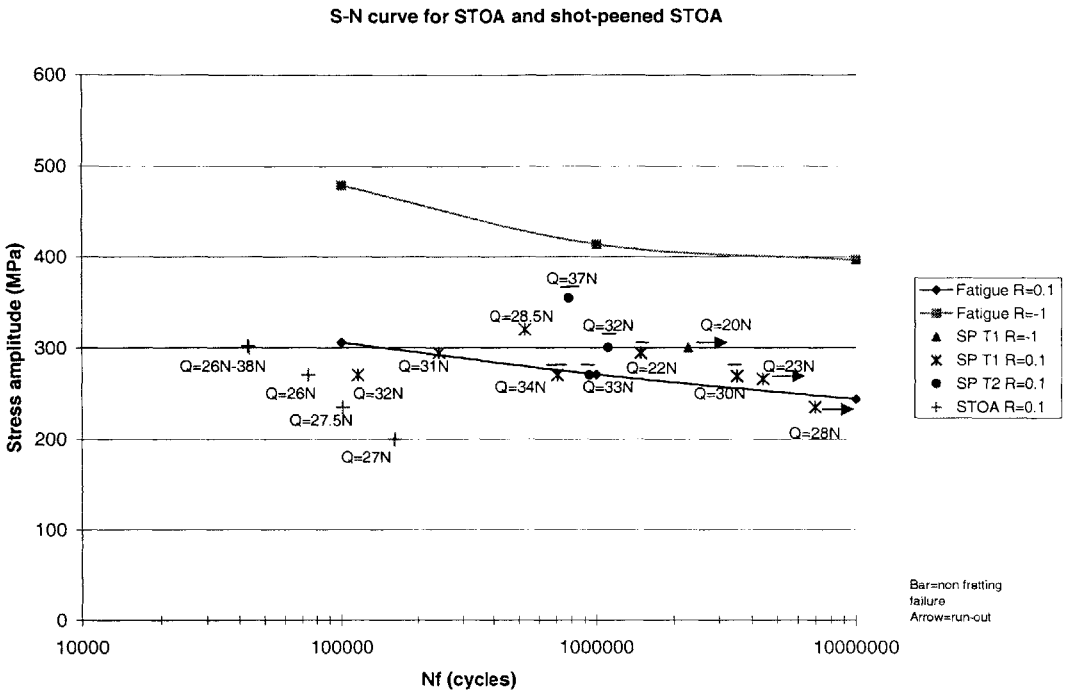

Figure 3-13: Summary graph of experiments on shot-peened specimens in the form of an SN curve (plain fatigue data from Bellows et al. [12])

the stick-slip boundary from meeting with the contact edge. As explained in more details in Section 4.1, experimental results suggest that this value may be conservative. Hence, although the required minimum was not always achieved in our tests, no definite conclusion could be drawn

2. plasticization at one of the contact edges: although the positive load ratio was chosen to avoid extensive plasticization (see Section 4.1), it did not completely eliminate the problem

3. an instability of the contact condition: the analysis of contact based on Hertz and Mindlin's theories assume small deformation and a quasi-static load varia-

tion, which may not be appropriate when too large an axial stress is imposed at 10 Hz

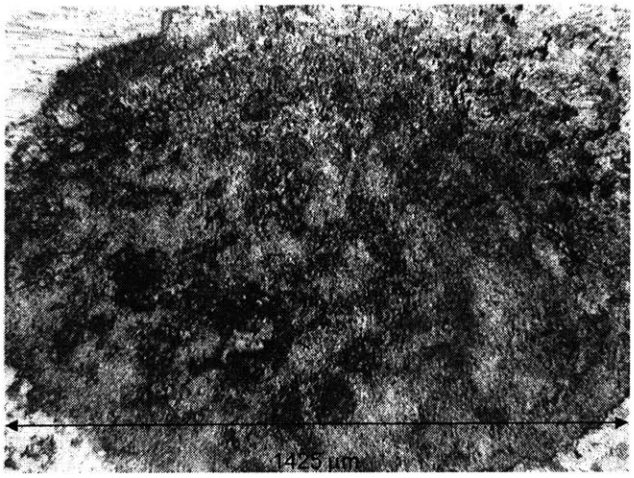

Figure 3-14: Scar obtained for P=50 N, Q~37 N, and a maximal axial stress over 600 MPa (stress ratio=0.1); the contact diameter predicted by Hertz theory is close to 400 μm

Decreasing the maximum bulk stress improves the quality of the scar and decreases the risk of non-fretting failure, but also increases the number of cycles to failure to several millions cycles, which is impractical at 10 Hz. Therefore, it was concluded that the current set-up was not well suited to study the failure of shot peened specimens.

Nevertheless, a few useful observations could be made. As regards the effect of shot peening on fretting fatigue resistance, the comparison between the shot peened and untreated materials for the same stress ratio clearly indicates a great efficiency of the fretting fatigue resistance for the geometry and range of loading investigated. Also, for the experimental conditions chosen, the fretting fatigue and plain fatigue lives are similar.

3.4.2 Interrupted tests and pad analysis

Tests to failure are not however essential for understanding the fundamentals of fretting fatigue. A crack of reasonable size can indeed be treated with classical linear

elastic fracture mechanics concepts (see Section 2.2.6). The "essence" of fretting is what happens in the early stages of the loading near the surface, primarily under the influence of the contact condition. Therefore, it is most interesting to either perform fretting experiments with little or no bulk stress, or try and observe what happens early under the surface. The first option was not experimentally feasible using the test frame presented in Section 3.1.1, yet the pads fulfill the requirements. Optical electron microscope observations of fretted pads revealed a definite crack-like pattern at a "macroscopic" level, well positioned with respect to the crack and the oxide built-up, as illustrated by Figure 3-15. However, optical and scanning electron microscope observations after polishing revealed that this pattern is not a crack but a step or gouge limited to the oxide layer, and that the underlying pad material is undamaged.

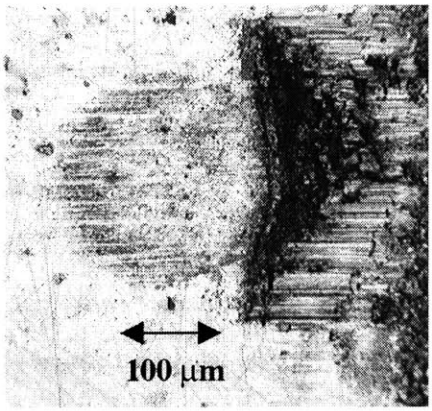

Figure 3-15: Macroscopic damage pattern on the pad after 2163277 fully reversed cycles, for Q=10 N, N=50 N, σ_{axial}=300 MPa

The other option was implemented by interrupting tests on both shot peened and untreated specimens at 10^5, $3x10^5$ and $6x10^5$ cycles, and $5x10^4$, 10^5, and $3x10^5$ cycles respectively. A stress ratio of 0.1 was used for the shot-peened specimens, whereas a ratio of -1 was used for the untreated ones, for which the expected number of cycles to failure was of the order of 4 to $5x10^5$ cycles. The specimens were cut near the centerline of the crack by EDM, polished and etched to try and reveal incipient cracks. The conditions and results are summarized in Table 3.4 and Figure 3-16.

Number/Type	Q (N)/ σ_{axial} (MPa)	Number of cycles	Crack	Slant/ straight length (μm)	Angle (°)
1/STOA	$19/300^{+}$	100000	Yes	39/20	60
2/STOA	$18.5/300^{+}$	300000	Yes	23*/208**	59
3/STOA	$14.5/300^{+}$	50000	No***	NA/NA	NA
4/T1	$34/270^{++}$	100000	No***	NA/NA	NA
5/T1	$27.5/270^{++}$	300000	Yes	15/NA	60
6/T2+T1	$33/270^{++}$	600000	Yes	37/NA	68

Table 3.4: Experimental conditions and observations for interrupted tests on STOA and shot peened specimens; +=stress ratio of -1, ++=stress ratio of 0.1, *tortuous initial path, maximum averaged path length given, **=total depth, ***=plane of cut misplaced

Four out of six experiments revealed the presence of cracks. For the two that did not show cracking, errors in the positioning of the plane of the cut don't allow to conclude that no damage was indeed present[6]. The available pictures show that, for the loading conditions chosen, cracking is well developped at about 25% of the expected life in the STOA. For the shot peened material, the loading may be bellow the endurance limit, or at least will not lead to failure before several million cycles. Yet damage is present at 300000 cycles, and is still limited at 600000 cycles.

A closer examination of the crack reveals that the initial slant portion for specimens number 2 and 6 seems to be pointing outwards rather than inwards as usual. It could not however be confirmed whether the cracks were present at the trailing or leading edge, so this unusual observation would need further investigation. For the STOA specimens, the length of transition for a slant path to a path normal to the surface varies between 20 and 40 μm. The initial angles do vary, but seem to remain below 70°. To the first order, no strong influence of shot peening on the initial angle could be detected.

[6]Note that the error in the positioning need not be big to hinder observations for both cases, as the cracks are expected to be small: only a few tens of microns suffice

The methodologies used are thus seen to yield valuable information on the nature of damage, its growth, and geometry. Although observations of very short cracks via this procedure seem quite difficult, it is the kind of objective that is most likely to help understand the fundamentals of fretting.

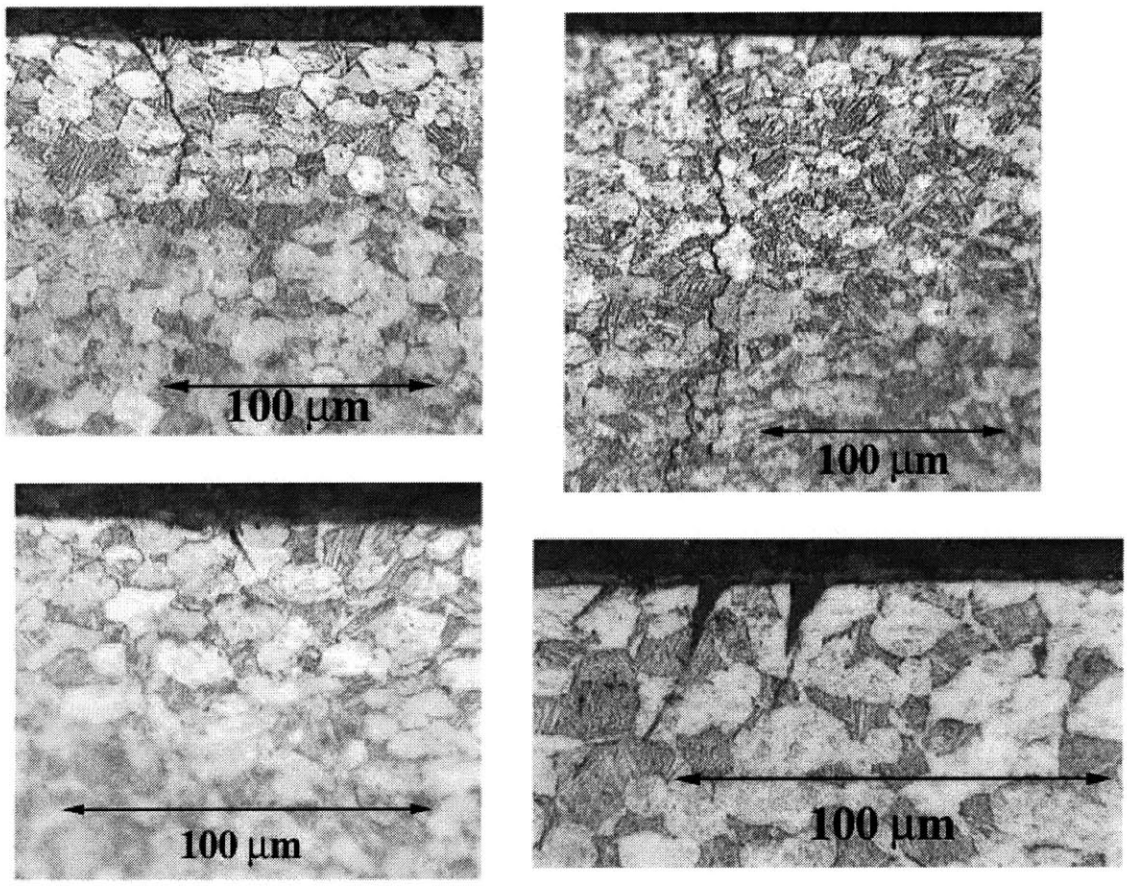

Figure 3-16: Cracks observed in specimens number 1 (top left), 2 (top right), 5 (bottom left) and 6 (bottom right) of Table 3.4

Chapter 4

Modeling of fretting fatigue

This section contains a detailed discussion of the characteristics of the stress field in a semi-infinite substrate under a spherical fretting pad, and their implication on the use of stress-based criteria. A description of the propagation-based model is then given, and the predictions of the approach are discussed in the light of experimental evidence.

4.1 Stress field under a spherical pad in fretting

In order to apply the stress-based criteria presented in Section 2.2.1, the knowledge of the whole stress history is required in principle: the contact loading and bulk loading may not be in phase, so it is not obvious a priori which points in a loading cycle will maximize the criteria. A program was written to compute the stress field below a rounded pad in the stick-slip condition. The principle is a superposition of Hamilton's analytical sliding solution [83], using the slip distribution derived by Mindlin [46], rather than the analytical solution by Sackfield and Hills [87], which is much more involved numerically. The program allows to compute the stress tensor at any location in the plane of symmetry, or anywhere in the substrate with minor modifications, for any given uniaxial, normal and tangential load. It also allows the computation of the stress field at any point of the loading cycle for a given maximum tangential load and uniaxial stress, assuming the relative displacement is due to the

latter as it is the case in our experiments.

From the above description, it is obvious that the computation is not fully representative of the test configuration due to:

1. the absence of finite width effect. As explained by Fellows et al. [88] in the case of normal indentation of a cylinder on a strip, finite thickness imposes tensile axial stresses, both in a layer near the surface and in depth, in order to achieve equilibrium. On the other hand, fully compressive stresses are present in a semi-infinite substrate. Finite thickness therefore raises the value of the axial stress at the edge of contact. For a line contact, they show that for thickness-to-contact radius ratio greater than 3, the axial stress is the only component significantly affected, due to the normal pressure only [1]. For a thickness-to-contact radius greater than 10, the tensile component of the axial stress is less than 10% of the mean contact pressure, so it is believed that the approximation, although unconservative, may not be too strong for our particular specimen size, where the thickness-to-contact radius ratio is of the order of 20

2. the absence of eccentricity. When the relative displacement is due to a stress in the substrate, the additional displacement induced by the bulk stress has to be taken into account to enforce the condition of no relative displacement in the stick zone. For a line contact, it was demonstrated [89] that this doesn't change the shape of the tangential traction distribution, but shifts it by:

$$e = \frac{\sigma a}{4\mu p_o} \tag{4.1}$$

where σ is the bulk stress, a the contact width, μ the friction coefficient and p_o the average contact pressure The same problem for a point contact was investigated by Wittkowsky et al. [34]. They showed that a similar shift of Mindlin's surface traction distribution allows to enforce the no-slip condition in the direction of relative displacement (x-direction with usual notations) in

[1] A finite width is found to have a very minor effect on the components due to tangential traction

the stick zone. However, there remains a very small relative displacement in the direction perpendicular to the direction of sliding away from the y-axis. Therefore, the simple shift in the distribution does not give an exact solution for the stress field, but the authors argue it yields a very close estimate, considering the magnitude of traction required to eliminate the transverse slip. The amount of shift is related to the same quantities as before, plus Poisson's ratio:

$$e = \frac{1-\nu}{4-3\nu}\frac{4\sigma a}{\pi\mu p_o} \tag{4.2}$$

The main effect of eccentricity is to enhance the axial stress at the trailing edge. This is true up to the point where the shifted stick-slip boundary reaches the contact edge. Then reverse slip occurs on one side of the contact, and the solution of the contact problem becomes more involved [89]. Using the above estimate of eccentricity for a 3D contact, it is possible to compute, for a given normal force, which combination of tangential force and axial stress results in reverse slip. The σ-Q curve shown in Figure 4-1 indicates the minimum tangential load required for any given axial load to avoid reverse slip for a normal load of 50 N. Experimental evidence would suggest that this value may be slightly overestimated, as it is always close to or greater than values used in actual experiments where no particular trouble was reported [3]. Thus it may be used as a lower bound when designing fretting experiments.

Bearing these limitations in mind, several quantities published in the literature such as the equivalent stress [83], the surface traction at maximum load [46] or when reverse slip zones exist [90], or the axial stress at the surface [42] during a loading cycle, were reproduced with satisfactory agreement, but it must be emphasized that very few results for a stick-slip condition with reversed sliding are available.

The results are given in Figure 4-2 to Figure 4-5, corresponding to cases of full sliding, stick-slip, stick-slip and stick-slip with reversed slip respectively.

For the first two cases, the agreement is very satisfactory, indicating a flawless derivation of the field by superposition and a correct implementation. On the other

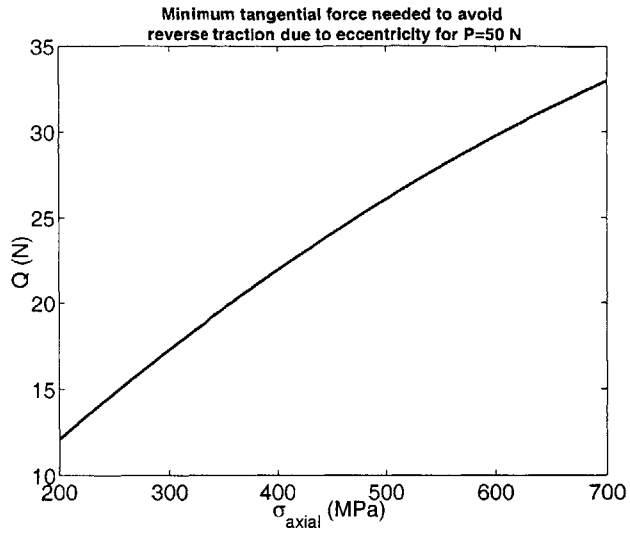

Figure 4-1: Minimum estimated tangential force needed to avoid reverse slip for a normal force of 50 N, as a function of the axial load

hand, the agreement with Chivers and Gordelier's formula [27] is seen to vary with the contact size in Figure 4-4. This appears because of an error in the derivation of the formula, which incorrectly scales the axial stress due to the normal force. Indeed, the authors start with Hamilton's formula for the axial stress due to a sliding indenter, and account for the reversed traction in the stick zone by scaling this formula with the contact radius, leading to:

$$\sigma_{xx} = \sigma_{xx}(\text{sliding formula}) \qquad (4.3)$$
$$-\frac{c}{a}\sigma_{xx}(\text{sliding formula with contact radius a replaced by stick-slip radius c})$$

However, Mindlin's solution is derived under the absence of coupling between the normal and tangential contact problems, and states that a state of equilibrating surface traction, not pressure, exists in the stick zone. Since the component of axial stress due to normal pressure decreases with contact radius, the error is small for large spherical pads (see Figure 4-4, bottom). In general however, as the axial stress due to normal contact is compressive everywhere for the case of the semi-infinite half-plane, Chivers

and Gordelier formula underestimates the axial stress at the trailing edge.

The kind of data needed for a validation of the method could only be found in Lamacq et al. [42]. They report calculations of the axial stress at various stages of the loading cycles for their aluminum specimens. As can be seen in Figure 4-5, only qualitative agreement is reached between their computation and ours. It should be noted that, when no reverse slip is present, the stress profile presented by Lamacq et al. doesn't match Chivers and Gordelier formula in the slip zone, in spite of a large 0.3 m pad radius, and that the size of the stick-zone is different from the theoretical value predicted by Mindlin for their reported coefficient of friction. For lack of details on the details of their numerical procedure, the reason for the discrepancies couldn't be explained.

4.1.1 Plasticity in fretting

Having presented a simple way to derive the stresses under a spherical fretting pad, computations can be carried to check for fundamental features of the stress field. A primary concern is the extent of plasticity for the loading conditions investigated. It's obvious that most of the analytical work on fretting has been carried out with elasticity in mind, and the present analysis is no exception. In particular, the treatment of the crack propagation problem is tractable only if plasticity remains confined. The computational tool developed will here be used to assess the extent of plasticity both of reference tests in untreated Ti specimens [3] and in the presence of residual stresses.

For a condition that can be considered as an upper-bound on the amount of axial stress induced at the trailing edge, Figure 4-6, a plot of the von Mises equivalent stress contours normalized by the yield strength in the plane of symmetry below the spherical pad, shows that, based on an elastic calculation, the region where the equivalent stress exceeds the yield strength is extremely small, both for traction and compression. Therefore, it can be considered that all the experiments reported in [3] were performed in the elastic domain.

However, this condition may not be respected if compressive residual stresses are

present. Figure 4-7 shows equivalent stress contours obtained by superimposing a "step" residual stress profile, with -500 MPa at the surface, -650 MPa down to a depth of 80 μm, and no equilibrating tensile stress beyond. It can be seen that the region where the equivalent stress exceeds the yield strength is very large. In fact, it can be shown by putting compressive stresses all the way through the specimen that two regions of potentially large equivalent stress exist, one starting at the surface at the trailing edge, and one below the surface outside the contact at the leading edge. Figure 4-7 shows that plasticity can occur in a region in excess of five times the contact radius (that's in excess of 1 mm in this case). Such an extensive yielding would certainly limit the validity of most of the concepts used to analyze the experiments, so a means to avoid or alleviate this was sought. This can include:

1. reducing the tangential force. However, this doesn't significantly reduce the size of the highly stressed region unless impractically low loads of only a few Newtons are imposed, which will fall below the fretting fatigue threshold (see Figure 4-8)

2. increasing the normal load, to increase triaxiality. This doesn't have much of an effect in practice

3. decreasing the axial stress. This is not a very effective way to solve the problem, as the high equivalent stress is largely due to the contact, not the bulk stress contribution. Therefore, for fully reversed loading, the axial stress would have to be reduced below the fretting fatigue threshold of the untreated material (see Figure 4-9). Experimentally, there are also limits in the reduction achievable while maintaining a reasonable tangential force, so the solution doesn't seem attractive overall

4. increasing the pad radius. For a given normal load, this will increase the contact size and decrease the average pressure, thus decreasing the stress level while increasing the length scale of the plots presented above. As can be seen on Figure 4-10, yielding can be confined to a very thin layer near the surface or

prevented altogether. It's an attractive solution, except that it may greatly increase the number of cycles to failure

5. change the stress ratio. As the trouble comes from superimposing compressive residual stresses and the compressive stress at the leading edge, limit the amount of compressive bulk stress seems like a straightforward answer. However, as the fatigue characteristics of titanium are rather more sensitive to the stress range than the stress ratio, keeping the stress amplitude to similar values requires relatively large maximum tensile loads. They can in turn induce concern with the extent of plasticity in the tension part of the cycle. The effect can be seen on Figure 4-11, where at minimum tension, in spite of a large tangential force of 35 N, the region of high equivalent stress is much reduced compared to Figure 4-7. On the other, at maximum tension, the stressing becomes severe at the trailing edge and below the layer affected by peening

As the above examples show, a useful outcome of the computation is the ability to carefully select loading conditions prior to testing. Another benefit is the ability to guide the choice of peening conditions to avoid yielding under a particular load, along the line suggested by Kirkpatrick [26].

An alternative to designing experiments to avoid yielding is to compute the evolution of the stresses during cycling, a complex problem as emphasized in Section 3.2.6.

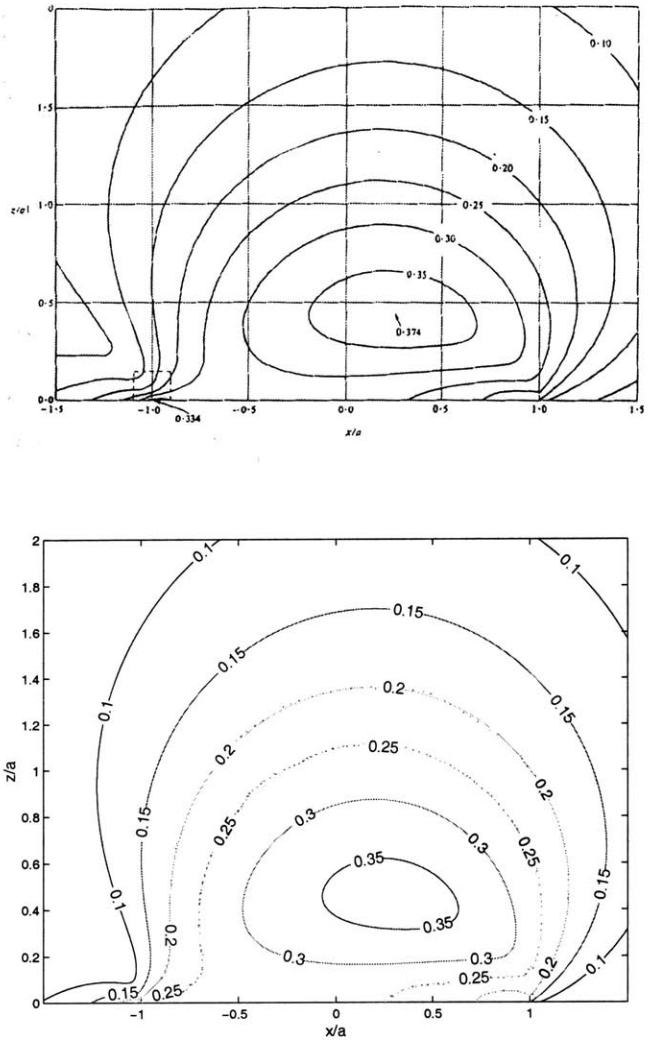

Figure 4-2: Equivalent stress contour, normalized by the average stress, under a sliding spherical indenter for $\mu = 0.25$, from Hamilton [83] (top), and from the present computation (bottom)

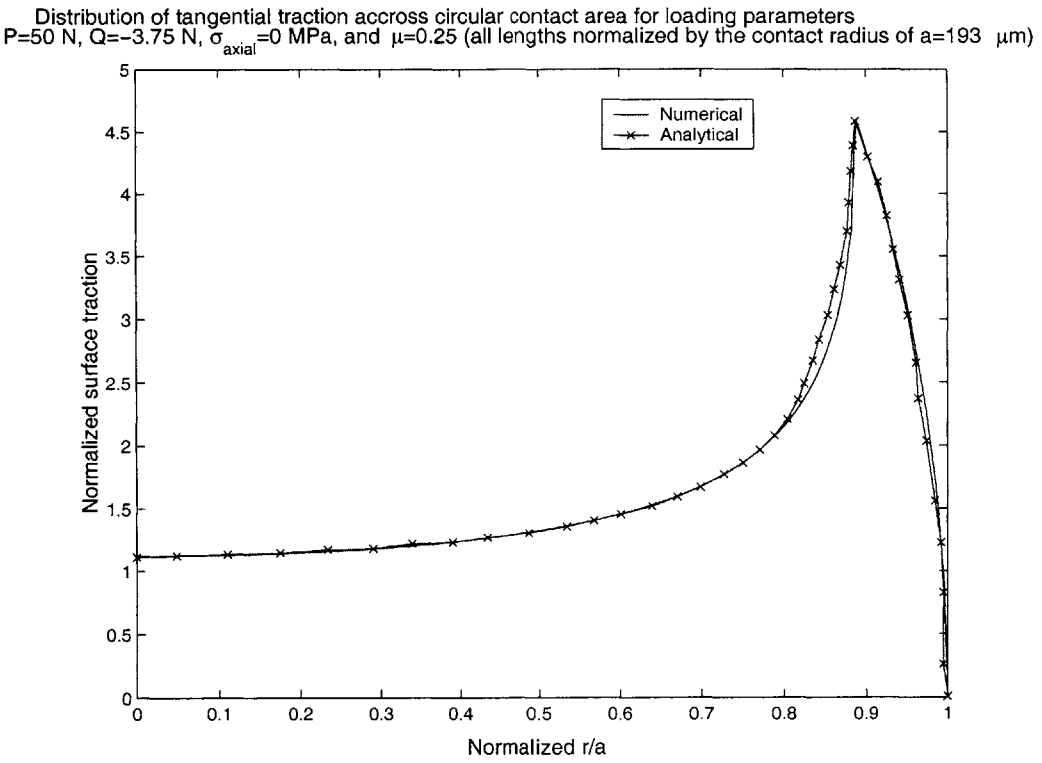

Figure 4-3: Surface traction in the plane of symmetry in the absence of reversed sliding for a stick-slip case

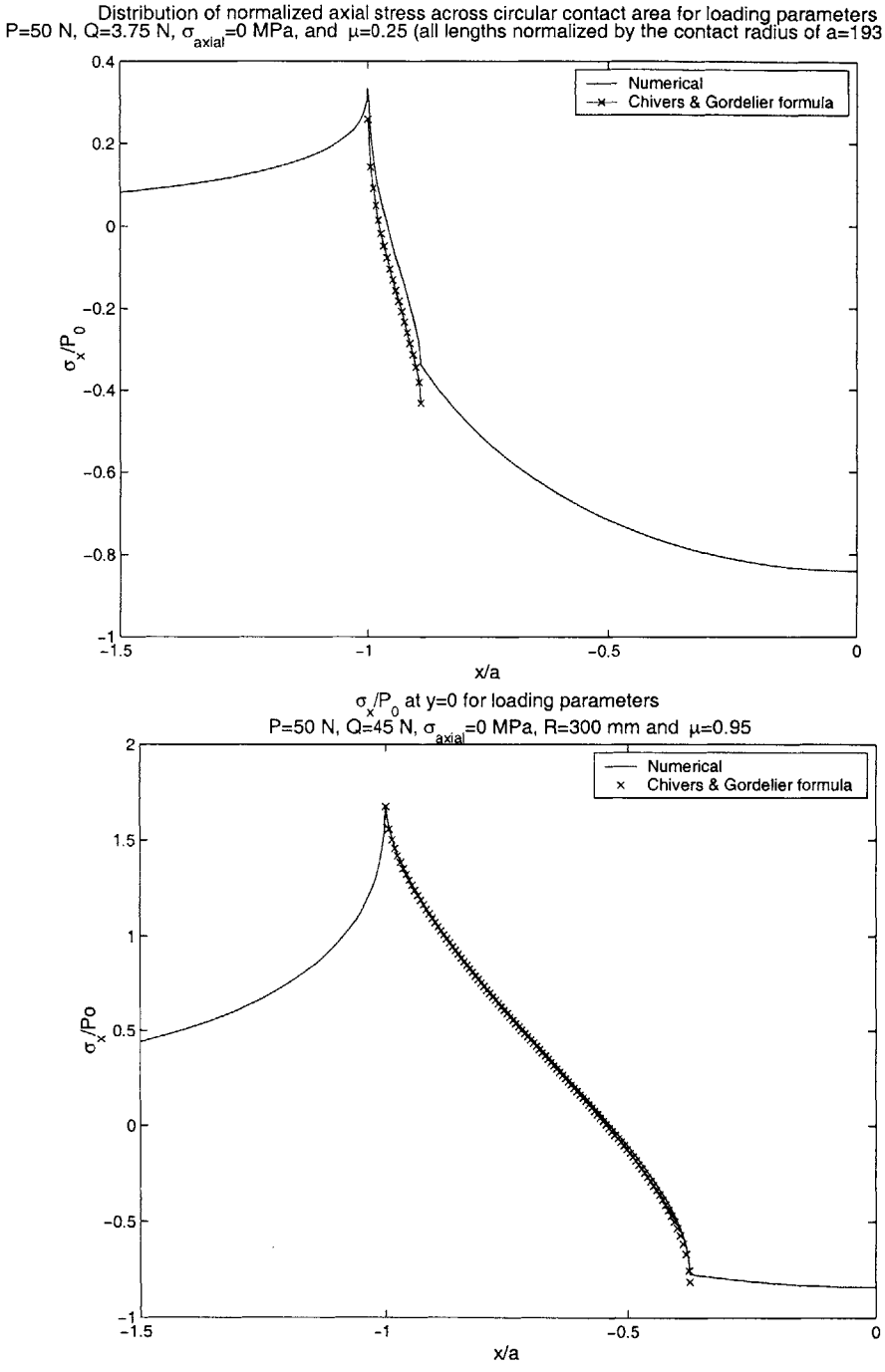

Figure 4-4: Axial stress at the surface in the slip region for pad radii of 12.7 mm and 300 mm

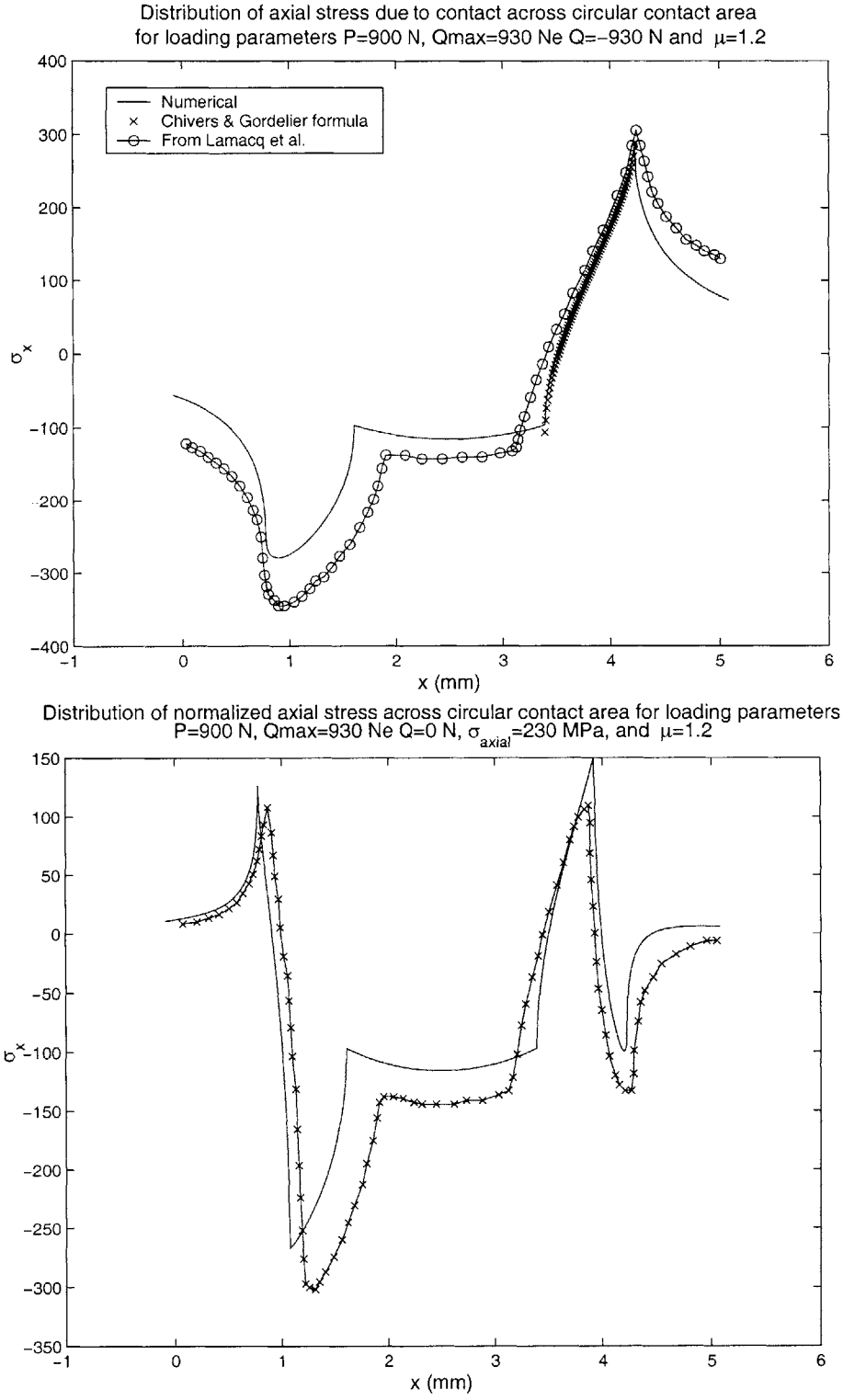

Figure 4-5: Axial stress at the surface in the plane of symmetry of the contact at minimum tangential load and at zero load

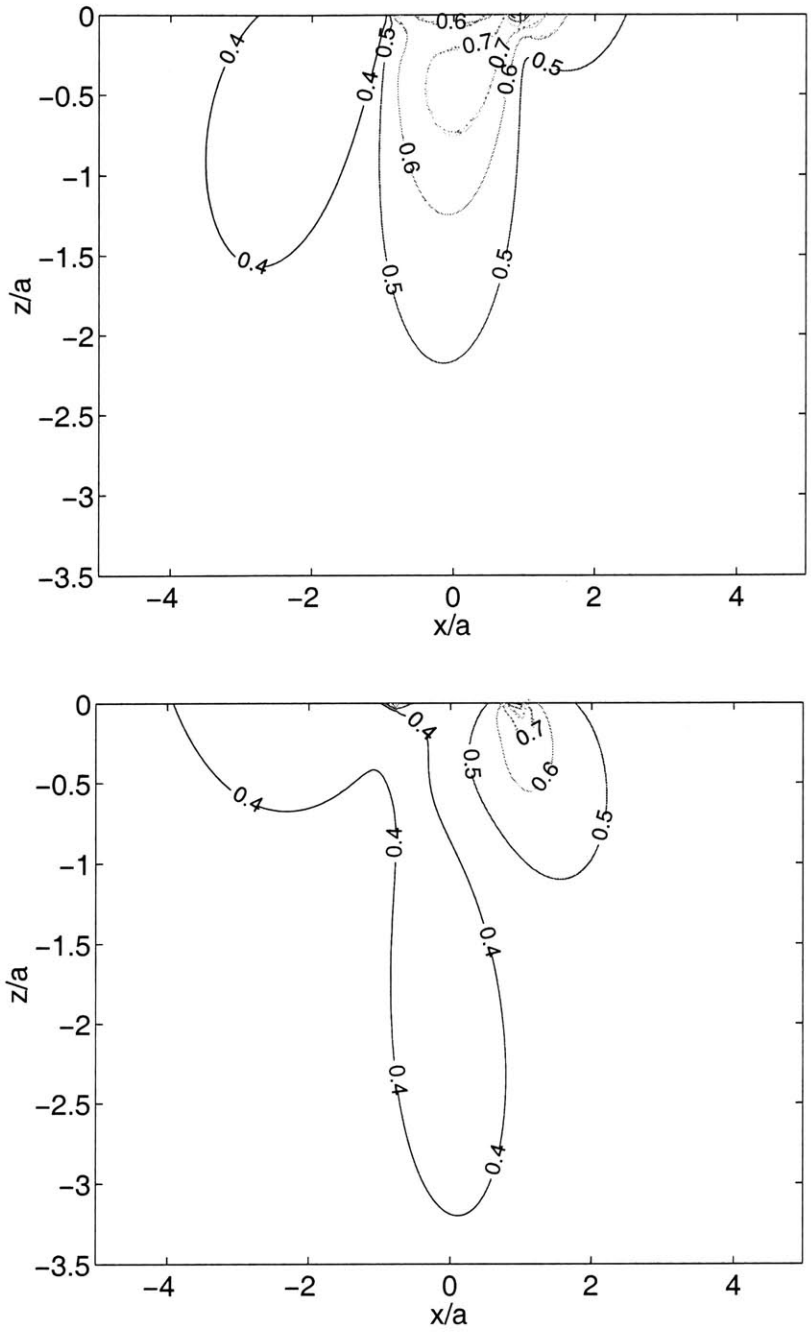

Figure 4-6: Von Mises equivalent stress contours, normalized by the yield strength, below a spherical pad for a normal load of 50 N, a tangential load of 26 N, and an axial stress of 400 MPa, at maximum tension (top; maximum σ_{eq}=1152 MPa) and maximum compression (bottom; maximum σ_{eq}=974 MPa)

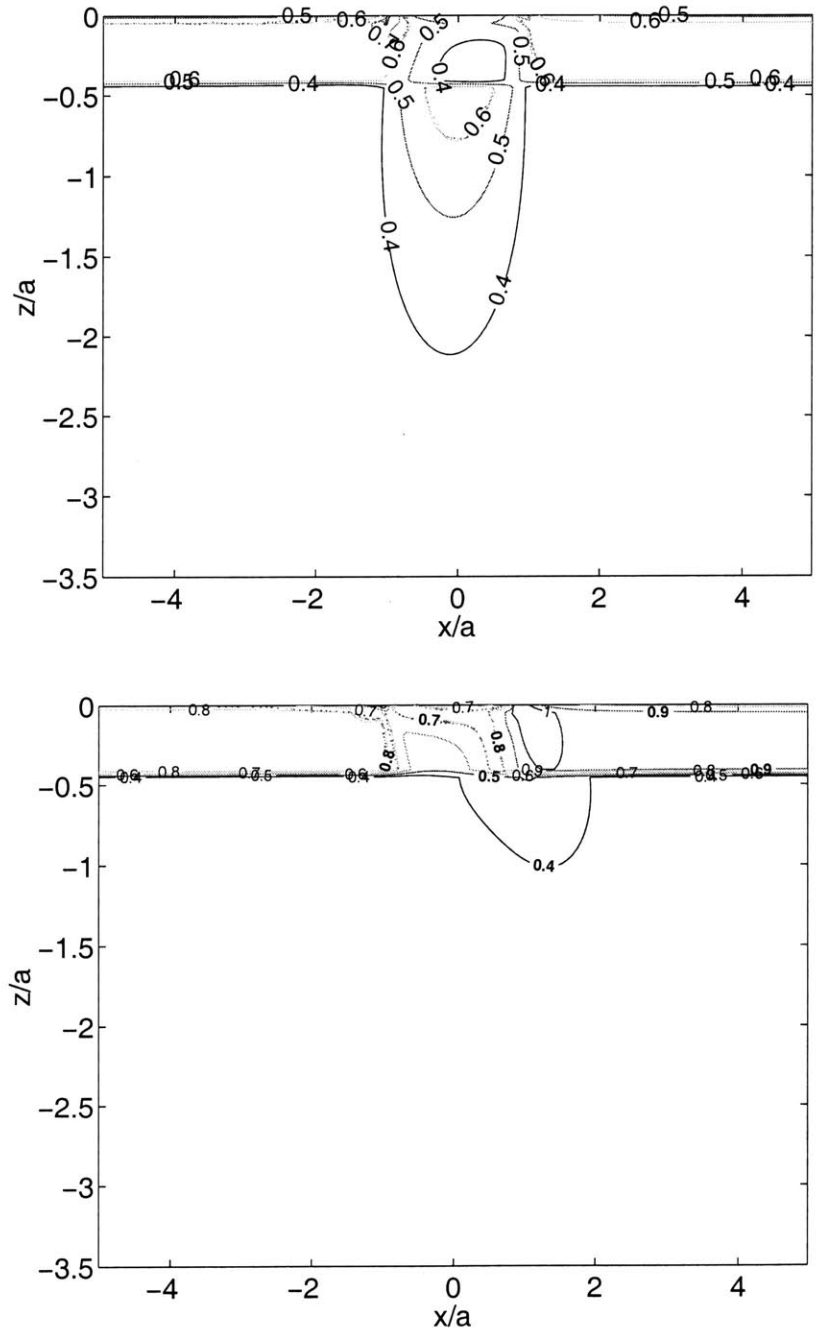

Figure 4-7: Von Mises equivalent stress contours, normalized by the yield strength, below a spherical pad for a normal load of 50 N, a tangential load of 20 N, an axial stress of 300 MPa, with a uniform residual stress of -650 MPa to a depth of 80 μm (-500 MPa at the surface) at maximum tension (top; maximum σ_{eq}=779 MPa) and maximum compression (bottom; maximum σ_{eq}=1203 MPa)

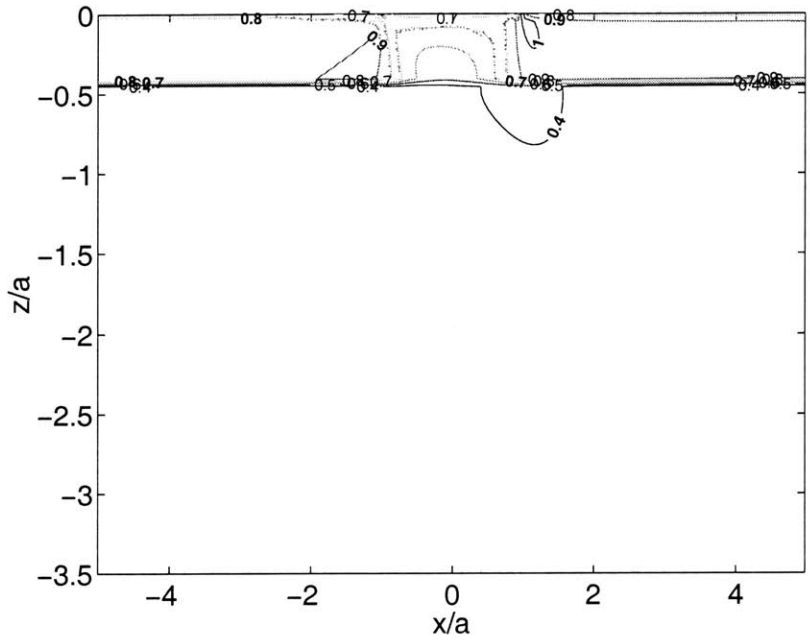

Figure 4-8: Von Mises equivalent stress contours, normalized by the yield strength, below a spherical pad for P=50 N, Q=9 N, σ_{axial}=-300 MPa, with residual stresses (-500 MPa at the surface, -650 MPa uniformly to a depth of 80 μm); maximum σ_{eq}=1017 MPa

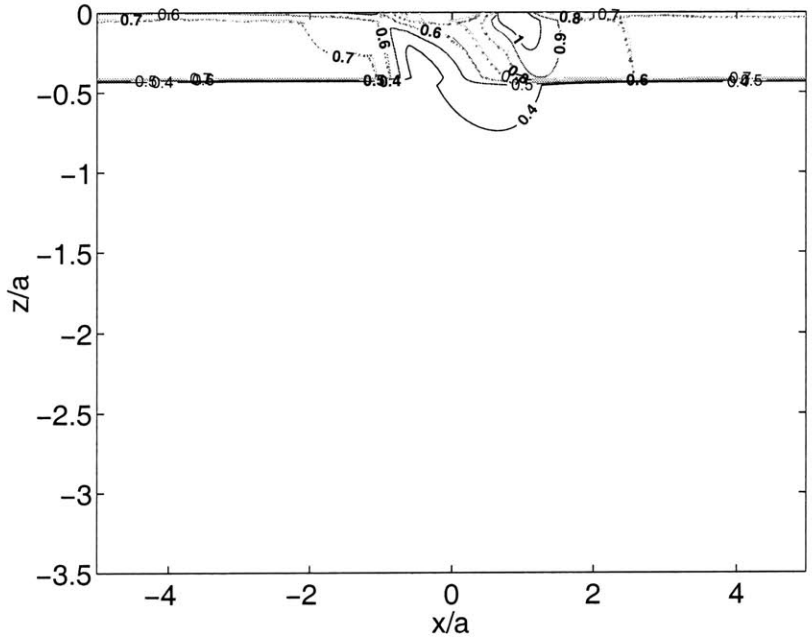

Figure 4-9: Von Mises equivalent stress contours, normalized by the yield strength, below a spherical pad for P=50 N, Q=35 N, σ_{axial}=-100 MPa, with residual stresses (-500 MPa at the surface, -650 MPa uniformly to a depth of 80 μm); maximum σ_{eq}=1223 MPa

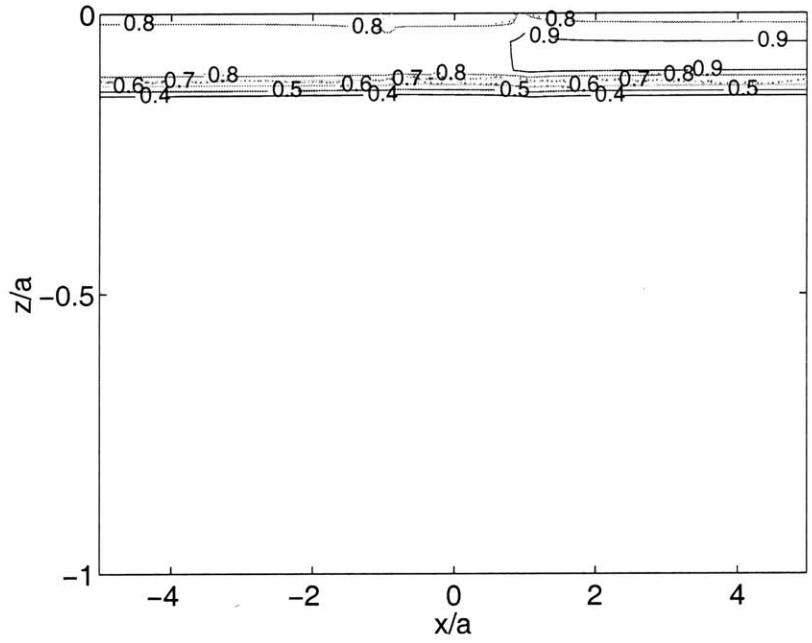

Figure 4-10: Von Mises equivalent stress contours, normalized by the yield strength, below a spherical pad of 254 mm radius for P=50 N, Q=20 N, σ_{axial}=-300 MPa, with residual stresses (-500 MPa at the surface, -650 MPa uniformly to a depth of 80 μm); maximum σ_{eq}=877 MPa

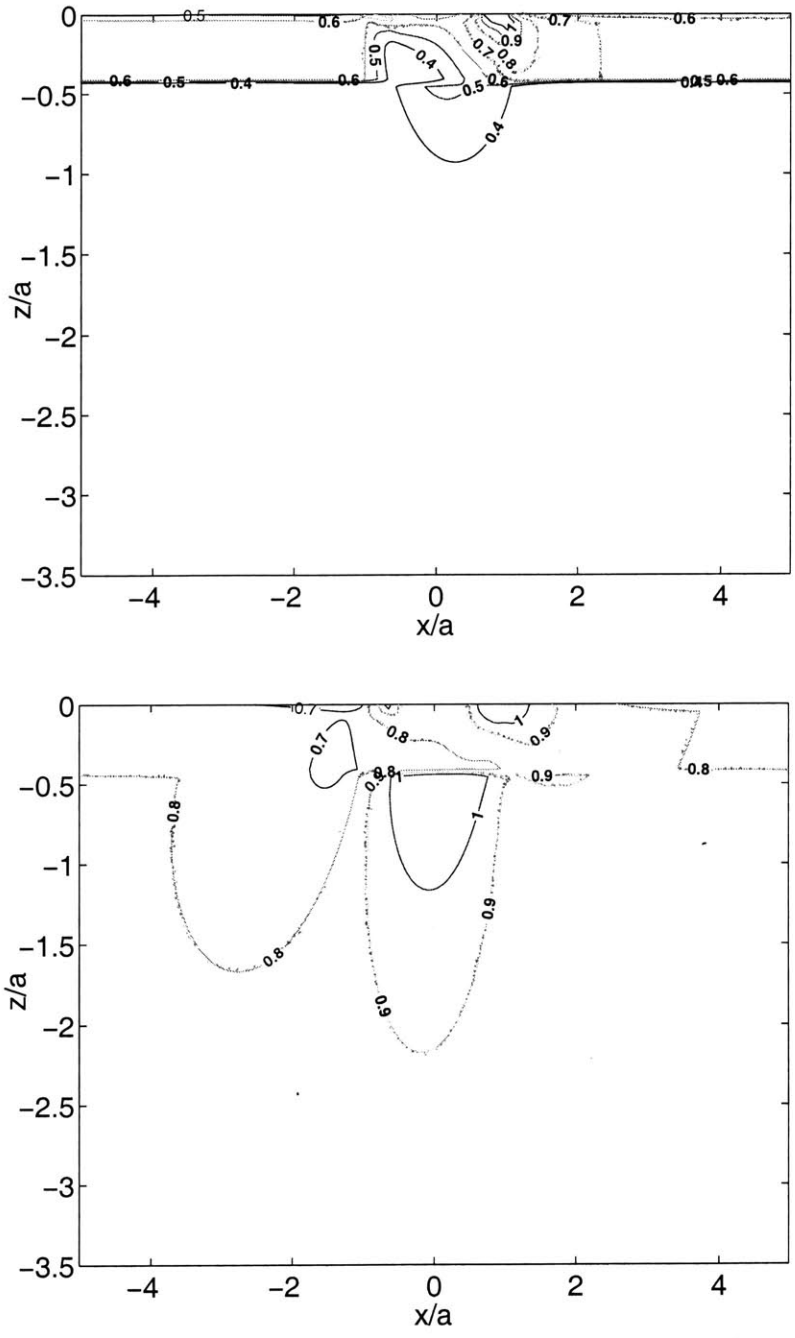

Figure 4-11: Von Mises equivalent stress contours, normalized by the yield strength, below a spherical pad for a normal force of 50 N, a tangential force of 35 N, a maximum axial stress of 778 MPa, and a stress ratio of 0.1, with residual stresses (-500 MPa at the surface, -650 MPa uniformly to a depth of 80 μm) at minimum tension (top; maximum σ_{eq}=1082 MPa) and maximum tension (bottom; maximum σ_{eq}=1420 MPa)

4.2 A fracture mechanics approach for fretting fatigue

In this section, we describe a model that allows to describe the entire life of a specimen subjected to fretting against a spherical pad in terms of crack propagation. A life-prediction methodology based on the ideas described in Section 2.2.7 is here proposed, and compared to actual data obtained on STOA specimens. The main assumptions of the model will be presented, and illustrated by the case of a variable tangential load for comparison with experiments, all other parameters being fixed. The effect of varying key parameters will then be presented, followed by comparisons with the experimental data available in [3]. The chapter closes on a discussion of the current capabilities and limitations of the model.

4.2.1 Principles of the model

It must first be noted that only the case of strong adhesion was considered in order to match the experimental observations [3]. Strictly following the adhesion-model leads to a prediction of weak adhesion in all the cases analyzed. The corrections on the critical debonding energies needed to match the experiments seem quite large, but proper optimization of these parameters has not been attempted yet. Another choice maintained throughout the analysis was the use of a coefficient of friction of 0.95, following the characterization of this parameter under fretting conditions for Ti-6Al-4V by Conner [3].

Compared to the methodology outlined in Section 2.2.7, the model presented here makes use of slightly different criteria for predicting the deflection of the crack, and uses a somewhat more sophisticate fracture mechanics approach to compute the stress intensity factor of the slant crack. As regards deflection, in the absence of convincing evidence in favor of any approach, the following assumptions were made:

1. for the initial angle, the maximum tensile stress criterion is applied when tension at the trailing edge is maximum. Therefore, the angle is sensitive to the normal

pressure through K_I, in order to account for the observations in [31] for a flat pad, which was the main reason behind modifying the methodology described in Section 2.2.8.

2. for the deflection normal to the remote uniaxial stress, it was assumed that the crack propagates in the direction where the propagation rate is maximal. As Paris's law was used in a simple form (see next paragraph) and the stress intensity factor solution for a 2D normal edge crack was used for the crack after deflection, this really means that the governing factor is the maximum stress intensity factor

Compared to the deflection criterion, the choice of appropriate stress intensity factor solutions can be a little more substantiated. First of all, the mode I stress intensity factor is considered as the single parameter determining crack propagation, an approach verified by Kitagawa et al. [48] on steel. Their work correlates the fatigue crack growth rate under uniaxial and biaxial loadings using apparent length and stress intensity factor, that is length and stress intensity factor projected along the direction the crack is progressively turning to, which is found to be the direction for pure mode I solicitation. In our case, it is assume that the slant crack propagates from the outset along such a constant direction, so projection is not needed.

Such a mode I stress intensity factor is given by the crack-analogue model (see Section 2.2.7) for the initial stage. Another is needed for the slant crack loaded by the contact and axial stress field. Among the methods presented in [91], Green's function method, or the more general weight function method, are the ones of choice for a first-time implementation. The problem of a semi-elliptical edge crack normal to the surface was studied, using the eigenstrain method [17][92], but no details of the solution were reported. To our knowledge, there are no published results for a slant semi-elliptical edge crack. On the other hand, Rooke et al. reported the detail of Green's functions for a 2D slant edge crack [93], obtained by including Bueckner weight functions into a boundary element method. Although it has been claimed that 3D calculations show some improvement over 2D for normal cracks at the edge

of contact [17], in the absence of a quantification or correlation to experiments, a 2D approach can be considered an acceptable choice for a first implementation. When the crack is "sufficiently long", it can be assumed that it propagates only under the influence of the remote axial stress. A reasonable assumption is then that the stress intensity factor at the tip of the kinked crack will become increasingly similar to the one experienced at the tip of a normal edge crack. Therefore, for long enough cracks, the solution for a 2D edge may seem appropriate. Alternatively, kinked-crack or 3D elliptical crack solutions could certainly be implemented. As the aspect ratio is not known for certain nor easily computed, and as the rest of the analysis is bidimensional, the approximation was considered sufficient and consistent. The reader is referred to Figure 4-12 for an illustration of the crack geometry and a summary of the modeling assumptions.

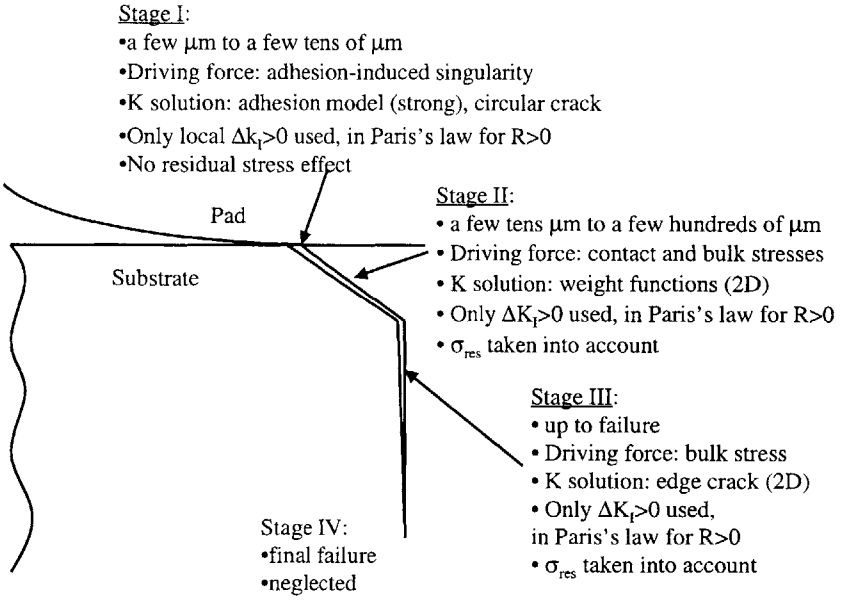

Figure 4-12: Summary of the modeling assumptions

Having define the deflection criteria and the three stress intensity factor solutions to be used, it is hypothesized that, at any stage, the solution giving the maximum mode I stress intensity factor is the driving parameter for crack propagation. As

illustrated for Figure 4-13 for instance, for a normal force of 50 N, a tangential force of 20 N, and an axial stress of 300 MPa, the crack would be driven by adhesion only up to about 4 μm, then the contact and axial stress would propagate it up to 50 μm, at which point the axial stress alone is sufficient to propagate it in a direction normal to the bulk stress. Note that at this point, the stress intensity factor is approximated by the one for a normal 2D edge crack under uniaxial stress. This modeling approach is consistent with the definition of stage I, II and III given in Section 2.2. The crack first propagates under the influence of the adhesion induced singularity only (stage I), then under the influence of the contact load as a slant crack (stage II), and finally under the influence of the bulk stress only (stage III).

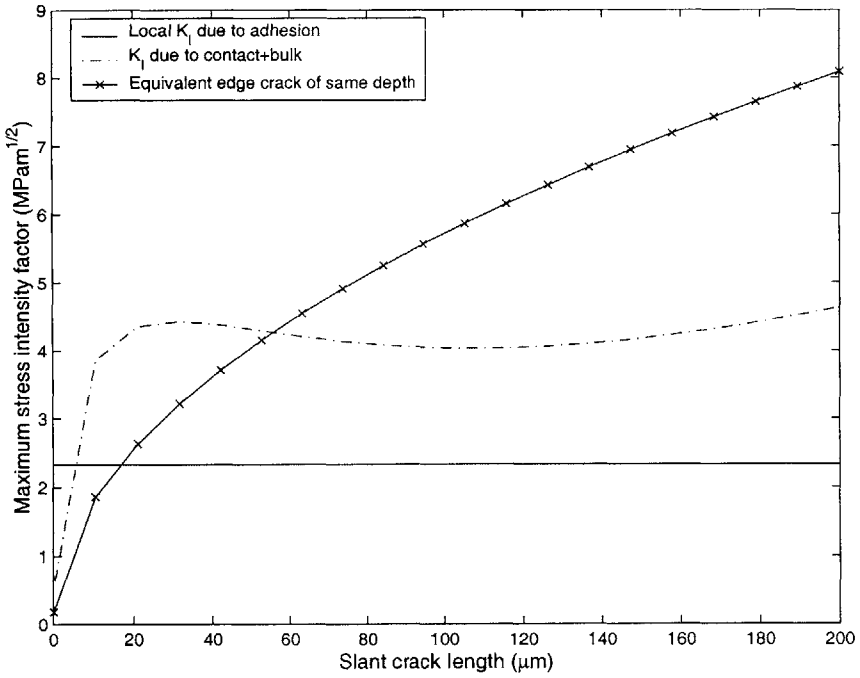

Figure 4-13: Variation of maximum stress intensity factors with length for P=50 N, Q=20 N, σ_{axial}=300 MPa; the crack angle is 67.1°

The numerical implementation is summarized in Figure 4-14.

At this point in the modeling, the variation of the initial angle with normal and tangential forces, and the deflection points as a function of normal, tangential and axial forces can already be examined. Figure 4-15 shows how the crack angle varies

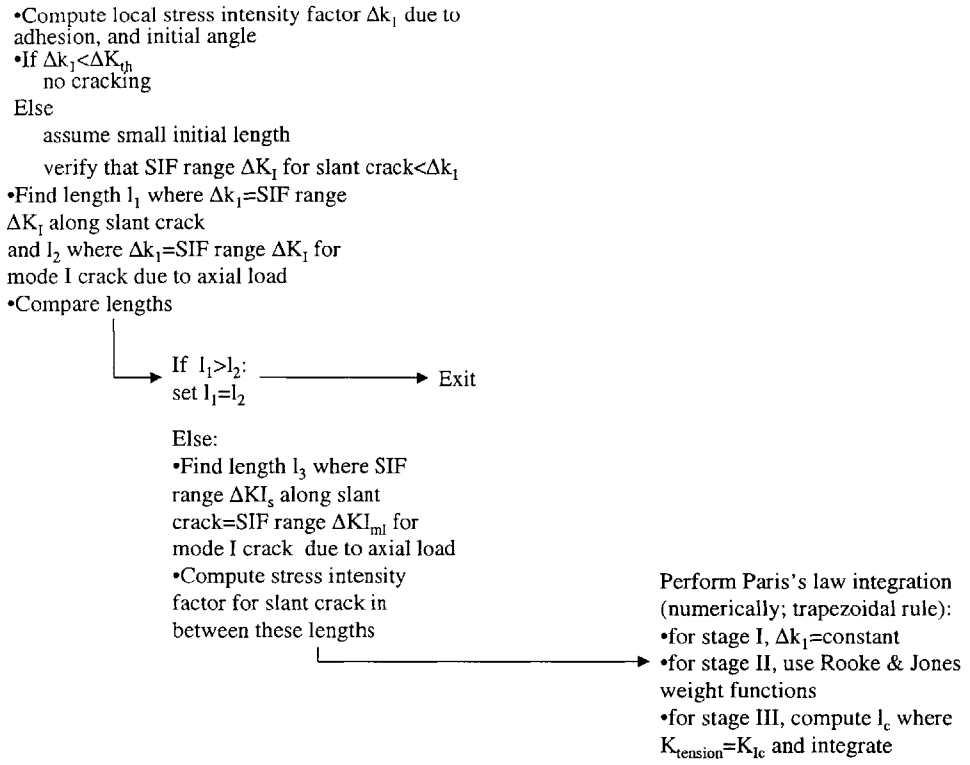

Figure 4-14: Flowchart of the numerical implementation of the fracture mechanics model

with the normal and tangential forces. An increase in the tangential force makes the crack steeper with respect to the surface, whereas an increase in the normal pressure makes the angle shallower. The variation is very limited for the geometry investigated. It is nonetheless consistent with the adhesion model formulation, where normal pressure really equates to mode I loading, and tangential force to mode II. However, at first sight, the latter prediction seems contradictory with the observations by Adibnazari and Hoeppner [31], on which the choice of the modification of the deflection criterion was based. This is an artifact of the data presentation. The authors based their observations on a flat-on-flat geometry, for which they were not able to report the variation in tangential force with normal pressure. As the third graph in Figure 4-15 shows, if it is assumed that the tangential and normal forces remain proportional when the normal pressure is increased, then the angle is indeed

predicted to increase.

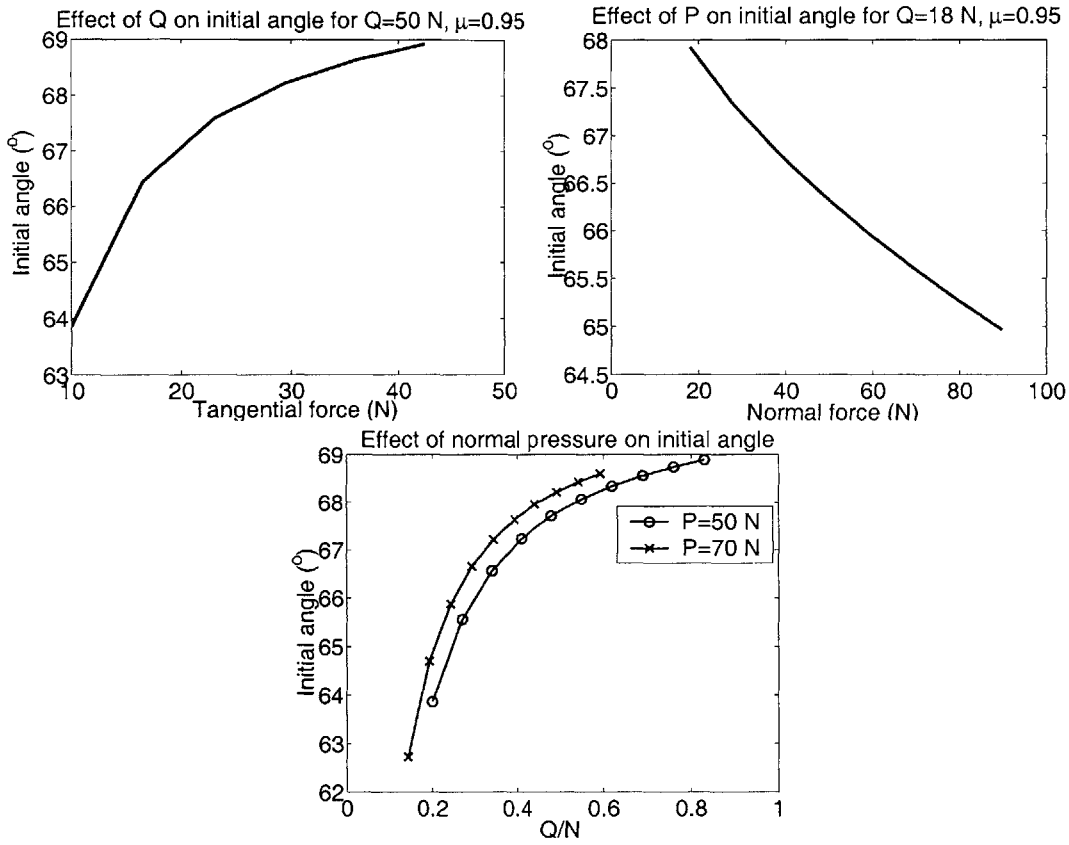

Figure 4-15: Variation of the initial crack angle with the tangential force Q for a normal force P=50 N (top left), with the normal force P for a tangential force Q=18 N (top right), and for different Q/P ratios (bottom)

Also, it is possible, for given loads, to determine the point where the contact stresses takes over from the adhesion-induced stresses, and the point of transition from slant to "normal" cracking. For illustration, the crack lengths for both transition are presented in Figure 4-16 as a function of the tangential force, for a fixed normal force of 50 N and a fixed axial stress of 300 MPa. Both lengths increase with increasing tangential force. Although this is expected for the slant-to-normal transition, as the magnitude of the contact stresses in depth will increase, it is less intuitive for the transition from adhesion to contact-induced cracking. In the latter case, it means that the strength of the adhesion-induced singularity decreases somewhat faster with the tangential force than the in-depth contrast stress. However tempting it could

be to try and infer what the consequences of these length variations with the load will have on the predicted life of the specimen, one has to bear in mind that the stress intensity factor magnitude will also play a strong role, so the discussion of the problem is deferred to the next section.

The increase of the length of transition with increasing tangential force, everything else being equal, is qualitatively in agreement with the experimental observations of Venkatesh et al. [21] on the STOA titanium alloy, but not on the mill annealed alloy. Quantitatively, the predictions underestimate the observations.

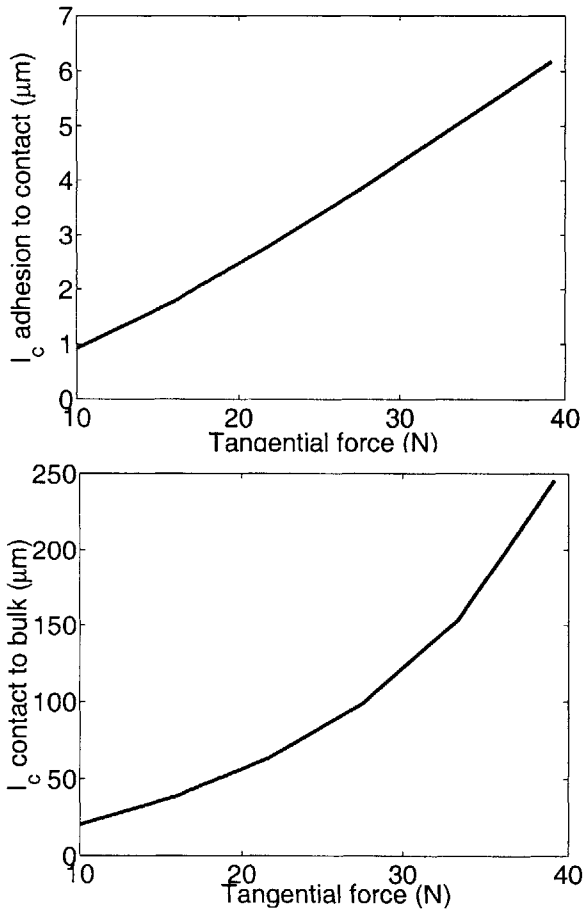

Figure 4-16: Variation of the length of transition from adhesion to contact-induced cracking (left), from contact to bulk stress-induced cracking (right), for a varying tangential force and a normal force of 50 N, an axial stress of 300 MPa

Once the crack path and associated stress intensity factors are defined, the next

important modeling assumption lies the choice of the crack growth law. Although the choice of a Paris's law is natural and hardly debatable, the question of whether and how to take closure into account is much more open. If crack growth data for the material investigated are available for the range of R ratio of interest in the problem, then, for long cracks, closure is taken care of in the data by similarity. In our case in particular, as it is often the case, data for our material at negative stress ratio were not available. As data for positive stress ratio have been published [50], a way to make use of them is to consider only the positive part of the stress strain history. The parameters depend on the R ratio (notably the coefficient), and, for Ti alloys, this dependence is largely due to plasticity-induced closure. Therefore, an option is to use data for high stress ratio, which usually exhibit minimum closure effects in the linear regime, if one doesn't want to include closure[2]. However, at low ΔK values, such data may include a significant amount of plasticity-induced closure. Another method could be to use stress intensity factor solutions that include displacement to readily check for closure, but the numerical complexity is greater and was not deemed essential for a first formulation in a short time-frame. The sensitivity to Paris's law parameters are discussed in the next chapter.

The last issue of interest at this point is the applicability of linear-elastic fracture mechanics. The parameters given by Giannakopoulos et al. [20] indicate that local and global plasticity will not occur due to contact alone. However, it was indicated in Section 4.1 that purely elastic conditions may not exist initially for all loading conditions when the contact and axial stresses are taken into account. This does not invalidate the use of LEFM concepts in the initial stage of the model as far as the crack size is concerned, as the relevant length scale is the contact size, which is much larger than the expected plastic zone. However, the size of the adhesion-induced K dominance zone may be a concern. For the mode I singular field induced by the normal force alone, the size of the K-dominance region, defined as the annulus of negative pressure, is about 3 μm for a typical normal force of 50 N. On the other

[2]The choice is in some sense not consistent with the use of the positive ΔK range, which is a step towards accounting for closure, yet forced by the lack of data rather than modeling choices

hand, for a relatively large value of Q of 45 N, the size of the plane-stress plastic zone due to the local K_I at the tip of the incipient kinked crack is around 10 μm. It drops to 0.5 μm for Q=10 N, and remains below 4.5 μm for the loads typically used by Conner [3]. No estimate for the mode II dominance is provided. Noting that, for typical loads, the point of transition between stage I and stage II is between 1 and 4 μm, the small-scale yielding condition can be expected to hold for the lowest loads, while the most severe conditions may not allow to enforce it.

4.2.2 Sensitivity to Paris's law (for the case of varying tangential load)

As just stated, a computation of plasticity induced closure was not attempted, but some insight may be gained by implementing several of the crack growth laws available in the literature, and discuss the model's responses to variations in the parameters and their implications. For comparison with experiments, the computations will be presented for the case of a constant normal and axial force, with variable tangential traction. Note that throughout the analysis, final failure is defined as the crack depth for which a semi-elliptical crack with an aspect ratio of 0.67 (the mean value reported by Conner [3]) reaches the edges of the specimen. Specifically, the Paris's law parameters selected are (with stress intensity factors in MPa$\sqrt{\text{m}}$, and lengths in meter):

- C=7.5x10^{-13}, m=4.1, derived by Conner [3] from Yoder and coworker's crack growth studies on mill-annealed Ti
- C=1.83x10^{-8}, m=3.01, obtained from Lenets and Bellows's work on Ti-6Al-4V STOA [94]
- C=2.43x10^{-11}, m=3.17, from the crack growth data of Boyce et al. [50] on Ti-6Al-4V STOA at a stress ratio of 0.8
- C=6x10^{-13}, m=4.4, from the review by Lykins et al. [40]

- C=5x10^{-12}, m=3.1, to illustrate the role and the physical importance of the exponent and the coefficient of the Paris's law

The choice of appropriate fatigue parameters directly relates to the ambiguous nature of the crack when the contact problem is cast into a fracture mechanics problem. From a physical point of view, it seems natural to consider the incipient fretting crack as a short crack free on closure effects. From a theoretical point of view, in the absence of clearcut provision in the derivation of the model, one can consider that the crack from which the fretting crack originates, although long, is just a mechanical artefact. So its length has no relevance to determine its closure properties. At most, some geometrical closure effect due to kinking under mixed-mode could be considered [95]. Therefore, the influence of using two different sets of Paris's law parameters, to account for a different behavior in the initial stage of crack growth, will be investigated.

Before presenting some results of the computation, a specific point of the numerical implementation should be emphasized: due to discretization, the number of cycles predicted by integration of the Paris's law is sensitive to the step size for the stress intensity factor computation. Step sizes were tried down to 0.1 μm: they make the computation exceedingly long for an improvement of at most 10% over 1μm increments. As the objective was not to fit the model to a particular application but to demonstrate its generic capabilities, the latter step size was considered acceptable.

Figures 4-17 to 4-20 compare the number of cycles to failure with data available in [3] for a normal force of 50N, and a fully-reversed axial loading of amplitude 300 MPa, for the Paris's law parameters given above. These computations don't take into account any threshold effect: the linear Paris regime is extrapolated down to the minimum value of ΔK, around 1.15 MPa$\sqrt{\text{m}}$.

The two laws with the lower Paris coefficients and higher exponents present a good agreement with the data (the implication of this observation will be discussed shortly). In particular, the rapid increase in total life at low tangential force is present in Figure 4-19 and 4-21, which is best illustrated with linear axis as in Figure 4-22. More significantly, as can be seen on Figure 4-23, this increase is predominantly due

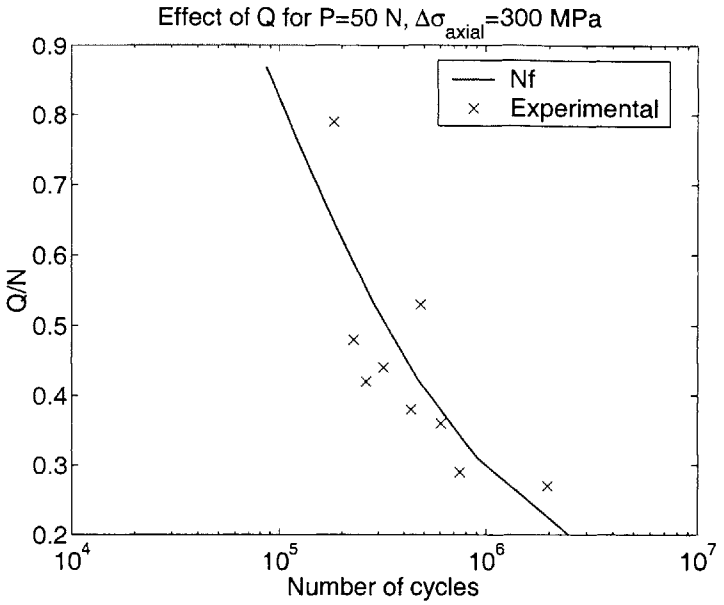

Figure 4-17: Number of cycles to failure for Paris's law parameters C=7.5x10^{-13}, m=4.1 (ΔK in MPa$\sqrt{\text{m}}$, length in meter)

to a longer stage I-II, which is in agreement with the observations by Conner [3]. The fact that the so-called stage I becomes predominant is also a satisfactory prediction. Recall indeed that the slant crack length for a low tangential force at the end of stage I is about 1 μm. This means that nucleating a sizeable crack takes an increasingly large number of cycles. This is consistent with the practical definition of nucleation as the existence of an observable defect, and the formulation includes some sort of asymptotical effect at low tangential force even when no threshold is specified. This observation also shed light on the initiation versus growth debate regarding fretting fatigue cracks. Physically, our understanding of fatigue crack growth mechanisms leads us to think that a phase of nucleation, where nothing happens but microphenomena that prepare for the appearance of substantial damage, takes place in the early phase. However, it is clear that the mechanics of the modeling implies quite unconventionally that a crack can start propagating right from the first cycle, albeit at a very slow rate. The analysis of Figure 4-23 and Figure 4-16 reconciles the two viewpoints, for all practical purposes, as at the end of the stage I phase, the crack

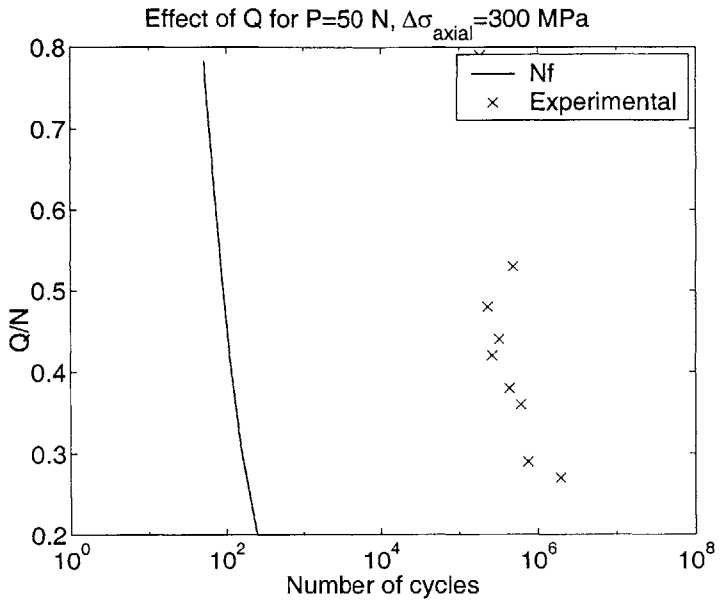

Figure 4-18: Number of cycles to failure for Paris's law parameters C=1.83x10^{-8}, m=3.01 (ΔK in MPa$\sqrt{\text{m}}$, length in meter)

length is predicted to be less than 10 μm. Yet, it is acknowledged and emphasized that the question whether a significant part of the total life is expanded to create a very small crack by either a nucleation or propagation process is a fundamental problem in fretting, and one of the most difficult to address practically. Interrupted tests or tests in the absence of bulk load, as illustrated in section 3.4.2, are seen as the best hopes to gain some insight on this topic.

Thus, it can be said that using only available linear crack growth data, with no tuning of the model, the agreement with experiments can be satisfactory, and more significantly, the trends are well captured. However two problems arise in this approach. First, the use of a linear crack growth law down to a very low stress intensity factor range, although advocated in the literature [94], may seem contradictory with the usual deceleration observed near the threshold. The slower growth at low ΔK is also valid for short cracks: although they are commonly said to propagate faster than long cracks for the same stress intensity factor range, the actual rate may be lower than an extrapolation of the Paris regime. And second, and more important, the

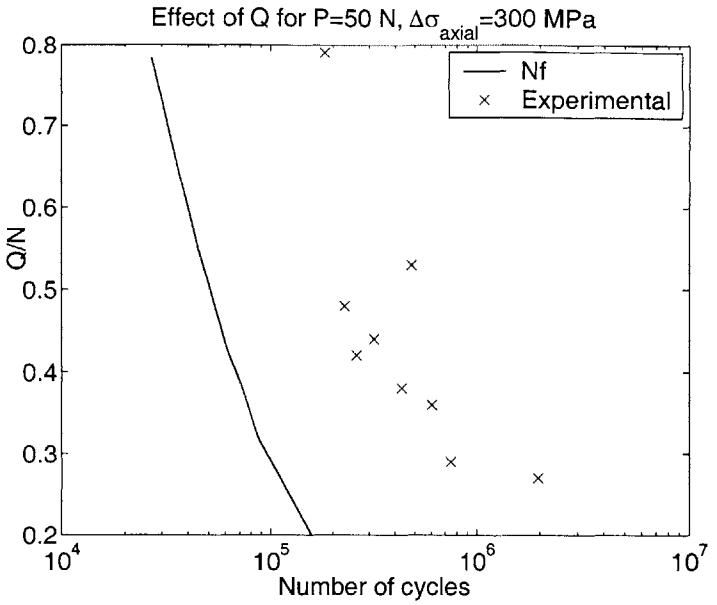

Figure 4-19: Number of cycles to failure for Paris's law parameters C=2.43x10^{-11}, m=3.17 (ΔK in MPa$\sqrt{\text{m}}$, length in meter)

agreement with the data is best when using an exponent close to 4, which corresponds to a mill-annealed Ti alloy rather than an STOA alloy, where an exponent of 3 would be more typical. The comparison of Figures 4-17 to 4-21 indicates that the value of the exponent, which is a material parameter, is critical to simulate the increase of endurance at low loads. The value of the coefficient, on the other hand, is dependent on the type of loading, and Figure 4-21 shows that a physically meaningful value for the STOA alloy (corresponding to a low stress ratio) can be used together with a representative exponent to simulate the behavior at high loads.

Therefore, it was inferred that two different regimes may have to be distinguished, one for the Paris regime and one for slow crack growth, which would account for the behavior at high and low loads respectively. Using crack growth rate data from [50], the possibility of using a non linear crack growth law was investigated. The high stress ratio law of [50] was approximated beyond the linear regime by a parabola, as shown on Figure 4-24. The linear regime for the solid curve is characterized by C=2.43x10^{-11} and m=3.17.

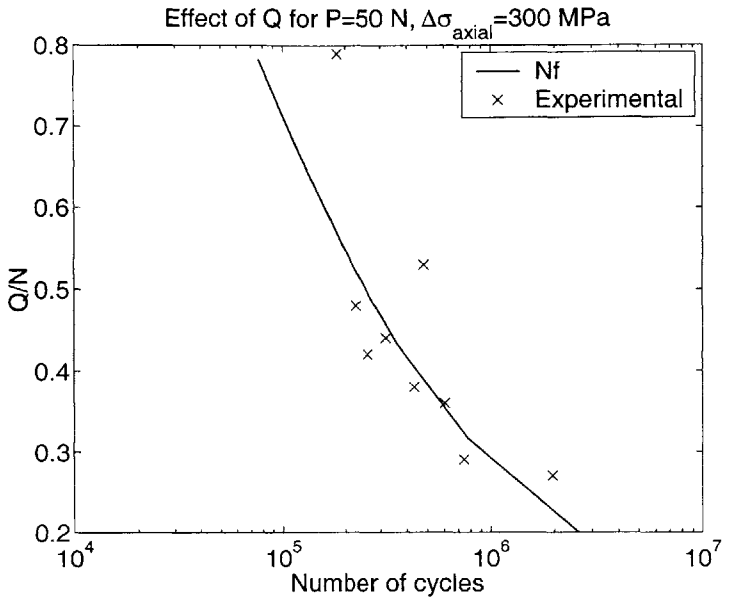

Figure 4-20: Number of cycles to failure for Paris's law parameters C=6x10^{-13}, m=4.4 (ΔK in MPa$\sqrt{\text{m}}$, length in meter)

As Figure 4-25 shows, and as intuitively expected, the use of a nonlinear law better captures the increase in total life at low tangential loads, without affecting too much the total life at lower cycles to failure. Combined with the previous observation that certain linear laws also allow to reproduce this behavior, it is clear that the key to a good agreement at low tangential loads is a slow crack growth rate (but not necessarily non linear), and that the nonlinear effect is really a consequence of the adhesion-induced initial cracking. Indeed, as discussed in Section 4.2.1 about Figure 4-16, the length over which the adhesion-induced field dominates decreases with decreasing tangential force. But so does the strength of the singular field, and the effects compound each other in a manner that leads to predictions consistent with experiments.

An important point must be made about the relevance of the parameters. First of all, the ideal situation in modeling occurs when only physical parameters are needed to make prediction. In our model, it is not exactly the case. Indeed, the Paris coefficient varies with the load, and Figures 4-25 and 4-26 use an upper and lower

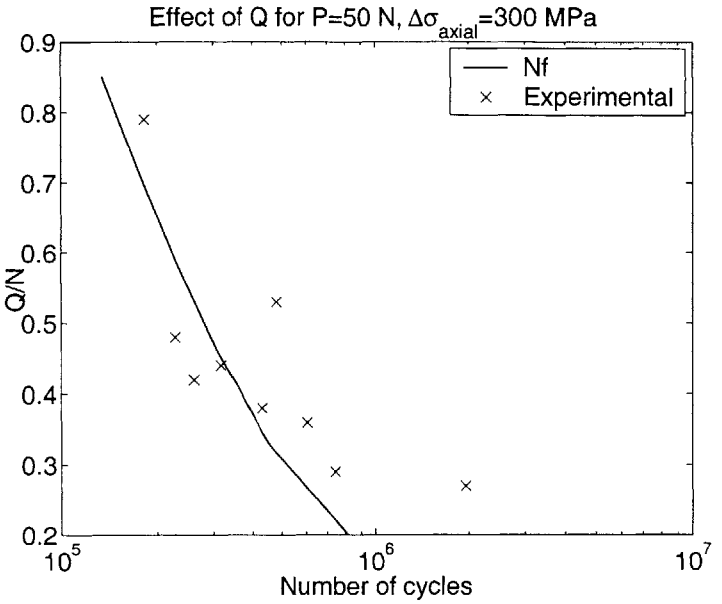

Figure 4-21: Number of cycles to failure for Paris's law parameters C=5x10^{-12}, m=3.1 (ΔK in MPa$\sqrt{\text{m}}$, length in meter)

band for the coefficient for large and small positive stress ratio respectively, with a parabolic decrease of the crack growth rates at low stress intensity factor amplitudes. For the latter case, which is somewhat more consistent with the use of the positive part of the stress intensity factor cycle, we can see that the agreement is rather good, with some underestimation. Unfortunately, crack growth rate data near the threshold is quite often dependent on the procedure used, and cannot be considered a material parameter. There is then some required tuning of the model to get a perfect agreement, and one must ensure that the tuned parameters remain physically appropriate. The only way to take the uncertainty out would be to compute the load ratio at any stage of crack growth and use corresponding crack growth rate data, but such a database is hardly available for any material. Alternatively, short crack growth data may be of interest, but availability in the literature may also be a problem. Another important consideration is that good results were obtained with parameters close to the expected physical values. As usual in modeling, if such parameters can be shown to be not physical but intrinsic, they constitute an apt choice from a modeling

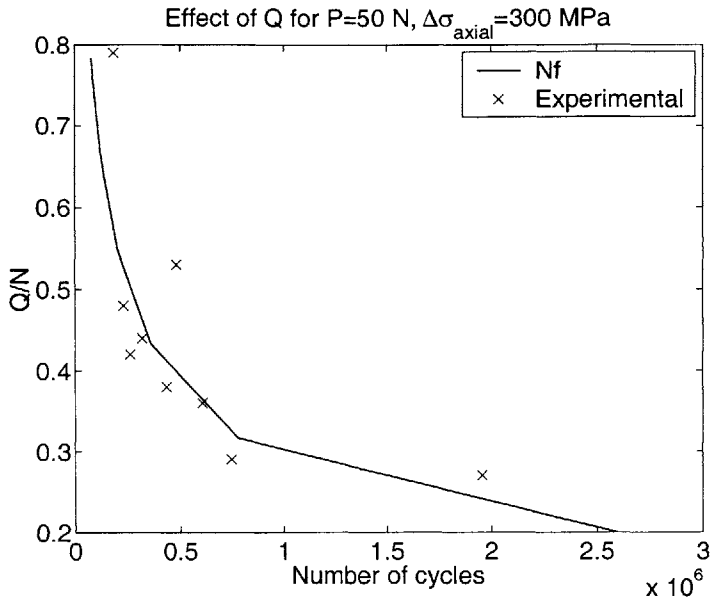

Figure 4-22: Number of cycles to failure and in stage I-II-III for Paris's law parameters C=6x10^{-13}, m=4.4, with linear axis (ΔK in MPa$\sqrt{\text{m}}$, length in meter)

point of view.

Lastly, a systematic study of the variations of the C and m parameters of the Paris's law was carried out. The results are shown on Figure 4-27.

The sensitivity of the total life to the Paris's coefficient is obviously strongly non linear, as it appears linear on a log scale when C is changed by factors of 10 (the exponent being constant throughout and equal to 4). The effect of changing the exponent for a fixed coefficient of C=5x10^{-13}, in terms of curve shift, is also gradual on a log scale. The most significant effect is the increasing non-linearity at low loads with increasing exponent. Therefore, for tuning of the model, these results suggest that the Paris's coefficient can be changed to position the curve, whereas the exponent will have a more direct effect on its shape, as previously mentioned. Beyond the "freedom" provided by the above considerations for fitting experimental data, a more fundamental point regarding the relevance of the modeling can be made: considering the breadth of parameters spanned in this study, it is encouraging that the ones which best agree with the experiments are both physical and close to published values for

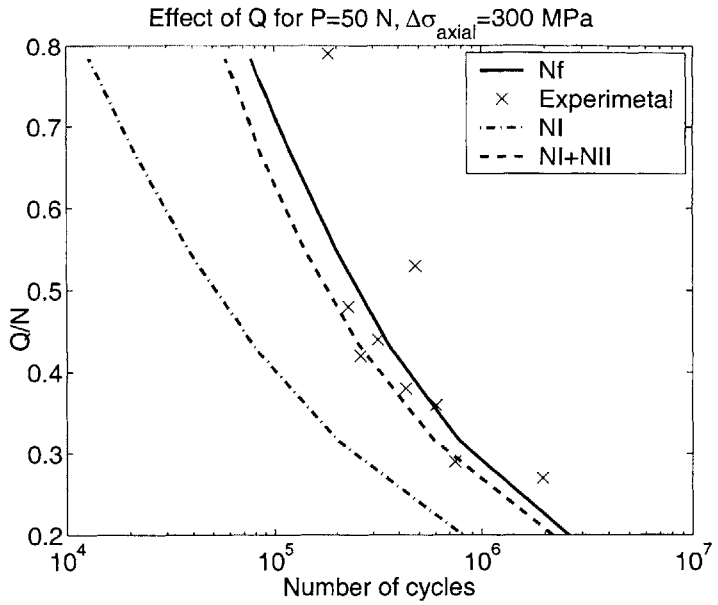

Figure 4-23: Number of cycles to failure and in stage I-II-III for Paris's law parameters C=6x10^{-13}, m=4.4, with linear axis, (ΔK in MPa$\sqrt{\text{m}}$, length in meter)

titanium alloys. However, the discrepancy mentioned previously about the exponent points to the probable need for more than one Paris's law, and it is emphasized that, although the parameters used are relatively physical, a finer identification of a physical crack growth law is yet to be performed.

4.2.3 Comparison with experiments for varying normal and axial loads

Some of the well-documented data by Conner [3] on the effect of the normal and axial loads are here compared to the model's predictions for a linear Paris law with C=7.5x10^{-13} and a parameter m=4.1. Note that, here, these parameters do apply to the mill-annealed Ti-6Al-4V alloy on which the experiments were performed. It is seen on Figure 4-28 and 4-29 that the agreement is satisfactory for the effect of the normal load, although the increase in life at large normal load may be less gradual than the simulation suggests. This pattern is similar to the one observed for the experiments with varying tangential load, and the cause is presumably the same.

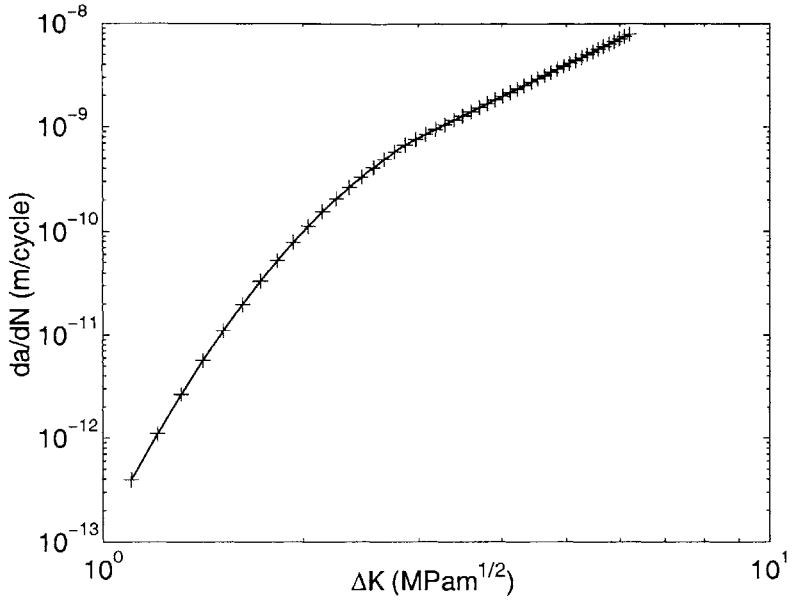

Figure 4-24: Example of a non-linear crack growth law for Ti-6Al-4V STOA

The effect of the axial stress, which was assessed for several tangential loads and pad radii, is not as well predicted. In this case, only the broad trends (increase in life with decreasing tangential force and increasing pad radius, with a marked effect of the former) are captured, although it can be argued that the data and predictions are still within a reasonable factor for a fatigue problem. Nevertheless, the slope in a log-linear format is not as well predicted as for the other set of experiments. This point will be discussed further in Section 4.2.6.

The effect of varying loads on the transition lengths was also examined. Figure 4-30 and 4-31 illustrates the effect of varying the normal force and the axial stress respectively, all other parameters being fixed. The latter is in the form of a log-linear graph to show how the pad radius affect the location of the curve, while the tangential load also affect its slope.

The decrease in the length of transition from stage II to III with increasing normal load is conform to intuition, as noted by Venkatesh et al. [21]. However the data they present for the mill annealed material show an increase at low loads and a decrease at high loads. As in Section 4.2.1, the predictions underestimate the observations (the

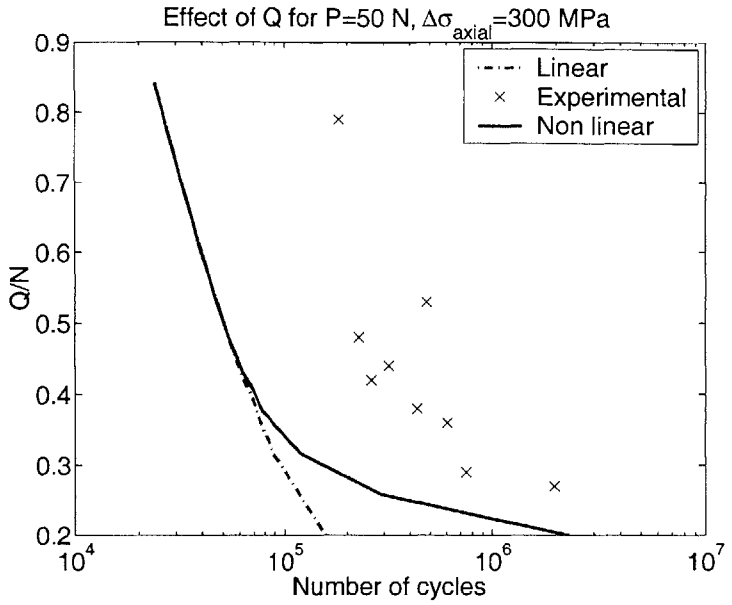

Figure 4-25: Number of cycles to failure for Paris's law parameters C=2.43x10^{-11} and m=3.17 beyond 3.1 MPa$\sqrt{\text{m}}$ (ΔK in MPa$\sqrt{\text{m}}$, length in meter), and a parabolic crack growth law below (solid curve), and a linear law only (dash-dotted curve)

materials are only slightly different).

On the other hand, the decrease in the transition length with increasing axial stress is fully consistent with the trend of the data of Venkatesh et al. [21]. Also, the increase with increasing pad radius, everything else being equal, is also captured by the model. Yet once again, the agreement is only qualitative, with underprediction by the model.

4.2.4 Effect of residual stresses

As the only measured residual stress values were at the surface (see Section 3.3), a stress profile for the T1 treatment was constructed using simulations obtained from Metal Improvement Co. , using the Peenstress^{TM} software. The stress at the surface is taken to be -500 MPa. Below the surface, a constant compressive stress of -650 MPa is imposed to a depth of 80 μm, where it drops to zero. Some comparisons of computations and experiments are qualitatively discussed on this basis. The

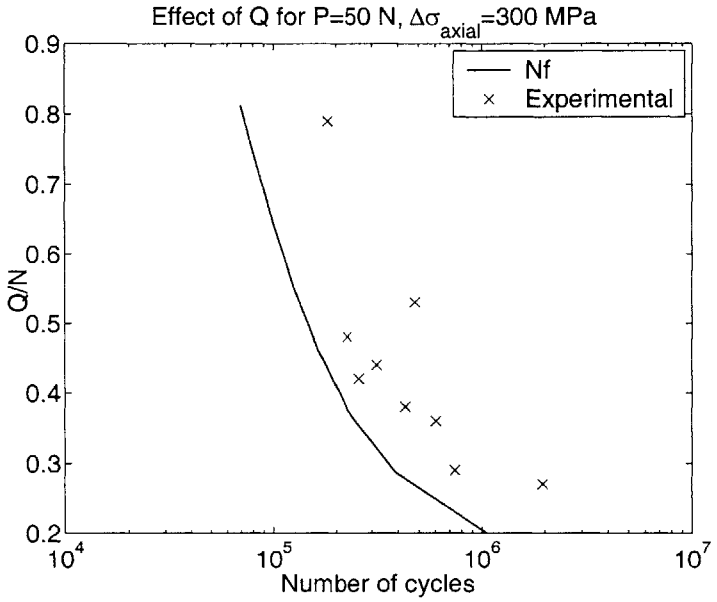

Figure 4-26: Number of cycles to failure for Paris's law parameters C=5x10^{-12} and m=3.17 beyond 5 MPa$\sqrt{m}$ (ΔK in MPa$\sqrt{m}$, length in meter), and a parabolic crack growth law below

three stages of crack growth distinguished so far require a different treatment of the residual stresses. Formally, the derivation of the adhesion-induced singularity presented in Section 2.2.7 is not modified by an additional stress in one of the contacting components[3]. Therefore, it is assumed as in the previous section that this singular field will drive the crack irrespective of the residual stress magnitude. On the other hand, the work of Wilks et al. [17] has shown that residual stresses in fretting fatigue can be normally superimposed in a weight function approach. Consequently, in the slant crack stage and the stage that follows, the contribution of the residual stresses is computed separately using weight functions (for a 2D slant crack or 2D normal crack respectively), and the resulting stress intensity factor added to the one due to the other loads. The difficulty that ensues is that, as one can intuitively figure, the adhesion-induced stress may remain much higher than the contact or bulk induced stress over a relatively large depth. It was seen in Section 4.2.1 that the depth over

[3]Provided the additional stress doesn't affect adhesion, which is may be the case to a first order

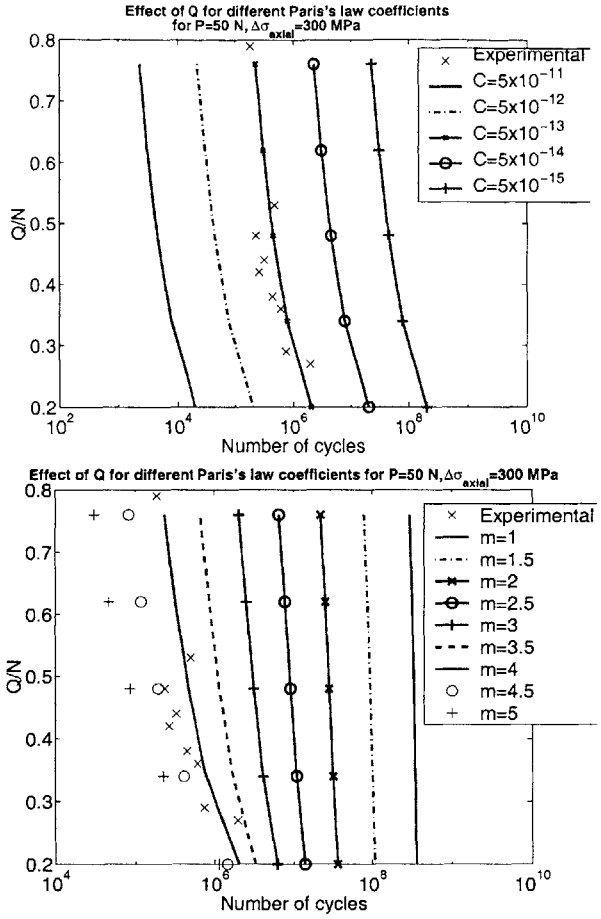

Figure 4-27: Number of cycles to failure for m=4 and various Paris's coefficients (top), and for C=5x10^{-13} and various Paris's exponents (bottom) (ΔK in MPa$\sqrt{\text{m}}$, length in meter)

which one can reasonably expect this singularity to be effective is of the order of a few microns only. The problem is illustrated on Figure 4-32, where the stress intensity factors as a function of depth have been computed for four of the experiments on the T1 treated specimens.

The two top simulations represent experimental conditions that lead to failure in less than 7x10^5 cycles, whereas the bottom ones didn't lead to failure after more than 4x10^6 cycles. The plots contain a reasonable value for the crack propagation threshold determined by Boyce et al. [50]. Negative values of the stress intensity factors have been set to zero. One way to consistently interpret these results is to note that for

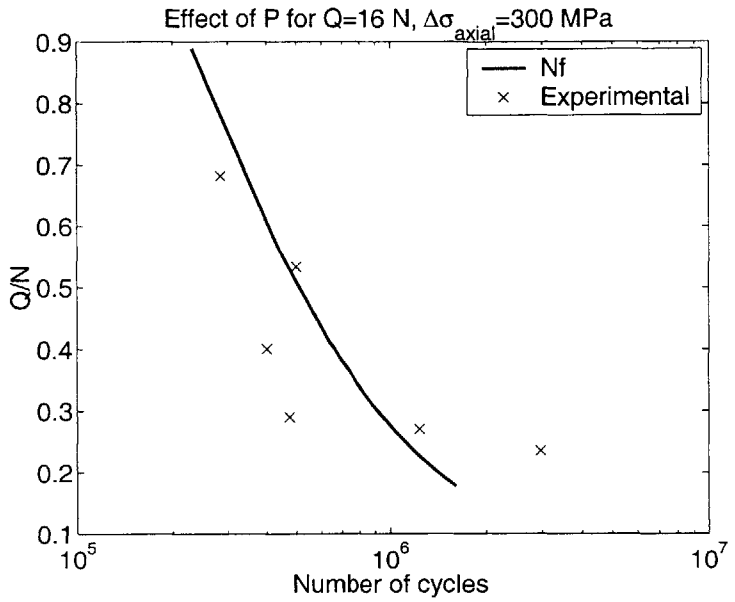

Figure 4-28: Number of cycles to failure for varying normal load and a fixed tangential force Q=16 N, and a bulk stress of 300 MPa

the experiments that did fail:

- the stress intensity factor for stage II exceeds the threshold value at a depth of about 5 μm
- the stage II stress intensity factor drops close or slightly below the threshold value before picking up again

On the other hand, for the two experiments that did not show failure, the stage II stress intensity factors barely exceeds the threshold value, and subsequently drop to zero. Clearly, the threshold effect could explain the occurence or absence of failure. The fundamental question however is how the transition between stage I and II can occur. The model predicts that a crack should propagate over a length of about 4 μm, where the adhesion-induced singularity is active. As can be seen on the two top plots, the stress intensity factor for stage II at this depth may not reach the stage I value, but still exceed the threshold value. It is then suggested that, under this condition, the stage II stress intensity factor may take over, and that relatively

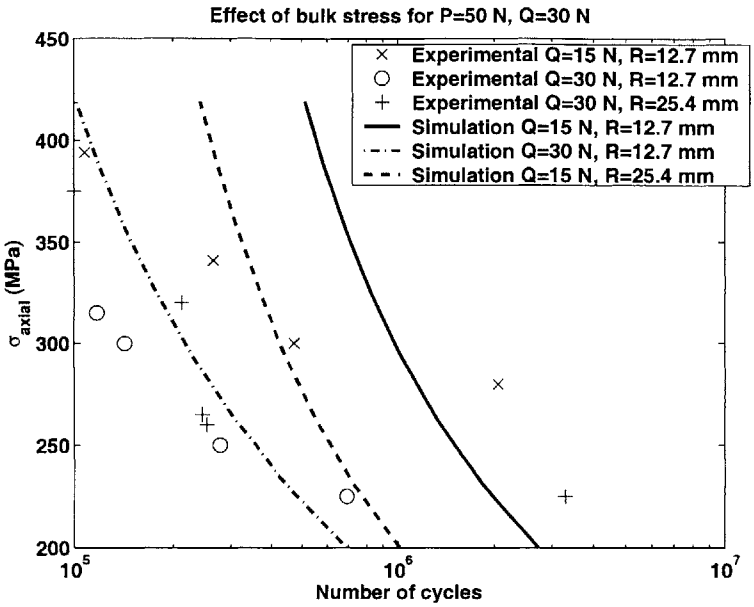

Figure 4-29: SN curves for various tangential forces and pad radii, for a fixed normal force of 50 N

long arrested cracks (on the order of 20 μm) might be expected for suitable rates of decrease of the stage II stress intensity factor. In other words, the transition may not necessarily occur if the slant crack stress intensity factor exceeds the adhesion-induced stress intensity factor, as it was assumed previously, but rather if the slant crack stress intensity factor reaches a large enough value above the threshold at the depth where the adhesion-induced singularity fades away. The measurement of the length of arrested cracks in known residual stress fields would help to choose the most relevant condition.

It must be emphasized that the above discussion is highly qualitative, due to the absence of precise measurement of the residual stress profile and the uncertainty on the threshold value. Also, the size of the plastic zone due to the contact and bulk stress is relatively deep for the tests analyzed (ranging from 4 to 13 μm). How this will affect the residual stress distribution near the contact edge is not known. However, as the high stress region extends rather outward from the contact edge, it may not impact the analysis too severely. In spite of these uncertainties, this modeling

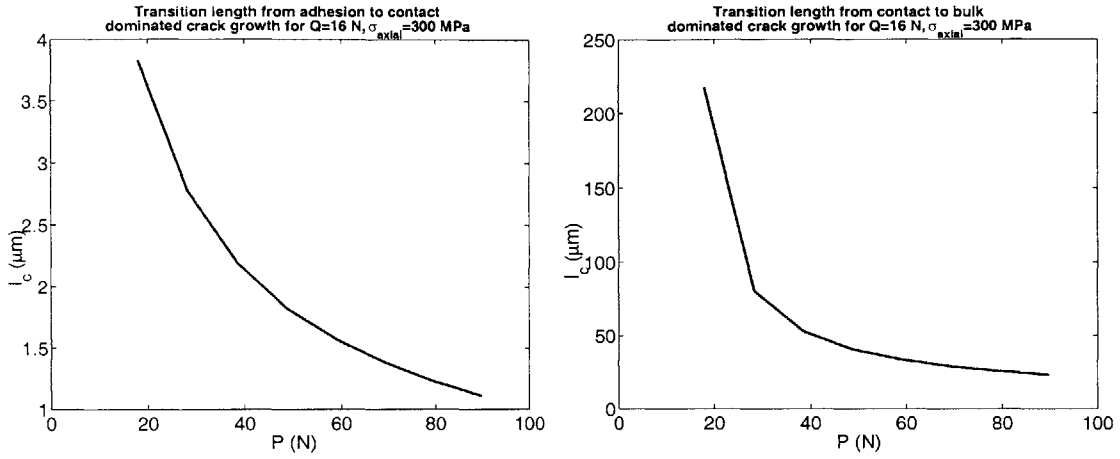

Figure 4-30: Variation of the length of transition a) from adhesion to contact-induced cracking, b) from contact to bulk stress-induced cracking, for a varying normal force and a tangential force of 16 N, an axial stress of 300 MPa

approach seems attractive because it is consistent, and lends itself to experimental verification via the measurement of the depth of arrested cracks.

4.2.5 Analysis in the absence of bulk stress

The analysis can be extended to the damage growth prediction in the absence of bulk stress, which can be related both to specimens in pure fretting or to the pads used for fretting fatigue experiments. This once again points to the need for a characteristic length over which adhesion is capable to propagate a crack.

Consider indeed Figure 4-33. The curves represent the maximum stress intensity factor (or equivalently the positive stress intensity factor range) for two experiments typical of Conner's work [3] and one from Lamacq et al. [42], who used the sphere-on-flat geometry. For the first two graphs, representative of Ti-6Al-4V, the normal force is 50 N and the tangential force 20 and 30 N, for a pad radius of 12.7 mm. For the third one, representative of a 7075 aluminum alloy, the normal force is 900 N and the tangential force is 930 N, for a pad radius of 0.3 m. For the first two cases, it is seen that the stress intensity factor due to contact peaks up above a reasonable threshold value at a length of about 5 μm at most, never reaches the magnitude of the

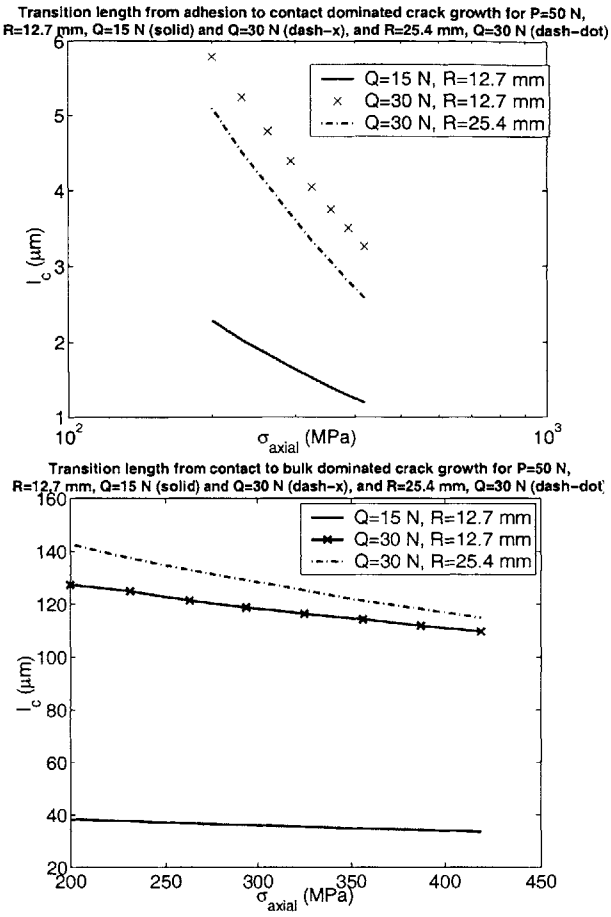

Figure 4-31: Variation of the length of transition a) from adhesion to contact-induced cracking, b) from contact to bulk stress-induced cracking, for a varying axial stress and a tangential force of 15 N and 30 N, a fixed normal force of 50 N, with two different pad radii

singularity due to adhesion, and then drops below the thershold value. As explained previously, it would be utterly unrealistic and unphysical to assume that just because the adhesion-induced stress intensity factor exceeds the threshold value, a crack will just grow to any length. It is more realistic to postulate that the adhesion-induced singularity can be efficient in propagating the crack over a length comparable to the K-dominance zone of the adhesion-induced singularity, which is about 3 μm. Then, if the stress intensity factor due to contact is high enough, the crack can grow further before arresting. As explained before, it is not obvious whether "high enough" means that the K factor should exceed the adhesion-induced K factor of just the threshold.

Settling this question would require a very precise knowledge of the threshold, of the K-dominance region for both loading modes (only mode I was considered here), carefully controlled experiments and difficult observations of arrested cracks. In any case, our model predicts that cracks ranging from a few microns (to possibly a few tens of microns, depending on the loads and modes of transition just discussed), should be observed in the pads used by Conner [3]. That is, however, in the absence of perturbative effects, such as those of the oxide layer outlined in Section 3, or instabilites in the contact location.

For the third case, the stress intensity factor due to contact is steadily increasing over the first 200 μm, after exceeding a value of 2 MPa$\sqrt{\text{m}}$ at about 10-15 μm. Note this threshold value is more indicative, as it is not as previously the result of extensive research on the same material, but a value used by Newman et al. [96] for 7075-T6 long crack threshold (0.9 MPa$\sqrt{\text{m}}$ was used as a small crack threshold). In this particular case, the K_I-dominance zone defined in Section 4.2.1 is about 32 μm. Therefore, all elements point at the possibility of propagation of cracks several tens of microns long in the absence of axial fatigue stress for this contact condition, as the curve picks up to 5 MPa$\sqrt{\text{m}}$ at about 400 μm, then decreases to 3 MPa$\sqrt{\text{m}}$ at 2mm. This is indeed what was reported by Lamacq et al. [42] both for the specimen under a constant axial load and for the pads, in which cracks longer than 100 μm and of at least a few tens of microns respectively were indeed observed. The latter example raises the interesting question of the relative importance of the size and the magnitude of the loads in such a result. From the expressions presented in Section 2.2.7, it can be seen that for a constant average pressure and a constant $\frac{c}{a}$ value, the mode II stress intensity factor due to adhesion scales as the square root of the spherical pad radius, leading to a faster initiation for large pads[4]. However, if the stick zone to contact radius ratio is not maintained, the mode II stress intensity factor varies as $\frac{Q_{max}}{R^{\frac{3}{2}}}$, where Q_{max} is the maximum tangential load and R the contact radius. Initiation can then be faster or

[4]This is another reason, besides ease of observation, why large pad radii may be preferable, as the strength of the mode II singularity may overcome possible shielding effects of wear and oxide build-up

slower depending on the exact loading conditions. Thus, as observed and rationalized by Hills and Urriolagoitia-Sosa [97] using a stress approach, the adhesion model used incorporates a size effect for initiation.

Thus it is seen that the model also rationalizes available observations in the absence of bulk stress. It must be emphasized that the propagation or arrest of cracks is really dictated by the fracture mechanics analysis of the slant crack under the influence of contact alone. The truly original prediction of the model is that very short cracks should be present very early on in the life, which may unfortunately be quite difficult to observe, all the more so as mechanical polishing can leave compressive residual stresses (see Section 3.2.3 and [56]).

4.2.6 Conclusions and perspectives on modeling

Overall, the fracture mechanics based fretting model developed in this work accounts for most of the characteristic trends observed in fretting, such as the effects of the various loads on the total life. Even when using simple Paris-type crack growth laws, the quantitative agreement is acceptable in most cases. The large increase in the early stage of crack growth at low loads is particularly well picked up. The model also exhibits good response to variations of the crack growth law, which leaves room for optimization and tuning within physical constraints. It was shown that different regimes of crack growth, depending on the crack length, can give a better description of the threshold effect at low loads. Some predictions, such as the variation of the transition length from stage II to III, can be compared only with limited reliable data, but seem to conform to the physics of the problem (see [21].

That being said, it is useful to emphasize some of the assumptions already mentioned and point to possible improvements of the modeling approach. One of the main differences with the theory by Giannakopoulos et al. [20] is the use of strong adhesion, when weak adhesion is expected for any tangential load in excess of 12 N. As can be seen on Figure 4-34, for a normal load typical of Conner's tests [3] and ours, weak adhesion would impose an initial stress intensity factor that remains very low compared to the threshold value of 2 MPa$\sqrt{\text{m}}$ proposed by Ritchie and coworkers [50].

This indicates that, although strong adhesion seems to be supported by observations and gives satisfactory predictions, more work may be needed to fully characterize the adhesive parameters used in the model.

Another "shortcoming" of the model is the lack of threshold effect. The easiest way to introduce a threshold effect is to implement a "cut-off value" of the stress intensity factor that stops the computation. A reasonable estimate could be the value of 2 MPa$\sqrt{\text{m}}$ just mentioned. But a threshold value of 2 MPa$\sqrt{\text{m}}$ would not allow for crack growth below a tangential force of about 17 N, whereas, in untreated specimens, failure was obtained for tangential loads as low as 10 N [3]. However, this objection is valid if the threshold value is taken as a mode I threshold for the local stress intensity factor at the tip of the incipient kinked crack. Another solution is to use the global mode II stress intensity factor to predict the possibility of kinking itself, as was done by Venkatesh et al. [21]. For strong and weak adhesion respectively, this parameter turns out to be 2 and 1.7 MPa$\sqrt{\text{m}}$ for a tangential force of 10 N[5]. Care must be taken here because, a priori, the threshold value obtained by Boyce et al. [50] for a mode I tension-tension configuration may not be directly relevant for the mode II fully-reversed loading just described. The extensive work by Campbell and Ritchie [98][99] on mixed mode threshold suggests that a value of 5 MPa$\sqrt{\text{m}}$ may be more appropriate as a mode II threshold at positive R ratio. Actually, the problem of accurately measuring an intrinsic mode II threshold is very difficult because of roughness closure. In our case, it is really an intrinsic value we are looking for, as a static mode I loading is present to open up the crack. As no reliable value for the mode II threshold at R=-1 was available, and as such a value would have been only indicative since a static mode I is superimposed, it was chosen not to implement any threshold effect. In support of the choice, it can be argued that the model does not necessarily requires it, as it naturally captures the high increase at low loads, although possibly at the expense of crack propagating in mode I for a positive stress intensity factor of about 1 MPa$\sqrt{\text{m}}$, and maybe some inaccuracy for large normal load/low tangential load combinations (see Figure 4-28). Also, any firm conclusion

[5]It must be emphasized that this is indeed a range, not the positive part of the cycle

on the appropriate threshold is made difficult by the short versus long crack dilemma already mentioned about the crack growth parameters (see Araújo and Nowell [41] for a discussion of the issues associated with the short crack threshold problem in fretting).

The last significant discrepancy between the predictions and experimental data was the effect of the axial stress. The possible explanation might be the relatively crude modeling of the crack in stage III by a 2D edge crack. The use of 2D kinked crack solutions or 3D semi-elliptical crack solutions might be advisable. The former was not implemented because the difference in the stress intensity factor with the 2D edge crack model was deemed not significant enough, at least for low values, while the latter raises the technical question of the aspect ratio, and the engineering question of the trade-off between modeling complexity and accuracy. An additional benefit of a more sophisticated stress intensity factor analysis could be to shed light on the closure problem mentioned in the previous section, thus helping in the choice of crack growth parameters.

Going to more technical details, the limitations discussed in Section 4.1 regarding the eccentricity and finite width effects should be born in mind, as well as the problem of shakedown for the severe loading conditions. Of course, as is almost always the case, the accuracy of the analysis may also benefit from more a sophisticate treatment of the numerical aspect of the modeling, such as the integration and interpolation processes, although separate validation of each modules suggest it would not be beyond a few percents.

Lastly, it is acknowledged that the material-related aspects of the problem, such as the effect of oxides, are still lacking in this predominantly mechanical framework. Some considerations on them are given in the appendices.

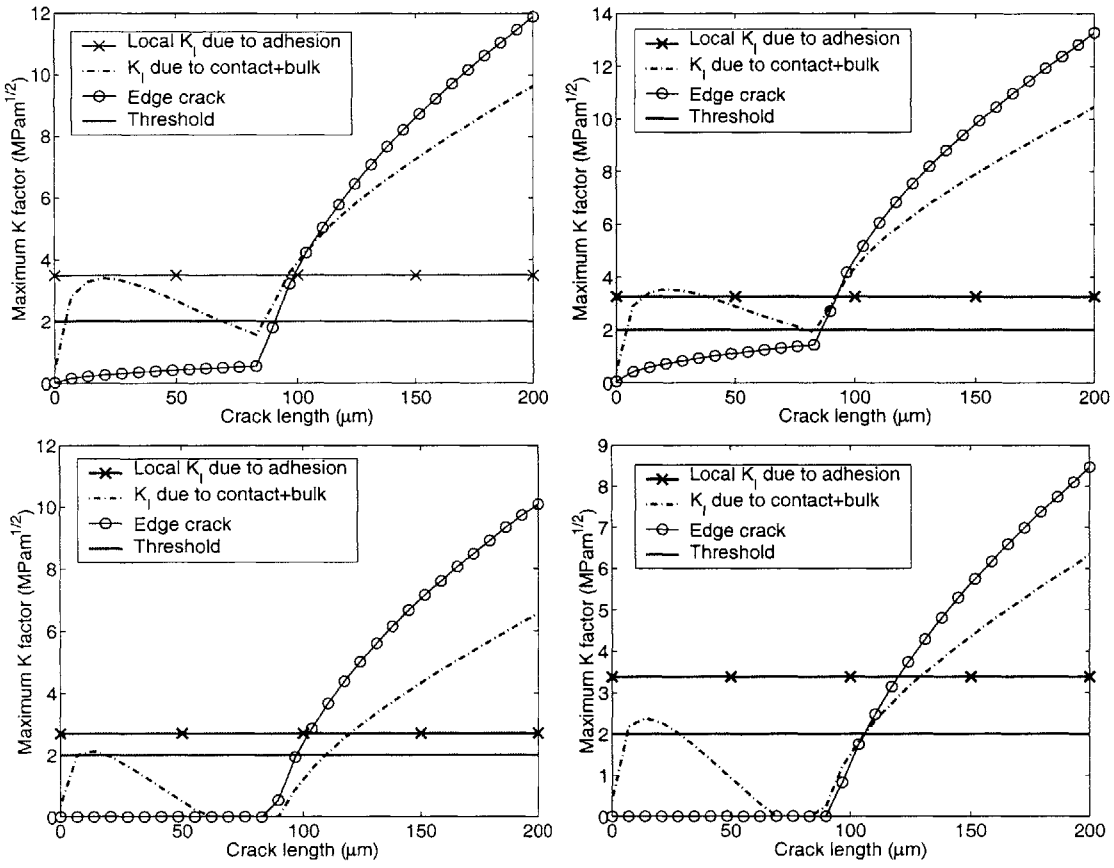

Figure 4-32: Variation of the stress intensity factors with crack length, for the first three stages of fretting fatigue, for two specimens which failed before 7x10^5 cycles (top), and for two specimens which did not fail after 3x10^5 cycles (bottom), in tension-tension tests; a residual stress profile of -650 MPa to a depth of 80 μm was used to simulate the T1 treatment (loading conditions: top left: Q=30 N, $\Delta\sigma_{\text{axial}}$=290 MPa, top right: Q=28 N, $\Delta\sigma_{\text{axial}}$=315 MPa, bottom left: Q=23 N, $\Delta\sigma_{\text{axial}}$=260 MPa, bottom right: Q=29 N, $\Delta\sigma_{\text{axial}}$=235 MPa)

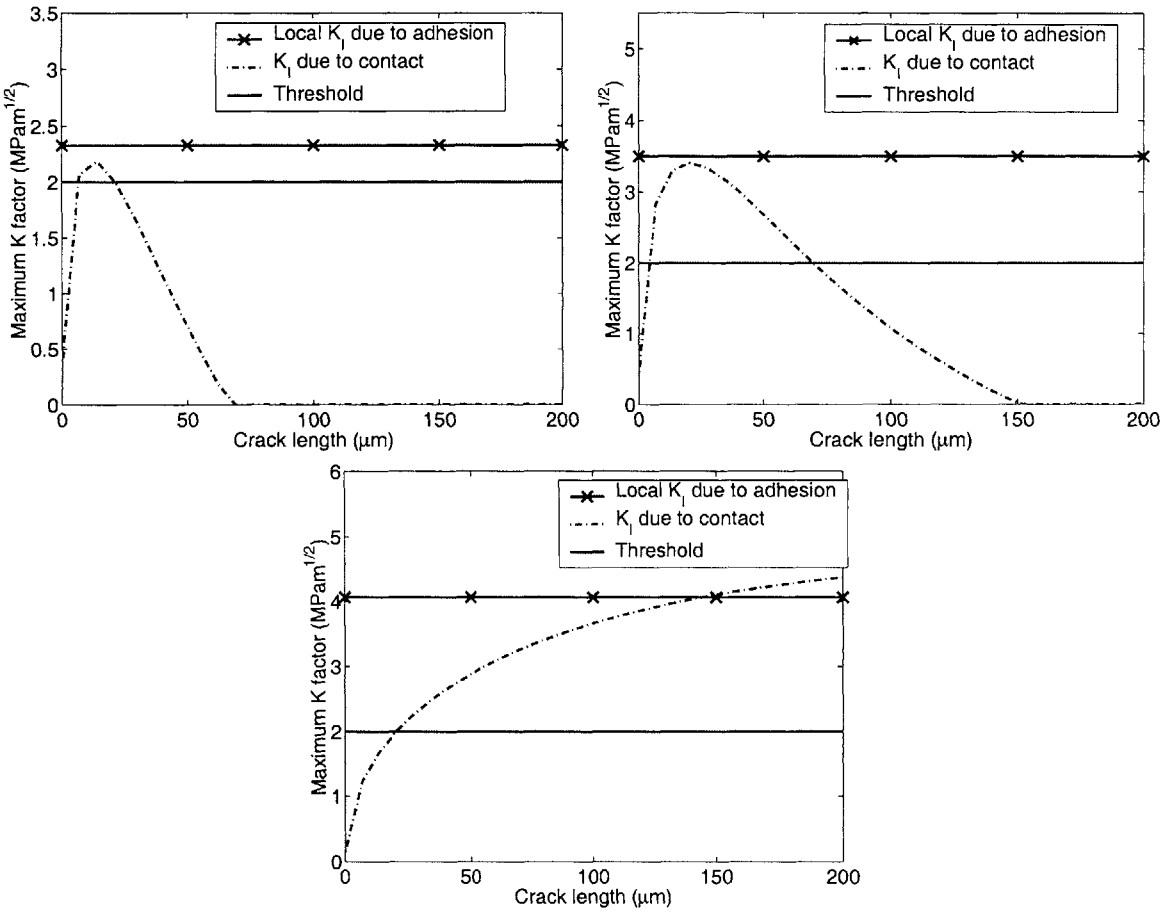

Figure 4-33: Positive stress intensity factor range induced by adhesion and contact as a function of length for Q=20 N, P=50 N, pad radius of 12.7 mm on Ti-6Al-4V (top), for Q=30 N, P=50 N, pad radius of 12.7 mm on Ti-6Al-4V (middle), for Q=930 N, P=900 N, pad radius of 0.3 m for a 7075 aluminum alloy (bottom)

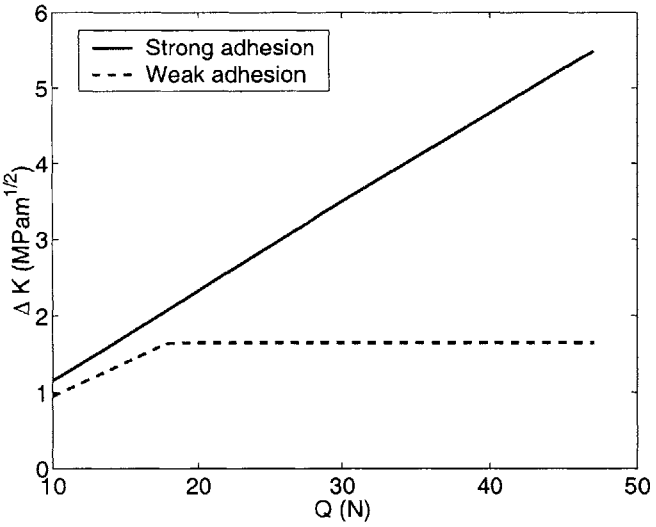

Figure 4-34: Local mode I stress intensity factor due to adhesion for a normal load of 50 N (the tangential load varies)

Chapter 5

Conclusions

The main objective of this work, which was to assess the validity of a novel fretting fatigue life prediction methodology relying only on fracture mechanics, has been achieved. A large portion of the experimental observations reported on fretting fatigue could be accounted for qualitatively, some with good qualitative agreement. The most significant feature of the methodology is that, however remote from an initiation-propagation model it can be in principle, it does in practice lead to an initial propagation phase that resembles a nucleation phase for all practical purposes. Of course, the true nature of damage accumulation in the early cycles of fretting fatigue would need to be ascertained to make this model physical as well as practical. The experiments carried out during the course of this study didn't allow to settle the question, partly because of the limitations of the set-up, partly because of pure experimental complexity. It is becoming clear however that early observations of damage, or characterizations of damage growth in the absence of bulk stress are the information needed to advance the fundamental understanding of fretting and its modeling. Unfortunately, these observations are also the most challenging.

As regards the details of the modeling, the results obtained so far are encouraging, but limited to the basic behavior of the model. The general trends due to variations in the tangential, normal and axial loads are captured when using physically relevant fatigue parameters. The distinction between different regimes of crack growth allows a better quantitative agreement, and to better simulate the asymptotic behavior at

low loads. For further development of the model, the parametric study showed that the Paris's law parameters represent good tuning parameters, although the allowable variation of the exponent in the Paris regime is rather limited. Difficulties yet to be resolved include the strength of the adhesion (and the possible need to refine the controlling material parameters), the crack growth threshold value, and the length of transition between the adhesion and contact dominated crack growth regimes. The latter seems to be amenable to a classical fracture mechanics analysis of dominance region, although the experimental verification, outlined in this work, may be quite difficult without proper selection of the experimental conditions.

Lastly, the experimental effort emphasized the need of a strict control of the load conditions, as plasticity greatly complicates the interpretation of experiments. Various experimental techniques for the observations of early cracks and short cracks in the absence of bulk stress were proposed and tested, and although they are very difficult to implement, they are believed to represent a better way to further the knowledge on the fretting process than the standard test to failure, as they may direct to a more fundamental understanding of the phenomenon, leading to truly physical and intrinsic modeling.

Appendix A

Preliminary investigation of ion glazing effects on fretting fatigue

A process using the high power (5 billion watt) of an accelerated ion beam has been developed at Los Alamos National Laboratories (LANL) to modify physical and mechanical properties over a depth of 1 to 10 μm. The process, called IBEST^{TM} (for Ion BEam Surface Treatment), relies on a very quick melting of the surface (on the order of 150 ns), followed by a very fast cooling by conduction of the molten layer (at a rate of about 1 billion degrees per second) to induce transformations of the surface roughness, hardness and microstructure primarily. Tensile residual stresses may also arise in the skin. On the other hand, the change in composition is normally very limited, since only 0.0001 times as many ions are implanted compared to conventional ion implantation, in which 20 to 30 atomic percent is commonly achieved [52]. A brief review of the few results available regarding the influence on fretting fatigue of ion implantation and laser glazing, two techniques somewhat similar to that described, will be followed by a discussion of the results obtained on ion glazed Ti-6Al-4V specimens, and their interpretation in the framework of stress and adhesive methodologies.

A.1 Influence of ion implantation and laser glazing on fretting fatigue

Although the process investigated in Appendix A is not strictly speaking an ion implantation process, some considerations on the results obtained by this technique may be useful to assess the experiments on ion glazed specimens. Ion implantation consists in bombarding a material with ions accelerated by a high voltage electric field[52]. As a general rule, in spite of significant improvement of plain fatigue properties by ion implantation[52][100], the benefits for fretting fatigue were limited by the very shallow depth of treatment (about 0.15 μm) initially achieved by particle accelerators [8]. Some benefits are reported however, and attributed to modifications of the adhesive properties (by formation of second phase precipitates which chemically stabilize the low-friction oxide layer), surface hardness (through solution strengthening) and residual stresses (up to -350 MPa at the surface) for implantation of C^+ and N^+ ions [53][52]. Specifically, improvements of the number of cycles to failure of 15% (for N^+) and 45% (for C^+) have been reported [53]. As higher energy beams of several hundred KeV are used, greater depth of tretament of the order of a few tens of microns could hopefully lead to further improvement in fretting fatigue resistance, warranting more sytematic studies of the fretting properties of the treated material. Another surface treatment more akin to the ion glazed process investigated in Section A is laser glazing. The process uses the energy of a laser beam to melt the surface, which affects the microstructure and hardness on a depth of several hundreds of microns (0.35 mm to close to 2 mm depending on the details of the process) and induces residual stresses whose sign depend on the material. The benefits are material and process dependent (as the atmosphere and the dpeth of treatment may strongly affect the results). A study by Malakondaiah and Nicholas[101] showed that the benefits of the treatment could be entirely attributed to the compressive residual stresses generated outside of the glazed region.

A.2 Material's characterization

Four specimens of Ti-6Al-4V, treated in four different ways, were obtained from QM Technologies for preliminary evaluation of the potential benefit of the technique against fretting fatigue. The details of the treatments are given in Table A.1. The depth of treatment varied from 1-2 μm for the so called low energy treatment to 2-3 μm for the high energy treatments, according to QMT estimations.

		Energy received	
		Low	High
Heat treatment:500°C 1hr furnaced cooled, encapsulated in Ar	Yes	1	3
	No	2	4

Table A.1: Number assigned to each treatment condition

This section first presents the expected or observed changes of material properties, and the results obtained. A brief interpretation of the experiments using the crack-analog methodology is given, which highlights the interest of this process to validate some aspects of this methodology, and the characterizations needed for a better understanding.

A.3 Influence of ion glazing on material properties

At least eight different parameters entering the analysis of fretting fatigue may be affected by the process, namely:

- the composition
- the Young's modulus
- the microstructure
- the surface roughness
- the friction coefficient

- the hardness
- and residual stresses.

As explained before, no significant change in composition is expected. The species usually used in ion implantation are carbon and nitrogen, as their beneficial effects in both wear and fatigue have been clearly demonstrated [52][100]. Tin, palladium and platinum have also shown favorable results in pin-on-a-disc test at LANL. The actual residual stress profile is not known, only its possible tensile nature has been recognized both from literature and LANL previous experience. Experiments on various materials have always shown, to our knowledge, an increase in hardness, but quantification of the change on our specimens remains to be done. The other parameters have been more or less characterized, with the exception of Young's modulus.

A.3.1 Modification of surface microstructure

A polished and etched cross-section of specimen # 1 is shown on Figure A-1. A martensitic layer is expected to form in the heat affected zone, over a depth of 1-2 μm for the low energy treatment and 2-3 μm for the high energy one. At this low magnification, no change in the surface microstructure can be detected. Further investigation is needed to confirm the absence of modification, and compare the result to specimen 2, which received no heat treatment, and specimen 3, which received a higher energy treatment.

It is also suspected that some change of the grain size in the surface plane may occur due to the thermal cycling. Metallographic preparation of the surface of low-energy specimens revealed an $\alpha + \beta$ microstructure very similar to the one observed on standard STOA. It is however difficult to confirm that no change occurred because the polishing required prior to etching may wear off the layer of interest.

A.3.2 Modification of surface topography

Profilometry data in two directions are available for each specimen. They show no significant change of the surface topography for the specimens treated at the lower

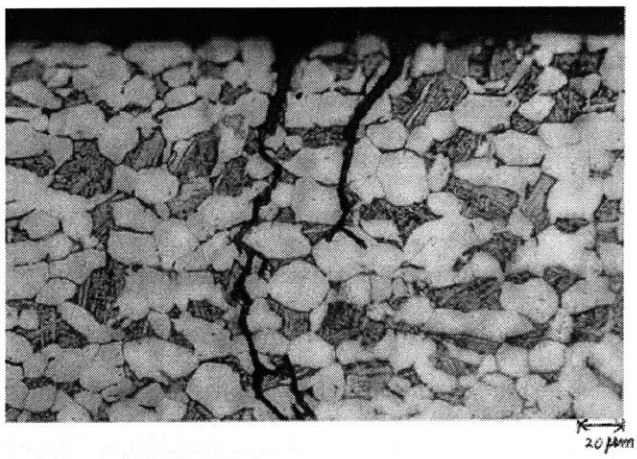

Figure A-1: Cross section of the low energy-heat treated specimen after cycling

energy level. However the topography on the specimens treated at the higher energy level is dramatically changed, as can be seen in Table A.2.

	Avg roughness R_a (μm)	Std dev R_a (μm)	Avg max height R_z (mm)	Std dev R_z (μm)	Rms wave length (mm)
Untreated	100	24	1.444	193	6.35-8.9
Low energy	139	9	1.702	99	6.35-8.9
High energy	354	89	3.227	518	19.3

Table A.2: Profilometry data in the fretting direction from Wyko profilometer, provided by QMT, Inc.

What may not be striking from these numbers is the change from serrated, anisotropic, statistically distributed profile to a wavy, isotropic, regular surface profile, as can be inferred from the pictures of Figure A-2, taken under an optical microscope.

A.3.3 Modification of the friction coefficient and experimental observations

The friction coefficient was measured for specimen # 4 only. The values obtained for the breakaway point and the kinetic coefficient of friction, 1 and 0.7 respectively, did not significantly differ from the values of 0.95 and 0.7 obtained for Ti-6Al-4V mill annealed. Since the surface topography obtained after the low energy treatment

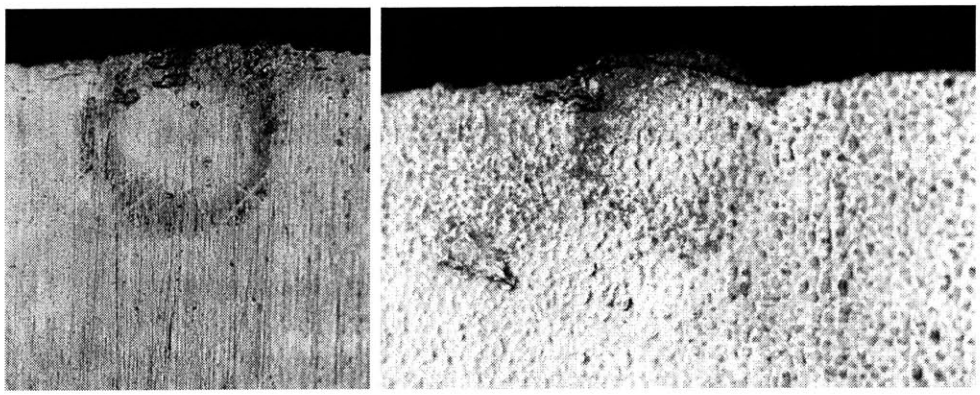

Figure A-2: Comparison of the surface aspect after low energy treatment (top) and high energy treatment (bottom)

is very similar to that of untreated specimens, and since no significant influence of composition is expected in any case, it can be said that the coefficient of friction is unaffected by these treatments, to the precision of our measurements.

A.3.4 Experimental results on ion glazed specimens

Comparison of life data with untreated material

A combination of normal, tangential and applied loads was chosen by reference to the standard Ti-6Al-4V STOA material, for which number of cycles to failure for a normal load of 50 N and an applied stress of 300 MPa were available for a range of tangential load. In order to obtain a finite life, but without falling in a low cycles-to-failure region where scatter is usually greater, a load of 15 to 20 N was selected.

Two of the tests didn't fail due to contact fatigue as expected: the test on specimen # 1 was interrupted by a pump failure on the fatigue machine, and specimen # 3 failed due to a fatigue crack initiating at the grip. Yet the examination of these particular specimens indicate that:

- a fairly large fretting fatigue had developed in specimen # 1. A fracture mechanics analysis, using simple semi-elliptical edge crack stress intensity factor for mode I, allowed to compute an estimate of the remaining life in stage III.

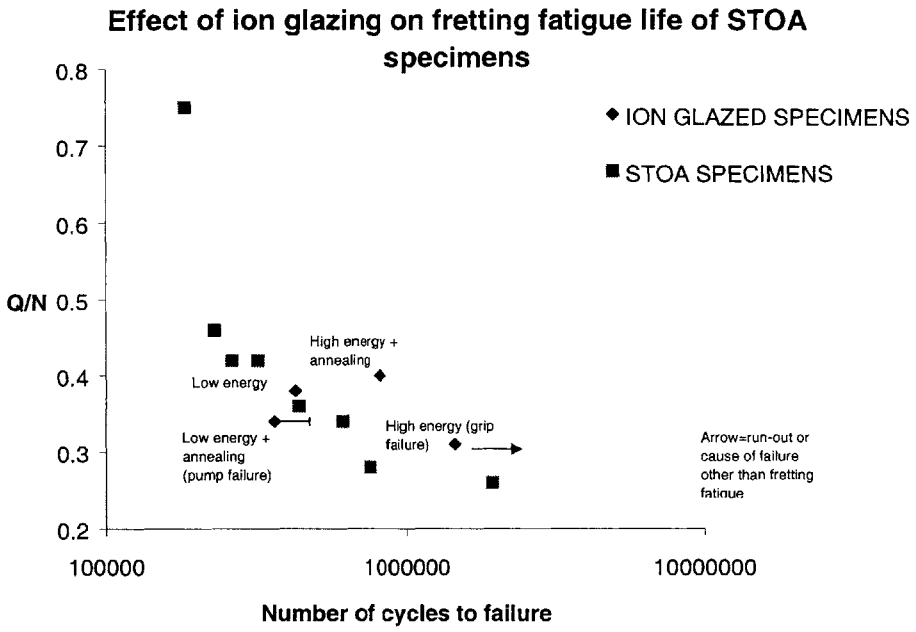

Figure A-3: Fretting fatigue life of STOA for various tangential forces, and of ion glazed specimens, for a fixed normal load of 50 N, and a fixed applied stress amplitude of 300 MPa

Knowing the data storage frequency, an upper-bound of the total life could be determined and is shown on the graph as an error bar.

- no fretting crack seemed to be present in specimen # 4. Only optical microscopy was used however to observe the fretting region. SEM may be required to ascertain this finding.

Figure A-3 indicates that the fretting fatigue resistance *for the particular loading investigated* was essentially unchanged by the lower energy treatment, whereas it was improved by about 50% for the higher energy treatment, and probably even more when used in conjunction with annealing.

Aspect of fretting scar

The fretting scars of specimens # 1 and # 2 were very similar to the ones usually observed on the untreated material, with the "classical" stick-slip pattern, as can be seen on the example of Figure A-2. In contrast the scars of specimens # 3 and # 4 were more representative of a distributed contact condition, where only a few spots, corresponding to the top points of the wavy surface, actually make contact with the pads. The pads actually provide a good mirror image of the distribution of high spots on the specimen, as can be seen of Figure A-4.

Figure A-4: Scar on one of the Ti-6Al-4V STOA pads used on specimen # 3

Fractography results

Specimen # 1 was cut parallel to the fretting direction in the middle of the scar, and polished and etched to reveal the crack geometry. Two cracks were present, as can be seen on Figure A-1. The longer was about 600 μm, and the characteristic turn from stage II to stage III could not be identified. The aspect ratio $\frac{a}{c}$ was about 0.86, as opposed to 0.67 on average for untreated specimens.

The fracture surface of the other failed specimens looked very similar to what is usually observed on STOA. On specimens # 2 and # 3, an aspect ratio of 0.41 and 0.59 respectively was estimated. This value does not take into account the correction

due to the inclination of the crack, which may increase these values by about 15%. It is not clear which of these aspect ratii is to be used for stage III calculations, but it will be shown later that this does not affect the final result significantly.

A.4 Interpretation of the results

The parameters cited above will influence the fretting fatigue life through stage I and stage II for the most part. Yet not all variations of life can be readily attributed to changes in these stages, because

1. residual stresses in depth may affect propagation, and
2. even in the case of a very shallow distribution, they may affect the aspect ratio of the crack, hence the life in stage III

. In order to draw valid conclusion on stage I-II in the absence of direct observation, the percentage of life spent in stage III has to be estimated. The aspect ratio of the detectable cracks was estimated for the first three specimens. As noted above, they were approximately 0.86, 0.41 and 0.69 respectively. The aspect ratio for specimen # 1 somewhat higher than usual, but was not obtained by the same procedure. It may hint towards a non-constant value of the parameter during crack propagation. On the other hand, the aspect ratios of the other two specimens were rather smaller than usual.

The uncertainty on the aspect ratio affects stage III life calculation within 5% only. However the error due to the lack of precise measurement of the turning point on specimen # 1 may easily give a 20% error on stage III calculation. Figure A-5 shows on top a comparison of the percentage of life spent in stage III for the first three ion-glazed specimens and standard STOA specimens at a similar $\frac{Q}{N}$ ratio. No clear trend can be inferred.

However, further analysis of the STOA data indicates that the percentage in stage 3 for the STOA specimen having a $\frac{Q}{N}$ ratio similar to the low-energy annealed specimen is somewhat lower than expected from the whole percentage data available,

presented on Figure A-6. A value of 45% seems to coincide better with the data trend.

Moreover, as indicated above, the calculation for the low-energy annealed specimen is highly sensitive to the initial crack length. The value on top of Figure A-5 is based on an initial length of 100 μm. Using a length of 150 μm, which is still in the range usually observed, the calculation decreases by about 15%. On the bottom of Figure A-5, this second possible initial length was used, as the values obtained for the ion-glazed specimens are compared to values extrapolated from Figure A-6 rather than exact values. It can be concluded that the uncertainties make a quantitative evaluation very difficult for the first ion-glazed specimen. Nevertheless it seems legitimate to say that there is little effect, if any, of the low energy treatment on the percentage of life spent in stage III.

On the other hand, the comparison of the percentage of life spent in stage III for specimens # 2 and # 3 (Figure A-5) indicate that it is twice shorter for the specimen treated at high energy than for the specimen treated at low energy and annealed. The comparison of the relative life of the high-energy annealed specimen with a typical relative life for STOA specimen also indicates that the percentage of life spent in stage III has been significantly decreased. Combined with the absence of visible crack in specimen # 4, these calculations lead to the conclusion that the ion-glazing treatment increases the time spent initiating and originally propagating a fretting fatigue crack.

Since the coefficient of friction is the same, a conventional stress analysis leads to the same results for the untreated and treated specimens. Thus only material parameters may account for modification of the fretting fatigue resistance. The differences would come from changes in the crack initiation resistance, which can be qualitatively related to surface hardening, and the crack propagation resistance, mainly under the influence of the microstructure and residual stresses. Note that the role of the latter would tend to be minimal according to this analysis, since the annealing does not show a distinct effect between specimens # 1 and # 2. On the basis of a conventional stress analysis, the absence of effect on the low energy treatment would actually indi-

cate that the microstructural modifications at the surface somehow compound each other and have no significant influence on fretting fatigue resistance, whereas they do influence the results for the higher energy treatment. In other words, since the only parameter that one can invoke is the depth of treatment, a purely stress based analysis would suggest the existence of a critical depth of treatment. The concept is not easy to rationalize for such shallow depths, especially considering the fact that the notion of critical length, related to stress gradients, is not yet firmly established in conventional stress-based analyses.

Examining the results in the light of the crack-analogue methodology gives a slightly different answer. The absence of effect for the low-energy specimens points once again towards a lack of significant influence of material's parameters such as the hardness, the crack growth rate, and the microstructure in general, possibly because the depth of the affected zone is very shallow [1]. Unlike stress-based models, the crack-analogue methodology indeed introduces, among other things, a length scale that compounds the importance of the modifications. A parameter that does change however between the specimens giving improved results and the others is the surface roughness. It is known that an increase of surface roughness reduces the sensitivity to fretting fatigue (see Section 3.2.2), and that this can be related to a change in adhesion, at least qualitatively [102]. At this stage of the investigation, it seems that this is the best way to rationalize the results obtained in the preliminary tests. Interestingly, it would indicate that the crack-analogue formulation may benefit from a qualitative treatment of roughness effects.

In order clarify the situation however, some more information would be needed regarding:

- the actual composition in the various affected layers, since significant variations of composition may alter the analysis presented above; it has been pointed out however that they are very unlikely

[1] As always, the absence of effect may be the compounded outcome of positive and negative factors, but these are hard to name in this case

- the microstructural changes and the depth of the affected zone; surface and through-thickness hardness measurement may help to evaluate the latter
- the actual residual stress profile
- the coefficient of friction, in order to really confirm the absence of modification, as this plays a key role in the mechanical analysis.

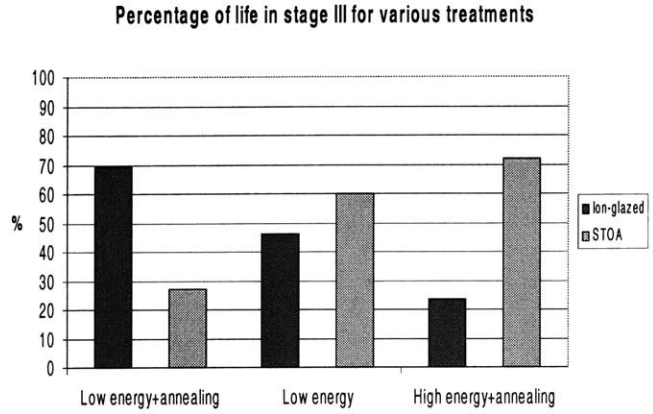

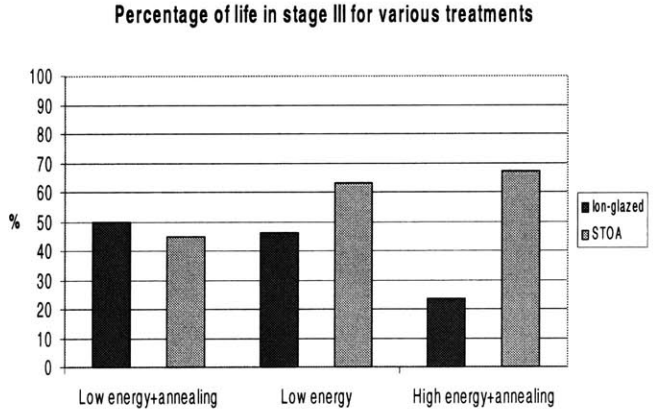

Figure A-5: Percentage of life in stage III at similar loadings, from semi-elliptical edge crack solution; a different aspect ratio based on observation is used in each case

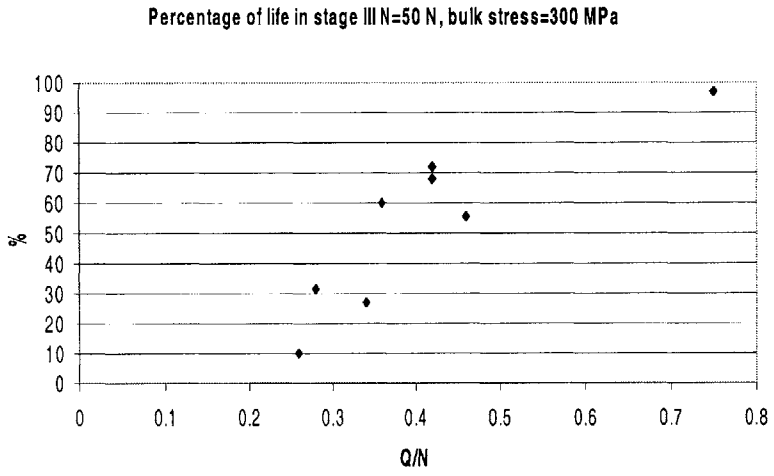

Figure A-6: Percentage of life in stage III for various tangential loads on STOA material (based on semi-elliptical edge crack solution)

Appendix B

Influence of the microstructure on the fretting resistance of Ti-6Al-4V

B.1 Effects of microstructure on crack growth rate and damage initiation resistance in relation to fretting fatigue

Although the model presented in Section 4 encompasses all stages of crack growth of fretting fatigue in the framework of fracture mechanics, the distinction between a stage of very slow crack growth corresponding to initiation and a stage of faster crack propagation remains valid, as in the classical partition of the fatigue phenomenon between damage initiation and growth. As it is known that the resistance of a metallic material to one or the other is usually a trade-off that can be influenced by material design, it may be of interest to investigate which kind of resistance yields an optimum against fretting fatigue. In the case of titanium alloys, fatigue crack growth is primarily a function of the morphology of the alpha phase, of the morphology and size of the prior beta grains, of the nature of the grain boundaries and on the type of matrix[1][103]. Larger alpha grain size, Widmanstätten colonies, larger prior beta

[1]The considerations are valid for room temperature and long crack behavior only; note that short crack propagation is influenced in a manner similar to high cycle fatigue strength

grain size or numerous alpha grain boundaries, and lower matrix strength (to a small extent) all lead to improved crack propagation resistance. On the other hand, damage initiation is better resisted by fine microstructures with large strength, although the separation of the alpha grains in the bimodal microstructure actually gives the best resistance. In order to evaluate the influence of some of these parameters on fretting fatigue resistance for the sphere-on-flat geometry, six different heat treatments were applied to a Ti-6Al-4V alloy.

B.2 Effects of heat treatment on the microstructure of Ti-6Al-4V

The various heat treatments performed after forging, and the corresponding microstructural features, are summarized in Table B.1. The STOA and mill-annealed materials were supplied directly, whereas the other microstructures were obtained by treating STOA forgings.

Material type	Heat treatment	Type of microstructure
Mill-annealed	2 hr at 704°C+AC	Equiaxed (with primary α grains elongated in the forging direction)
STOA	1.25 hr at 925°C+AC to; room temperature; 2hr at 704°C+ FaC in Ar to room temperature	Bimodal with 60 vol% of primary α 40 vol% of lamellar colonies of $\alpha + \beta$; primary α grain size~10-20μm
Coarse STOA	48 hr at 932°C+AC; 12 hr at 700°C+AC	Same as above with grain size~20-25μm
Acicular	0.5 hr at 1050°C+AC	Coarse lamellar (colony diameters~300μm
Widmanstätten	0.5 hr at 1050°C+FC to 700°C (1 hr)+ AC to room temperature	Lamellar; typical width ~15-20μm
Martensitic	0.5 hr at 1050°C+WQ	Fine needle-like

Table B.1: Heat treatments and type of microstructure obtained for the Ti-6Al-4V (AC indicates Air Cooling, FaC Fan Cooling, FC Furnace Cooling, WQ Water Quenching)

The various microstructures were expected to give different crack propagation resistance according to the rules stated above, with the Widmanstätten exhibiting the

best crack propagation resistance, the mill annealed the worst, and the martensitic structure having a significantly better damage initiation and short crack propagation resistance.

B.3 Experimental results

The fretting fatigue resistance of the treated materials was compared for a normal force of 30 N, an axial stress amplitude of 300 MPa, and a varying tangential force. The data are plotted on Figure B-1. No major effect was observed for this test condition, yet some differences appeared. The mill annealed material tends to perform the poorest, and the STOA and martensitic microstructures the best. For the latter, it must be noted that a few test points suggest it may achieve a significantly better fretting fatigue resistance. This is hard to confirm due to the very brittle nature of the material, which often leads to non-fretting failure. Interestingly, for material design, this suggests that the use of a strong microstructure might be beneficial for the type of load and geometry investigated, the brittleness of which would likely impose the choice of a coating or graded design.

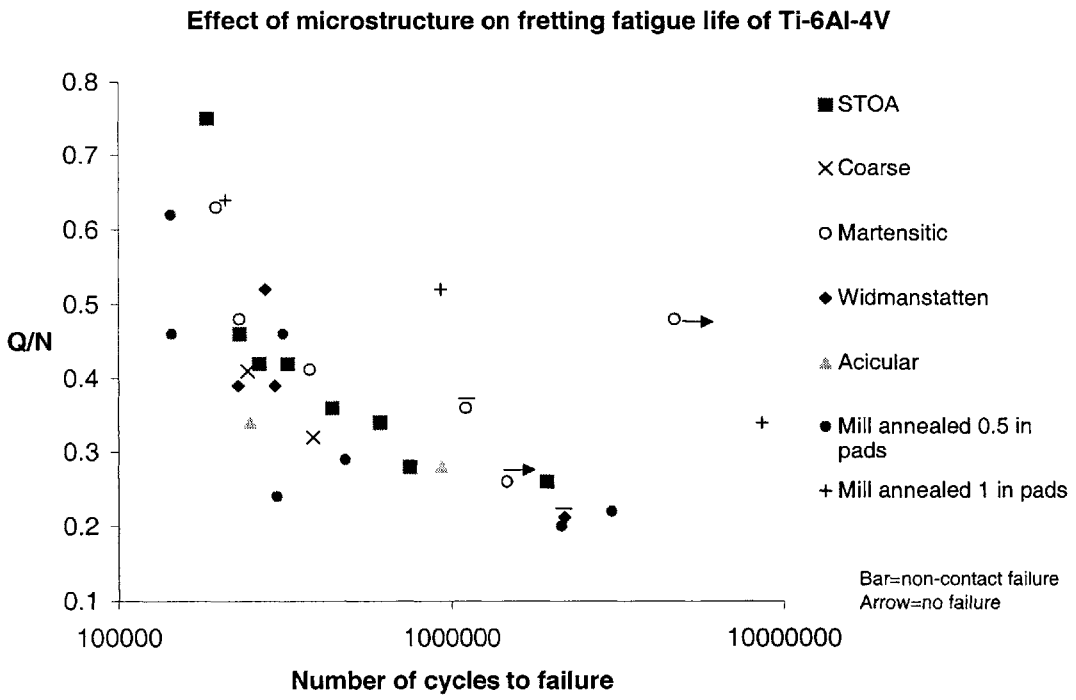

Figure B-1: Effect of microstructural changes on the fretting fatigue resistance for a normal force of 50 N and an axial stress amplitude of 300 MPa

Bibliography

[1] V. LAMACQ. *Amorçage et propagation de fissures de fatigue ous conditions de fretting, Approches théoriques et expérimentales.* Thèse de doctorat, INSA Lyon, 1997.

[2] A. E. GIANNAKOPOULOS, T. C. LINDLEY, S. SURESH. Aspects of equivalence between contact mechanics and fracture mechanics: theoretical connections and life-prediction methodology for fretting fatigue. *Acta Materialia*, 46(9):2955–2968, 1998.

[3] B. C. CONNER. Mechanical and microstructural effects on fretting fatigue of Ti-6Al-4V. Master's thesis, Massachusetts Institute of Technology, May 2000.

[4] L. WAGNER. Mechanical surface treatments on titanium alloys: fundamental mechanisms. In *Surface Performance of titanium*, pages 199–215, Cincinatti, 1996. Minerals, Metals and Materials Society/AIME.

[5] G. LEADBEATER, B. NOBLE, R. B. WATERHOUSE. Metallurgical observations on the fretting of shot peened aluminum surfaces. In R. B. WATERHOUSE and A. NIKU-LARI, editors, *Metal treatments against wear, corrosion, fretting and fatigue*, pages 67–86, 1988.

[6] H. WOHLFAHRT. The influence of peening conditions on the resulting distribution of residual stresses. In *2nd International Conference on Shot Peening*, pages 316–331, Chicago, Illinois, May 1984.

[7] T. HIRSCH, P. MAYR. The effect of manufacturing induced residual stress states on the mechanical behaviour of components. In *49th International Congress on the Technology of Metals and Materials*, pages 59–77, Sao Paulo, Brazil, 1995. Associacao Brasileira de Metalurgia e Materiais.

[8] T. C. LINDLEY, R. B. WATERHOUSE. Prevention of fatigue by surface engineering. In J. H. BEYNON, M. W. BROWN, R. A. SMITH, T. C. LINDLEY, B. TOMKINS, editor, *Engineering against fatigue*, pages 487–499, 1999.

[9] C. B. DANE, J. HACKEL, J. DALY, J. HARRISON. Shot peening with lasers. *Advanced Materials & Processes*, pages 37–38, May 1998.

[10] S. D. THOMPSON, D. W. SEE, C. D. LYKINS, P. G. SAMPSON. Laser shock peening vs. shot peening-a damage tolerance investigation. In *Surface Performance of titanium*, pages 239–251, Cincinatti, 1996. Minerals, Metals and Materials Society/AIME.

[11] O. VÖHRINGER, Th. HIRSCH, E. MACHERAUCH. Relaxation of shot peening induced residual stresses of TiAl6V4 by annealing or mechanical treatment. In *Titanium-Science and Technology*, volume 4, pages 2203–2210, Münich, FRG, 1985. Deutsche Gesellschaft für Metallkunde.

[12] R. S. BELLOWS, K. R. BAIN, J. W. SHELDON. Effect of step testing and notches on the endurance limit of Ti-6Al-4V. In *Mechanical Behavior of Advanced Materials*, volume 84, pages 27–32. ASME-MD, 1998.

[13] T. HATTORI. Fretting fatigue problems in structural design, fretting fatigue. In T. C. Lindley R. B. WATERHOUSE, editor, *Fretting Fatigue*, number 18 in ESIS, pages 103–109, 1994.

[14] T. HATTORI, M. NAKAMURA, H. SAKATA, T. WATANABE. Fretting fatigue analysis using fracture mechanics. *JSME International Journal, Series 1*, 31(1), 1988.

[15] T. HATTORI, M. NAKAMURA, T. WATANABE. A new approach to the prediction of fretting fatigue life that considers the shifting of the contact edge by wear. In C. B. ELLIOT D. W. HOEPPNER, V. CHANDRASEKARAN, editor, *Fretting Fatigue: Current Technology and Practices*, number 1367 in ASTM STP, 1999.

[16] M. C. DUBOURG, V. LAMACQ. A theoretical model for the prediction of crack field evolution. In T. C. Lindley R. B. WATERHOUSE, editor, *Fretting Fatigue*, number 18 in ESIS, pages 135–147, 1994.

[17] M. D. B. WILKS, D. NOWELL, D. A. HILLS. The influence of residual stress on crack growth rate. In *Proceedings of the fourth International Conference on Residual Stresses*, Baltimore, MD, June 1994. Society for Experimental Mechanics.

[18] L. J. FELLOWS, D. NOWELL, D. A. HILLS. Analysis of crack initiation and propagation in fretting fatigue: the effective initial flaw size methodology. *Fatigue Fract. Engng. Mater. Struct.*, 20(1):61–70, 1997.

[19] S. FOUVRY, P. KAPSA, L. VINCENT. A multiaxial fatigue analysis of fretting contact taking into account the size effect. In C. B. ELLIOTT III D. W. HOEPPNER, V. CHANDRASEKARAN, editor, *Fretting Fatigue, Current technologies and practices*, number 1367 in ASTM STP, pages 167–182, 2000.

[20] A. E. GINNAKOPOULOS, T. A. VENKATESH, T. C. LINDLEY, S. SURESH. The role of adhesion in contact fatigue. *Acta Materialia*, 47(18):4653–4664, December 1999.

[21] T. A. VENKATESH, B. P. CONNER, C. S. LEE, A. E. GIANNAKOPOULOS, T. C. LINDLEY, S. SURESH. An experimental investigation of fretting fatigue in Ti-6Al-4V: the role of contact conditions and micrsotructure. 2000.

[22] R. B. WATERHOUSE. Effects of material and surface condition on fretting fatigue. In R. B. WATERHOUSE and T. C. LINDLEY, editors, *Fretting Fatigue*, number 18 in ESIS, pages 339–349, 1994.

[23] A. BIGNONNET. Some observations of the effects of shot peening on fretting fatigue. In R. B. WATERHOUSE and T. C. LINDLEY, editors, *Fretting Fatigue*, number 18 in ESIS, pages 475–482, 1994.

[24] D. W. HOEPPNER, S. ADIBNAZARI. Fretting fatigue in aircraft joints. volume 1, pages 191–206, June 1993.

[25] M. P. SZOLWINSKI, T. N. FARRIS. Observation, analysis and prediction of fretting fatigue in 2024-t351 aluminum alloy. *Wear*, (221):24–36, 1998.

[26] K. W. KIRKPATRICK. Fretting fatigue analysis and palliatives. Master's thesis, Massachusetts Institute of Technology, June 1999.

[27] T. C. CHIVERS, S. C. GORDELIER. Fretting fatigue and contact conditions: a rational explanation of palliative behaviour. *Proc Instn Mech Engrs*, 199:325–337, 1985.

[28] H. P. LIEURADE, A. BIGNONNET. Fundamental aspects of the effect of shot peening on the fatigue strength of metallic parts and structures. In *Shot Peening: Science, Technology, Application*, volume 2, pages 343–359, Garmisch-Partenkirchen, FRG, 1987.

[29] J. FOULQUIER, C. PETIOT. Fretting fatigue behaviour of major helicopters alloys and influence of surface protections. In *Proceedings of the 17th Symposium of the International Committee on Aeroanautical Fatigue, Durability and Stuctural Integrity of Airframes*, volume 2, pages 899–909, June 1993.

[30] A. H. CLAUER. Laser shock peening for fatigue resistance, surface performance of titanium. In *Surface Performance of titanium*, pages 217–230, Cincinatti, 1996. Minerals, Metals and Materials Society/AIME.

[31] S. ADIBNAZARI, D. W. HOEPPNER. The role of normal pressure in modelling fretting fatigue. In T. C. Lindley R. B. WATERHOUSE, editor, *Fretting Fatigue*, number 18 in ESIS, pages 125–133, 1994.

[32] I. V. PAPADOPOULOS, P. DAVOLI, C. GORLA, M. FILIPPINI, A. BERNASCONI. A comparative study of multi-axial high-cycle fatigue criteria for metals. *Int. J. of Fatigue*, 19(3):219–235, 1997.

[33] M. FOGUE, J-L ROBERT, J. BAHUAUD. Contribution à l'analyse comparative de critères de fatigue multiaxiaux périodiques. *Mécanique Industrielle et Matériau*, 48(3), September 1995.

[34] B. U. WITTKOWSKI, P. R. BIRCH, J. DOMINGUEZ, S. SURESH. An experimental investigation of fretting fatigue with spherical contact in 7075-t6 aluminum alloy. In C. B. ELLIOT D. W. HOEPPNER, V. CHANDRASEKARAN, editor, *Fretting Fatigue: Current Technology and Practices*, number 1367 in ASTM STP, 1999.

[35] M. P. SZOLWINSKI, J. F. MATLIK, T. N. FARRIS. Effects of HCF loading on fretting fatigue crack nucleation. *Int. J. of Fatigue*, 21:671–677, 1999.

[36] D. COURATIN, P. DE ROO, T. LIM. Taking into account residual stresses in fatigue criterion in the case of shot peening. In *Residual Stresses in Science and Technology*, pages 793–799, Garmisch-Partenkirchen, FRG, 1987.

[37] I. V. PAPADOPOULOS, V. P. PANOSKALTSIS. Gradient dependent multiaxial high cycle fatigue criterion. In *4^{th} international conference on biaxial/multiaxial fatigue, Paris, France*, pages 461–476, June 1994.

[38] C. BLEUZEN, M. CHAUDONNERET, J. FLAVENOT, N. RANGANATHAN, M. ROBERT. Validation of life prediction models from representative testings on aluminium alloys specimens. In *Proceedings of the 17^{th} Symposium of the International Committee on Aeronautical Fatigue,*

Durability and Stuctural Integrity of Airframes, volume 1, pages 141–173, June 1993.

[39] M. CIAVARELLA, D. A. HILLS, R. MOBOLA. Analysis of plane and rough contacts, subject to a shearing force. *International Journal of Mechanical Sciences*, 41:107–120, 1999.

[40] C. D. LYKINS, S. MALL, V. JAIN. An evaluation of parameters fro predicting fretting fatigue crack initiation. *Int. J. of Fatigue*, 22:703–716, 2000.

[41] J. A. ARAÚJO, D. NOWELL. Analysis of pad size effects in fretting fatigue using short crack arrest methodologies. *International Journal of Fatigue*, 21:947–956, 1999.

[42] V. LAMACQ, M-C DUBOURG, L. VINCENT. Crack path prediction under fretting fatigue-a theoretical and experimental approach. *Journal of tribology*, 118:711–720, 1996.

[43] K. L. JOHNSON, K. KENDALL, A. D. ROBERTS. Surface energy and the contact of elastic solids. *Proc. R. Soc. London A*, 324:301–313, 1975.

[44] A. R. SAVKOOR, G. A. D. BRIGGS. The effect of tangential force on the contact solids in adhesion. *Proc. R. Soc. London A*, 356:104–114, 1977.

[45] M. BARQUINS, D. MAUGIS. Adhesive contact of axisymmetric punches on an elastic half-space: the modified Hertz-Huber's stress tensor for contacting spheres. *Journal de Mécanique théorique et appliquée*, 1(2):331–357, 1982.

[46] R. D. MINDLIN. Compliance of elastic bodies in contact. *Journal of Applied Mechanics*, pages 259–268, September 1949.

[47] S. M. A. KHAN, M. K. KRAISHEH. Analysis of mixed mode crack initiation angles under various loading conditions. *Engineering Fracture Mechanics*, 67:397–419, 2000.

[48] H. KITAGAWA, R. YUUKI, K. TOHGO, M. TANABE. Δk-dependency of fatigue crack growth of single and mixed mode cracks under biaxial stress. In K. J. MILLER and M. W. BROWN, editors, *Multiaxial Fatigue*, number 853 in ASTM-STP, pages 164–183, 1985.

[49] B. U. WITTKOWSKI, P. R. BIRCH, J. DOMINGUEZ, S. SURESH. An apparatus for quantitative fretting-fatigue testing. *Fatigue and Fracture of Engineering Materials and Structures*, 22(4):307–320, April 1999.

[50] R. O. RITCHIE, B. L. BOYCE, J. P. CAMPBELL, O. RODER, A. W. THOMPSON, W. W. MILIGAN. Thresholds for high-cycle fatigue in a turbine engine Ti-6Al-4V alloy. *Int. J. of Fatigue*, 21(7):653–662, August 1999.

[51] L. VINCENT, Y. BERTHIER, M. GODET. Testing methods in fretting: a critical approach. In M. H. ATTIA and R. B. WATERHOUSE, editors, *Standardization of fretting fatigue test methods and equipment*, number 1159 in ASTM STP, pages 33–48, 1992.

[52] J. E. ELDER, R. THAMBURAJ, P. C. PATNAIK. Optimising ion imlantation conditions for improving wear, fatigue, ad fretting fatigue of Ti-6Al-4V. *International Materials Reviews*, 33(6):289–313, 1988.

[53] A. K. KOUL, L. XUE, W. WALLACE, M. BIBBY, S. CHAKRAVARTY, R. G. ANDREWS, P. C. PATNAIK. An investigation on surface treatments for improving the fretting fatigue resistance of titanium alloys. *AGARD-CP 589, Tribology for Aerospace Systems*, October 1996.

[54] M. M. HAMDY, B. NOBLE, R. B. WATERHOUSE. Fatigue-crack initiation in imi 829 caused by high-temperature fretting. *Journal of Materials Science*, (18):493–502, 1983.

[55] P. D. NICOLAOU, E. B. SHELL, T. E. MATIKAS. Microsturctural and surface characterization of Ti-6Al-4V alloys after fretting fatigue. *Materials Science and Engineering A*, 269:98–103, 1999.

[56] L. WAGNER, G. GERDES, G. LÜTJERING. Influence of surface treatment on fatigue strength of Ti-6Al-4V. In *Titanium-Science and Technology*, volume 4, Münich, FRG, September 1985. Deutsche Gesellschaft für Metallkunde.

[57] Y. FU, N. L. LOH, A. W. BATCHELOR, D. LIU, X. ZHU, J. HE, K. XU. Improvement in fretting wear and fatigue resistance of Ti-6Al-4V by application of several surface treatments and coatings. *Surface Coatings Technology*, (106):193–197, 1998.

[58] R. B. WATERHOUSE. Residual stresses and fretting crack initiation and propagation, advances in surface treatments. In A. NIKU-LARI, editor, *Technology-Applications-Effects, International guidebook on residual stresses*, volume 4, pages 511–525, 1987.

[59] R. B. WATERHOUSE. The effect of surface treatment on the fatigue and fretting fatigue of metallic materials. In R. B. WATERHOUSE and A. NIKU-LARI, editors, *Metal treatments against wear, corrosion, fretting and fatigue*, pages 31–40, 1988.

[60] E. BROSZEIT, K. H. KLOOS, B. SCHWEIGHÖVER. The fretting behaviour of titanium alloy Ti-6Al-4V. In *Titanium-Science and Technology*, volume 4, pages 2171–2178, Münich, FRG, 1985. Deutsche Gesellschaft für Metallkunde.

[61] J. BEARD. Palliatives for fretting fatigue. In R. B. WATERHOUSE and T. C. LINDLEY, editors, *Fretting Fatigue*, number 18 in ESIS, pages 419–436, 1994.

[62] H. E. FRANZ, A. OLBRICHT. Optimization of shot peening to improve the fatigue strength of Ti6Al4V. In *Shot Peening: Science, Technology, Application*, volume 2, pages 439–446, Garmisch-Partenkirchen, FRG, 1987.

[63] Th. HIRSCH, O. VÖHRINGER, E. MACHERAUCH. Optimizing the bending fatigue behaviour of Ti-6Al-4V by shot peening. In *Titanium-Science and Technology*, volume 4, pages 2163–2170, Münich, FRG, 1985. Deutsche Gesellschaft für Metallkunde.

[64] J. BROICHHAUSEN, W. CALLES. Effect of residual stresses on the fatigue behaviour, crack origin and growth velocity of cold-worked Ti-6Al-4V. In *Residual Stresses in Science and Technology*, volume 2, pages 729–734, Garmisch-Partenkirchen, FRG, 1987.

[65] T. DÖRR, L. WAGNER. Fatigue behavior of shot peened timetal 1100: Effects of microstructure and stress gradient. In *Surface Performance of titanium*, pages 231–238, Cincinatti, 1996. Minerals, Metals and Materials Society/AIME.

[66] G. LÜTJERING, A. GYSLER. Fatigue. In *Titanium-Science and Technology*, volume 4, pages 2065–2183, Münich, FRG, 1985. Deutsche Gesellschaft für Metallkunde.

[67] S. ADACHI, L. WAGNER, G. LÜTJERING. Influence of microstructure and mean stress on fatigue strength of Ti-6Al-4V. In *Titanium-Science and Technology*, volume 4, pages 2139–2146, Münich, FRG, September 1985. Deutsche Gesellschaft für Metallkunde.

[68] K. L. JOHNSON. *Contact Mechanics.* Cambridge University Press, 1987.

[69] *Selection & Use of Titanium, a design guide.* The Institute of materials, London, 1995.

[70] W. CHENG, M. GREMAUD, A. ROSSELET, R. D. STREIT. The compliance method for measurement of near surface residual stresses: application and validation for surface treatment by laser and shot-peening. *J. Eng. Mater. Technol.*, 116(4):556–560, October 1994.

[71] J. E. HACK, K. S. CHAN, J. W. CARDINAL. The prediction of the crack-opening behavior of part-through fatigue cracks under the influence of surface residual stresses. *Eng. Fract. Mech.*, 21(1):75–83, 1985.

[72] R. FATHALLAH, G. INGLEBERT, L. CASTEX. Prediction of plastic deformation and residual stresses induced in metallic parts by shot peening. *Materials Science and Technology*, 14:631–639, July 1998.

[73] D. KIRK. Shot peening. *Aircraft Engineering and Aerospace Technology*, 71(4):349–361, 1999.

[74] H. GUECHICHI, L. CASTEX, J. FRELAT, G. INGLEBERT. Predicting residual stresses due to shot peening. In *Residual Stresses in Science and Technology*, volume 1, pages 449–456, Garmisch-Partenkirchen, FRG, 1987.

[75] S. T. S. AL-HASSANI. An engineering approach to shot-peening mechanics. In *2nd International Conference on Shot Peening*, pages 275–282, Chicago, Illinois, May 1984.

[76] C. P. DIEPART. Effect of residual stresses induced by shot peening on metal fatigue. In *Residual Stresses in Science and Technology*, pages 457–466, Garmisch-Partenkirchen, FRG, 1987.

[77] T. J. MEISTER. Overcoming detrimental residual stress in titanium by the shot peening process. In *Surface Performance of titanium*, pages 253–263, Cincinatti, 1996. Minerals, Metals and Materials Society/AIME.

[78] P. PEYRE, L. BERTHE, R. FABBRO, X. SCHEPEREEL, E. BARTNICKI, G. LEDERER, N. CELATI. Paper series. In L. BECKMAN, editor, *Lasers in material processing*, pages 546–575, June 1997.

[79] W. BRAISTED, R. BROCKMAN. Finite element simulation of laser shock peening. *International Journal of Fatigue*, 21(7):719–724, August 1999.

[80] P. MILLE, E. M. M. SUTTER, A. CORNET. Relationship between surface treatment and fatigue damage on Ti-6Al-4V titanium alloy. In *Titanium-Science and Technology*, volume 4, pages 2155–2162, Münich, FRG, 1985. Deutsche Gesellschaft für Metallkunde.

[81] A. BIGNONNET. Shot peening of welded joints and residual stress relaxation during fatigue. In *Shot Peening: Science, Technology, Application*, volume 2, pages 659–666, Garmisch-Partenkirchen, FRG, 1987.

[82] A. BIGNONNET, H. P. LIEURADE, L. PICOUET. Fatigue strength of shot-peened Grade 35 NCD16 steel. variation of residual stresses introduced by shot peening according to type of loading. In *Shot Peening: Science, Technology, Application*, volume 2, pages 585–593, Garmisch-Partenkirchen, FRG, 1987.

[83] G. M. HAMILTON. Explicit equations for the stresses beneath a sliding spherical contact. *Proc Instn Mech Engrs, C*, 197:53–59, 1983.

[84] A. E. GIANNAKOPOULOS, S. SURESH. A three-dimensional analysis of fretting fatigue. *Acta Materialia*, 46(1):177–192, 1998.

[85] A. KAPOOR, K. L. JOHNSON. Effect of changes in contact geometry on shakedown of surfaces in rolling/sliding contact. *International Journal of Mechanical Science*, 34(3):223–239, 1992.

[86] K. DANG VAN, M. H. MAITOURNAM. Elasto-plastic calculations of the mechanical state in reciprocating moving contacts: application to fretting fatigue. In T. C. Lindley R. B. WATERHOUSE, editor, *Fretting Fatigue*, number 18 in ESIS, pages 161–168, 1994.

[87] A. SACKFIELD, D. A. HILLS. Some useful results in the tangentially loaded hertzian contact problem. *Journal of Strain Analysis*, 18(2):107–110, 1983.

[88] L. J. FELLOWS, D. NOWELL, D. A. HILLS. Contact stresses in a moderately thin strip (with particular reference to fretting experiments). *Wear*, 185:235–238, 1995.

[89] D. A. HILLS, D. NOWELL. *Mechanics of fretting fatigue.* Kluwer Academics Publishers, 1994.

[90] R. D. MINDLIN, H. DERESIEWICZ. Elastic spheres in contact under varying oblique forces. *Journal of Applied Mechanics*, pages 327–344, September 1953.

[91] D. P. ROOKE. The development of stress intensity factors. In R. B. WATERHOUSE and T. C. LINDLEY, editors, *Fretting Fatigue*, number 18 in ESIS, pages 23–58, 1994.

[92] D. N. DAI, D. A. HILLS, D. NOWELL. Stress intensity factors for three-dimensional fretting fatigue cracks. In R. B. WATERHOUSE and T. C. LINDLEY, editors, *Fretting Fatigue*, number 18 in ESIS, pages 59–71, 1994.

[93] D. P. ROOKE, D. B. RAYAPROLU, M. H. ALIABADI. Crack-line and edge green's functions for stress intensity factors of inclined edge cracks. *Fatigue and Fracture of Engineering Materials ans Structures*, 15(5):441–461, 1992.

[94] Y. N. LENETS, R. S. BELLOWS. Crack propagation life prediction for Ti-6Al-4V based on striation spacing measurements. *Int. J. of Fatigue*, 22:521–529, 2000.

[95] S. SURESH. Crack deflection: implications for the growth of long and short fatigue cracks. *Metallurgical Transactions A*, 14:2375–2385, November 1983.

[96] Jr. J. C. NEWMAN, Jr., E. P. PHILLIPS, R. A. EVERETT. Fatigue life and crack growth prediction methodology. *AGARD meeting on "An assessment of fatigue damage and crack growth prediction techniques"*, September 1993.

[97] D. A. HILLS, G. URRIOLAGOITIA-SOSA. Brief note: some observations on the parametric relationships in hertzian fretting fatigue tests. *Journal of Strain Analysis*, 35(5):441–443, 2000.

[98] J. P. CAMPBELL, R. O. RITCHIE. Mixed-mode, high-cycle fatigue-crack growth thresholds in Ti-6Al-4V i. a comparison of large- and short-crack behavior. *Engineering Fracture Mechanics*, 67:209–227, 2000.

[99] J. P. CAMPBELL, R. O. RITCHIE. Mixed-mode, high-cycle fatigue-crack growth thresholds in Ti-6Al-4V ii. quantification of crack-tip shielding. *Engineering Fracture Mechanics*, 67:229–249, 2000.

[100] V. A. SHULOV, N. A. NOCHOVNAYA, G. E. REMNEV. Thermomechanical processing of titanium alloys by high power pulsed ion beams. *Materials Science and Engineering A*, 243:290–293, 1998.

[101] G. MALAKONDAIAH, T. NICHOLAS. The influence of laser glazing on fatigue crack growth in ti-24al-11nb. *Metallurgical and Materials Transactions A*, 25:183–192, January 1994.

[102] K. N. G. FULLER, D. TABOR. The effect of surface roughness on the adhesion of elastic solids. *Proc. R. Soc. Lond. A*, 345:327–342, 1975.

[103] G. W. KUHLMAN, A. K. CHAKRABARTI. Room temperature fatigue crack propagation in beta-titanium alloys. In A. K. CHAKRABARTI and J. C. CHESNUTT, editors, *Microstructure Fracture Toughness and Fatigue Crack Growth Rate in Titanium Alloys*, pages 3–15. The Metallurgical Society Inc., 1987.